UNIVERSIDAD COMPLUTENSE DE MADRID

FACULTAD DE FARMACIA

TESIS DOCTORAL

Título

Espectroscopía Raman Laser de substancias de interés biológico y nutricional

Laser raman spectroscopy in substances of biological and nutritional interest

MEMORIA PARA OPTAR AL GRADO DE DOCTOR

PRESENTADA POR

Alicia González Gonzálvez

Director

Ángel González Ureña

Madrid, 2013

©Alicia González Gonzálvez, 2013

Espectroscopia Raman Laser de Substancias de Interés Biológico y Nutricional

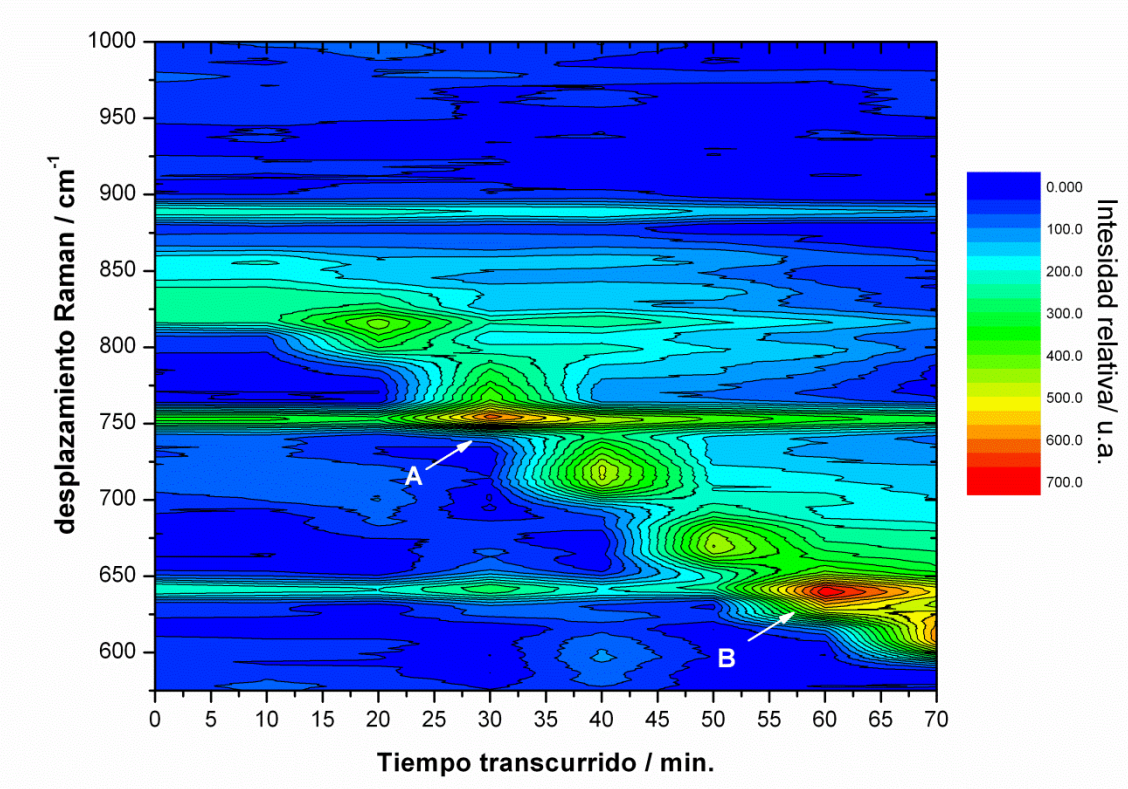

Laser Raman Spectroscopy in Substances of Biological and Nutritional Interest

Alicia González Gonzálvez

Tesis Doctoral

Madrid Septiembre 2012

Espectroscopia Raman Laser de Substancias de Interés Biológico y Nutricional

Alicia González Gonzálvez

Director de Tesis:

Ángel González Ureña

Instituto Pluridisciplinar

Unidad de Láseres y Haces Moleculares

Universidad Complutense de Madrid

Tutor del Programa de Doctorado

de Ciencias Farmacéuticas:

Montaña Cámara Hurtado

Facultad de Farmacia

Universidad Complutense de Madrid

Laser Raman Spectroscopy in Substances of Biological and Nutritional Interest

Alicia González Gonzálvez

Director of the Thesis:

Ángel González Ureña

Instituto Pluridisciplinar

Unidad de Láseres y Haces Moleculares

Universidad Complutense de Madrid

Tutor of the Pharmaceutical Sciences

PhD Program:

Montaña Cámara Hurtado

Facultad de Farmacia

Universidad Complutense de Madrid

A mis abuelas Mami y Gloria

Acknowledgments

I would like to thank all the people who have contributed in one way or another to the realization of this Doctoral Thesis.

First, I would like to thank the Director of my Thesis, Prof. Dr. Angel González Ureña, who gave me the opportunity to join the "Laseres y Haces Moleculares" Research Department in the Instituto Pluridisciplinar (U.C.M). He supervised my work during this period, offering me his unconditional support, help and interest; His continued encouragement, day by day, made me enjoy the scientific research. I would like to remark all the knowledge and experience he has taught me initiating my interest in the Physical-Chemistry and Spectroscopic fields, in particular in Laser Chemistry and Spectroscopy, expressing all his confidence always.

To my current colleagues of the "Laseres y Haces Moleculares" Department, and those who their period ended: Jorge, Khaled, Montse, Cristina, Jesús, Vitaly, Mercedes, Richard, Tania, Nerea, Dani, Karla, Gustavo, and, especially, to the secretary Arantxa - not anymore between us- who contributed to the nice atmosphere for the laboratory work. I would like to acknowledge a FPI contract from the Spanish MICCIN under grant CTQ2007-61749 and the Complutense - B. Santander programme of research groups.

I also thank the facilities provided by the mechanic and electric workshop of the Instituto Pluridisciplinar (U.CM).

To my tutor in the Nutrition and Food Science Department II, Prof. Dr. Maria de la Montaña Camara Hurtado, for her help and advice during my Doctorate Program in Pharmaceutical Sciences. I would like to thank the personal of this Department, Its

successive directors Profs. Zapata, Díez and Tenorio, professors and colleagues: Mª de Cortes Sánchez, Virginia Fernández, Amparo Díaz, Mª Cruz Matallana, Mercedes Garcia, Araceli Redondo, Nieves Bosch, Mª Luisa Pérez, Mº Teresa Orzaez, Esperanza Torija, Mª Jose Villanueva, Raquel San José, Patricia Morales, Inmaculada Mateos, Fernando Durán, Javier Prieto, Patricia García.

One part of this work was carried out in the group of Prof. Dr. Gert van der Zwan (Depatment of Chemistry, Faculty of Sciences, LASERLAB Centre, Vrije Universiteit, Amsterdam, The Netherlands), whom I would like to thank for giving me the opportunity to join his research group and for the warm hospitality received during my ten months of stay in his group. His help and contribution to increase my knowledge in Raman Spectroscopy is very much appreciated. I would like to thank Prof. Dr. Cees Jooger, Head of the Department, and Prof. Dr. Freek Ariese of the Department of Chemistry of Vrije Universiteit, Amsterdam, for their constant support and scientific attention during my stay in their University. Acknowledgement that I would like also to extend to all the personal of this Department for their help and good atmosphere for scientific research: Ingeborg, Jan-Hein, Heelen, Ivone, Guinevere, Joust, Cecilia and, Jacques. My thanks also go to Ingeborg, Jan-Hein, Rafa, Maria, Marina and David for the great moments I spent with them during my stay in Amsterdam.

I also thank Professor Helmut H. Telle for useful discussion about molecular spectroscopy during his summer visit to our Institute in 2012.

Last but not the least, I would really like to thank my parents and sister for their continous, invaluable help and support and to Mick, who since I met in Amsterdam continues to give me support to work and finish this doctoral Thesis. Without them, I would have never been able to accomplish this Doctoral Thesis.

This research received financial support from the Spanish Ministerio de Ciencia e Innovación (MICINN, grant CTQ2007-61749), the Government of the Madrid Region and from the Complutense University of Madrid. I acknowledge both a FPI fellowship and a visiting fellowship under the “Estancia Breves” programme of the MICINN of Spain in the Vrije University of Amsterdam.

Contents

List of Acronyms, Symbols and Units

ATR: Attenuated Total Reflectance

FTIR: Fourier Transform Infrared

HPLC: High Performance Liquid Chromatography

IR: Infrared

LOD: Limit of Detection

LOQ: Limit of Quantification

NIR: Near Infrared

RRS: Resonance Raman Spectroscopy

RS: Raman Spectroscopy

scatt: scattering

SERS: Surface Enhanced Raman Spectroscopy

SORS: Spatially Offset Raman Spectroscopy

t-res: trans-resveratrol

TRR: Transmission Resonance Raman

TRRS: Transmission Resonance Raman Spectroscopy

TRS: Transmission Raman Spectroscopy

ty: tyrosinase

UV: Ultraviolet

Vis: Visible

ν: frequency

λ: wavelenght

$\tilde{\upsilon}$: wavenumber

c: speed of light

h: Planck´s constant

E: Energy

$\boldsymbol{E}$: Electric field

I: Raman signal intensity

α: molecular polarizability

$\boldsymbol{\mu_d}$: inducted electric dipole moment

μ: permanent electric dipole moment

Γ: electronic transition width

m: meter

cm: centimetre (10^{-2} m)

micron.(μm): micrometre (10^{-6})

nm: nanometre (10^{-9}m)

s: second

fs: femtosecond (10^{-15}s)

Chapter 1

Introduction: Raman Spectroscopy, Objectives and Structure of the Thesis

1.1 Introduction to Laser Spectroscopy

The laser has revolutionized the world of Science and Technology in multiple fields as, for example, that of Spectroscopy, scientific area of great relevance for the study of molecular structure and dynamics as well as for chemical analysis.[1,2] The Spectroscopy[3,4] is based on the interaction of atoms and molecules present in matter with electromagnetic radiation. This radiation is the combination of an oscillating electric and magnetic field, mutually perpendicular, which propagates through space carrying energy from one location to another. Electromagnetic radiation extends to a range of spectral regions, e.g., infrared or visible radiation (visible light), X-rays or gamma rays.

Electromagnetic radiation is characterized by **its wavelength** or **frequency. The wavelength**, λ, is the distance between successive peaks. A **cycle** is part of a wave between two successive crests (or between any two successive points having the same phase). The **frequency**, ν, is the number of cycles that pass a given point in time unit [5.]

These magnitudes are described in Figure 1.1 and are interrelated by the following equation:

$$\nu \cdot \lambda = c \qquad (1)$$

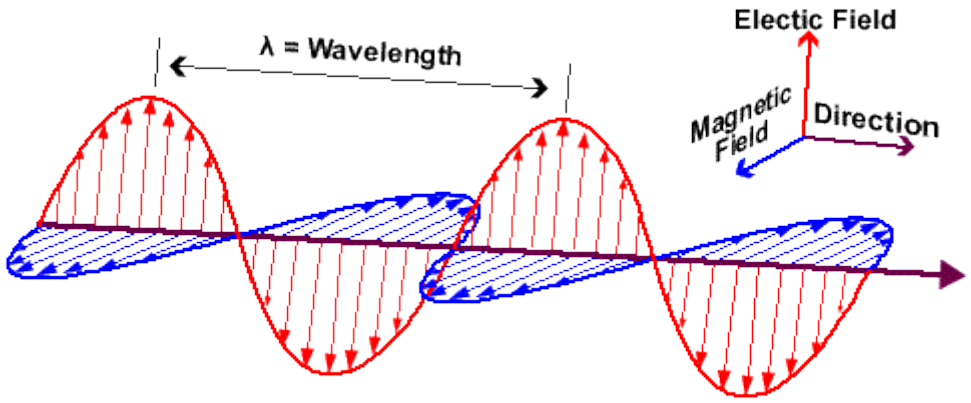

Figure 1.1: Diagram showing the propagation of an electromagnetic wave. Adapted from http://www.google.es/search?q=electromagnetic+radiation

where c is the **speed of light** (in vacuum c = 2.997928 · 10^8 m · s^{-1}**).** A light quantum (photon) of frequency ν has an energy, *E*, given by:

$$E = h \cdot \nu = \frac{h \cdot c}{\lambda} = h \cdot c \cdot \text{ŭ} \; ; \; \text{ŭ} = \frac{1}{\lambda} \qquad (2)$$

Where *h* is the Planck´s constant, *ν* the frequency of the oscillating electromagnetic field, *c* the speed of light, λ the wavelength and ŭ is the wavenumber and inverse of λ which is usually measured in cm^{-1}. Spectroscopic methods make use of electromagnetic radiation with **wavelengths** between 200 nm to a few microns.

The spectral regions of the electromagnetic radiation are fully illustrated in Figure 1.2.

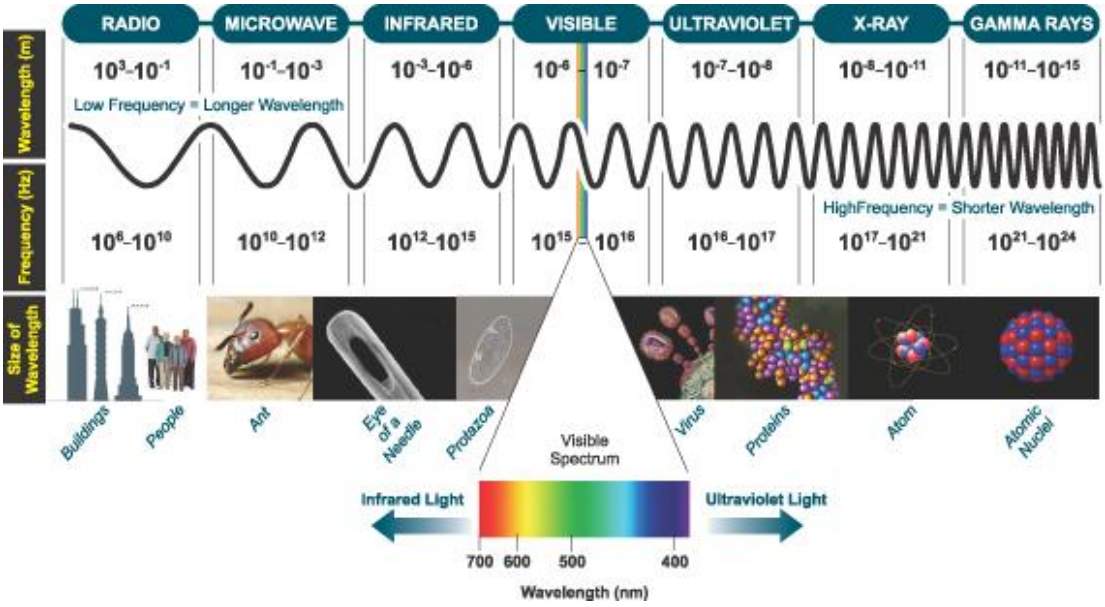

Figure 1.2: Schematic illustration of the spectrum of electromagnetic radiation. Adapted from http://www.google.es/search?q=electromagnetic+radiation.

Spectroscopy studies the absorption and emission of electromagnetic radiation by matter. In a broader sense, Spectroscopy deals with all the interactions of electromagnetic radiation with matter and, therefore, also includes the scattering and transmission of radiation. The intensity of radiation absorbed by a sample as a function of frequency is its **absorption spectrum** and, consequently, the intensity of radiation emitted by said sample as a function of frequency is its **emission spectrum.**[3,4] In laser spectroscopy[2,6] the used electromagnetic radiation comes from a laser which has become a powerful tool in the field of experimental science. This is due to the specific properties of laser light: These include:

- Its brightness.

- Its monochromatic and tuneable character.

- Its high directionality

- Its temporal and spatial coherence.

- Its polarization.

- The ability to analyze molecules using ultra-short pulses, e.g. femtoseconds (1fs $=10^{-15}$ s).

Brightness, also called radiance, is defined as the power emitted by the laser source per emitting surface unit and per solid angle unit. The high brightness of laser light is not only due to its small angular divergence but also to its high intensity. Thanks to its high radiance laser light can be focused with all its intensity on very small areas. This makes it possible industrial applications such as drilling and machining of materials or cutting tissue in medicine when used as an optical scalpel. In fundamental research, high power lasers enable a nonlinear spectroscopy causing molecular excitation and fragmentation phenomena by multi-photon absorption.[2,4,6]

The high monochromatic character and tunability of the laser light are two features that provide a high-resolution to the laser spectroscopy. The interaction of laser radiation with molecules can be very selective, allowing the excitation and analysis of certain functional groups and the probing of molecular reactions which absorb radiation at specific wavelengths. One area where this great spectral purity of the laser light has a wider application is in analytical chemistry as each molecule or atom has a characteristic absorption spectrum at a specific wavelength.

In most laser outputs, the light is polarized. The electromagnetic radiation can propagate in multiple planes of polarization, determined by two vectors: the propagation direction of the electromagnetic wave and another perpendicular to this one, determined by the electric field. When the electric field is directed vertically to the propagation direction of light, then the light is vertically polarized. If it is directed perpendicular to

the propagation of light but forming a horizontal plane with the propagation direction, then the light is polarized horizontally. Finally if the electric field is perpendicularly directed to the propagation direction of light but in all directions within a plane perpendicular to the propagation axis, then we have unpolarized light.

The polarization of the laser light provides an indispensable feature for studying the dynamics of chemical reactions and vector properties as is usually studied in Stereodynamics. Also the polarization of both Raman and Infrarred spectroscopic lines constitutes a basic information to elucidate the mechanism of radiation-matter interaction and the molecular structure.

The coherence of the laser light is one of its most remarkable properties. This property is directly related to the monochromaticity of laser light. If a laser beam is less monochromatic, i.e. it has a large bandwidth (if that bandwidth were too large it would become a very powerful lamp), the waves that form within a short time would not be on phase between them and we would say that the temporal coherence is very small. If instead the bandwidth is very narrow, the emitted photons represented by its respective electromagnetic radiation waves would be in phase, which could travel a certain time without out of phase. Then it could be said that the radiation has a great coherence.

The coherence associated with the laser propagation direction is defined as temporal or longitudinal coherence. By contrast, spatial coherence is associated with the phase in the direction perpendicular to the laser light propagation direction. The temporal coherence makes possible the existence of pulsed lasers, allowing the study of ultra-fast reactions, using laser excitation techniques in infinitesimal time scales such as the fs (10^{-15}s). These techniques allow the study of

chemical processes such as a bond rupture or biological processes as photosynthesis in real time.[2,6] One of the main applications of coherent laser light is holography, i.e. the technique in which three-dimensional images are formed.

1.2 Fundamentals of Raman Spectroscopy

Raman Spectroscopy (RS) is the branch of Spectroscopy that studies the light scattering by matter and specifically the inelastic scattering. Suppose a collision between a photon with frequency ν_0 and a molecule, the majority of the light is transmitted, some is absorbed and another is scattered. The photon-molecule collision can scatter the photon, i.e., it can change the movement direction of the photon and its energy.[5,6]

In this interaction there is an instantaneous photon absorption which is immediately reemitted. Therefore, the molecule state changes from the ground state S_0 to a more energetic state, called virtual state (dashed line in Figure 1.3), since it is not a real state of the molecule as for example the excited state S_1. Immediately after the molecule undergoes an energetic deactivation and returns to the ground state S_0. This phenomenon of light scattering is depicted in Figure 1.3.

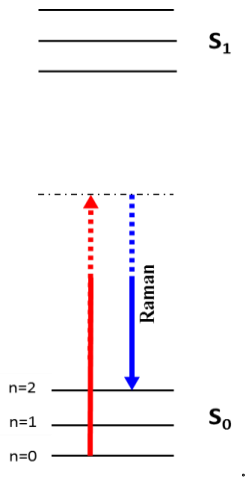

Figure 1.3: Diagram of Raman scattering.

Most scattered photons have the same frequency as the incident ones forming the so called **"elastic or Rayleight scattering ".** However, a small fraction of scattered photons exchange energy with the molecule resulting in a change in its frequency. This phenomenon is called the **"inelastic or Raman scattering "**, an effect, predicted by Kramers and Heisenberg[7] and first observed by C.V. Raman and K.S. Krishnan[8] in 1928, hence the name of this spectroscopy. Two years later Raman was awarded the Nobel Prize in Physics in 1930.

Let ν_0 and ν_{scatt} be the frequencies of the incident and Raman scattered photons, respectively. The increase or decrease in frequency, results, in a frequency variation, called "Raman shift" that is represented by $\Delta\nu_R$, and is the typical measurement in a Raman spectra. $\Delta\nu_R$ can be positive or negative, i.e. $\Delta\nu_R = (\nu_0 - \nu_{scatt}) > 0$, called Stokes, or $\Delta\nu_R = (\nu_0 - \nu_{scatt}) < 0$, called Anti-Stokes Raman scattering.

As seen in Figures 1.4 and 1.5, Stokes lines (Anti-Stokes) appear on the right (left) of the excited line when using the wavelength of the scattered radiation, in the X-axis. Let E_a and E_b be the energies of the molecule before and after the photon scatters. The energy conservation implies

$$h\nu_0 + E_a = h\nu_{scatt} + E_b \quad (3)$$

$$\Delta E \equiv E_b - E_a \equiv h(\nu_0 - \nu_{scatt}) \equiv h\Delta\nu_R \quad (4)$$

Here ΔE is the difference between the energies of two molecular stationary states, therefore the measurement of the **Raman shift** $\Delta E \equiv (\nu_0 - \nu_{scatt})$ gives the spaced molecular energy levels.

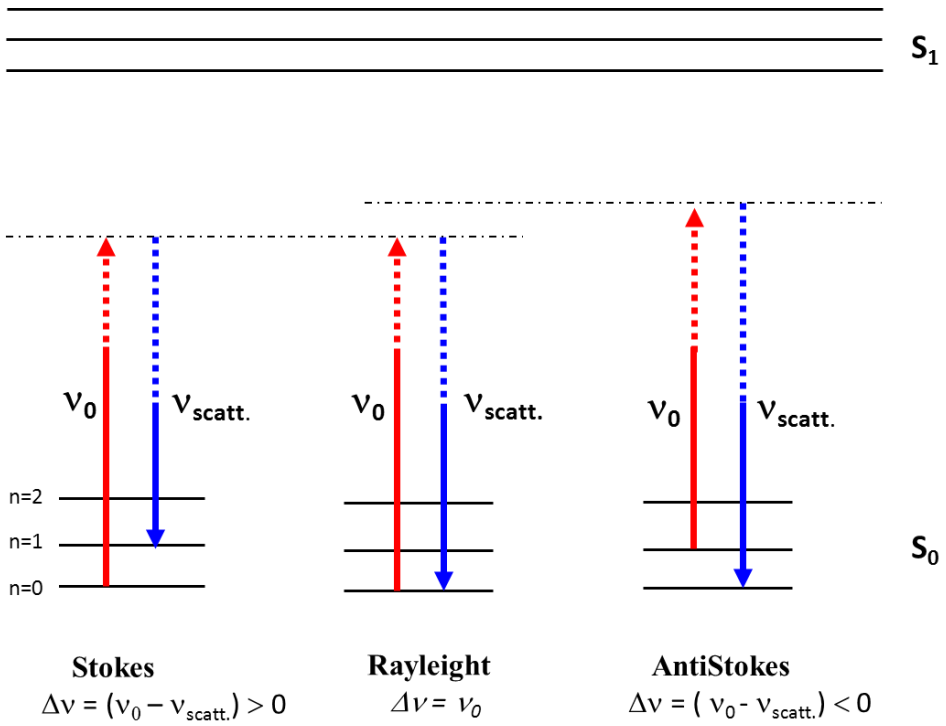

Figure 1.4: Energy level diagram of the Rayleigh, Raman Stokes and Antistokes scattering.

Before the advent of the laser, the radiation source was typically a lamp and it was usually employed an atomic mercury line whose scattered light was observed through a photographic plate with very long exposure times.

Since anti-Stokes lines come from a more excited vibrationall state than the initial one, with smaller population, the Antistokes lines have a lower Raman intensity than the Stokes lines, as seen in Figure 1.5.

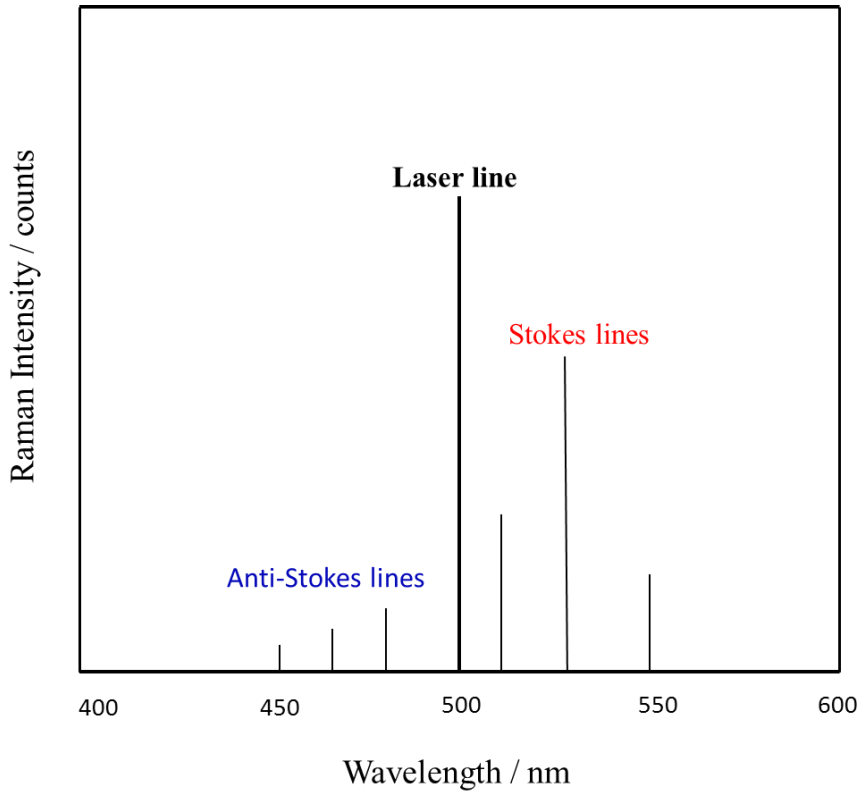

Figure 1.5: Simulated Raman Spectrum Anti-Stokes and Stokes lines are depicted.

With respect to the units in which a Raman spectrum is expressed, the x-axis can be measured in wavelengths (λ, nm), as seen in Figure 1.5, but nowadays the use of Raman shift $\Delta\tilde{\upsilon}_R$ in cm^{-1}, is becoming the standard unit in Raman Spectroscopy.

Apart from the Raman phenomenon described above, a number of photophysical processes can take place after the photon absorption by a molecule. All these processes are illustrated in the **Jablonski diagram** shown in Figure 1.6 and are of vital importance in Photophysics and Photochemistry.

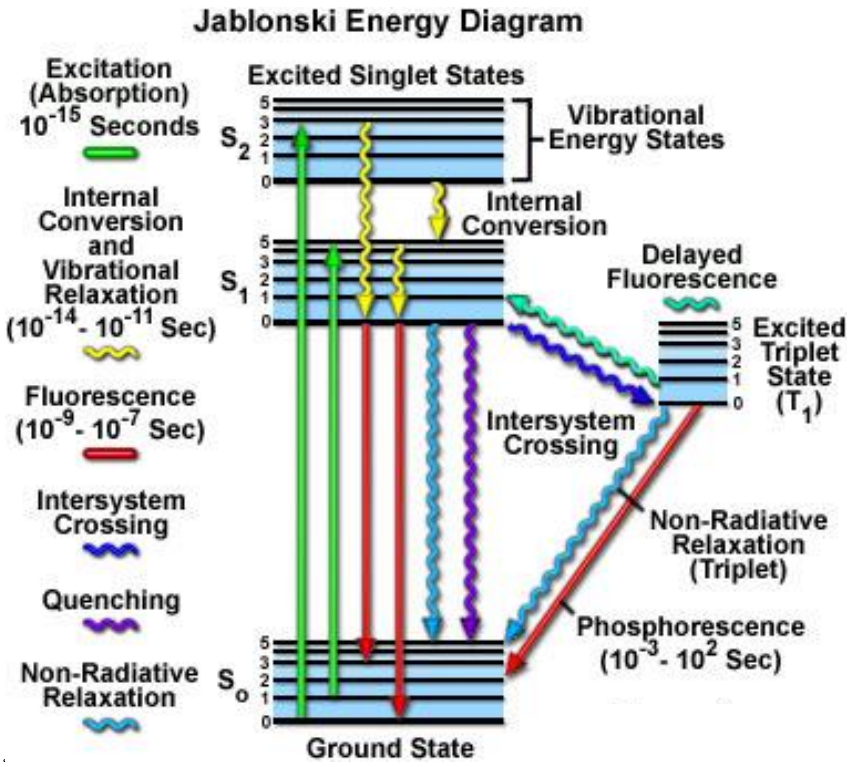

Figure 1.6: Jablonski Diagram

In the process of **absorption,** during the photon-molecule interaction, the photon is absorbed by the molecule in its ground state S_0 (singlet ground state), with all electron spins paired to an excited electronic state S_1 (singlet excited state) less populated. The absorption process is represented by $S_0 + h\nu \rightarrow S_1$. Electronic transitions associated with the absorption process occur within a too short lifetime of 10^{-15}s to involve significant nuclear displacements as the Frank-Condon principle establishes.

After the absorption process, the excited state S_1 of the molecule can transfer its energy to another molecule during the collision, thus returning to the ground state S_0, a process called non-radiative deactivation ("quenching"), which is shown in the Jablonski diagram by a wavy line.

Also intermolecular collisions could take place, which transfer the extra vibrational energy to other molecules, resulting that in the S_1 state, the molecule loses most of its vibrational energy to reach the lowest vibrational state of S_1, a process called **vibrational relaxation** [9].

The molecule in the state $v = 0$ of S_1 can undergo a transition without radiation to a different electronic state. If both states are singlets for example the case of non-radiative transition $S_1 \rightarrow S_0$ where the electronic energy of the latter is less than the initial one, then due to the energy conservation principle, there would be an energy conversion from the electronic energy to the vibrational energy. This process is called **internal conversion** ($S_1 \rightarrow S_0$) if no change of multiplicity takes place. If however, the states are a singlet and a triplet or vice versa, i.e. if the multiplicity changes, then this process is called **crossing between systems.**

The S_1 excited state of the molecule can lose electronic energy by spontaneous emission of a photon, falling back to a lower singlet ground state S_0. The process that occurs is: $S_1 \rightarrow S_0 + h\nu$ and it is called **Fluorescence**. Here, the emission of radiation takes place such that the total electron spin does not change, ($\Delta S = 0$)**.** The process of fluorescence is favoured in gases at very low pressure, because the time between collisions is relatively long. A typical lifetime of a state S_1 is 10^{-8} s in the absence of collisions.

Moreover, the triplet T can emit a photon and fall to the singlet ground state S_0. This process of radiation emission $T \rightarrow S_0 + h\nu$ is called **phosphorescence.** The phosphorescence violates the general selection rule of spin conservation $\Delta S = 0$, so that

there is a low probability of occurrence. The lifetime of the lowest excited triplet state is usually 10^{-3} to 1 s, in the absence of collisions.

The classic treatment of Raman scattering, see reference 10, Chapter 3, is based on the induction of an electric dipole, with moment **(μ_d),** by the electric field ***E*** of the incident electromagnetic radiation. This induced electric dipole moment is given by the relation[10]:

$$\boldsymbol{\mu_d = \alpha \cdot E} \qquad (5)$$

The molecular polarizability, **α,** is a measure of the degree to which the electrons in the molecule can be displaced relative to the nuclei.[4] In general the polarizability of a molecule, is an anisotropic property, which means that, at equal distances from the centre of the molecule, **α** can have different magnitudes when measured in different directions. Thus, for example, on a surface drawn such that the distance from the origin to any point on said surface has a length $\boldsymbol{\alpha}^{-1/2}$, where α is the polarizability in this direction, forms an ellipsoid. In general, this has elliptical cross-section in the xy and yz planes, as illustrated in Figure 1.7.

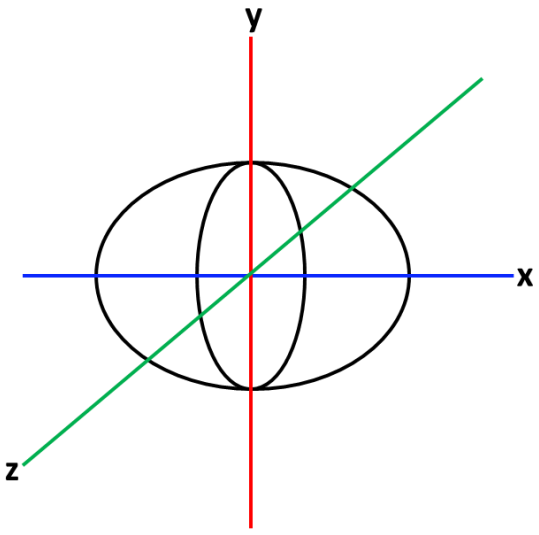

Figure 1.7: Ellipse of the Molecular Polarizability

From this model derives the particular selection rules of Raman scattering, which postulate that any molecular vibration that changes the molecular polarizability **(α)** will be active in Raman spectroscopy, i.e. we could see it in the Raman spectrum[6,11].

By contrast, in the case of infrared spectroscopy (IR) the model differs, being different the selection rules, i.e. only those molecular vibrations that induce a change in the permanent electric dipole moment of the molecule **(μ)** will be active**,** thus appearing in the IR spectra. In most cases the molecular vibrations that are inactive in Raman are active in IR and vice versa. That is why they are considered as two complementary spectroscopic techniques.

According to the mutual exclusion Principle, for a molecule with a centre of symmetry, the same vibration cannot be active in Raman and IR simultaneously. Thus, the symmetric molecular vibrations are forbidden in IR, meaning that are not active in IR, but are active in Raman. On the contrary asymmetric molecular vibrations are inactive in Raman but are active in IR. See example in Figure 1.8 which identifies two vibration modes for the CO_2 molecule.

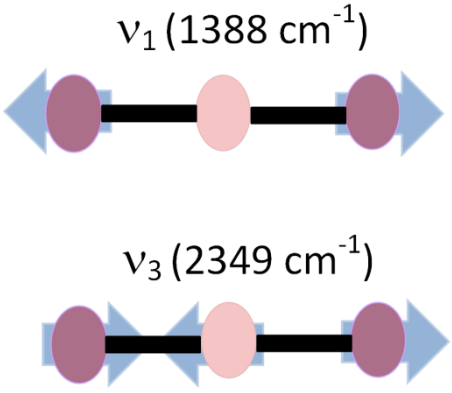

Figure 1.8: Vibration and CO_2. **Above)** symmetric stretching vibration, no change in the dipole moment μ (inactive in IR, Raman active). **Down)** asymmetric stretching vibration (change in the dipole moment μ, active in IR, Raman inactive).

1.3 Resonance Raman Spectroscopy

Conventional Raman scattering is a process of a very low probability (one in 10^7 photons results inelastically scattered), but this can be increased by several orders of magnitude if the excitation light beam has the same energy as the electronic absorption energy of the target species. This considerably increases the Raman radiation intensity associated with the vibrational modes located in the molecular region responsible for the electronic absorption. Figure 1.9 shows how in a photon-molecule interaction the photon is absorbed by the molecule reaching the excited state S_1. Therefore the scattering process is associated with the real excited states of the molecule.

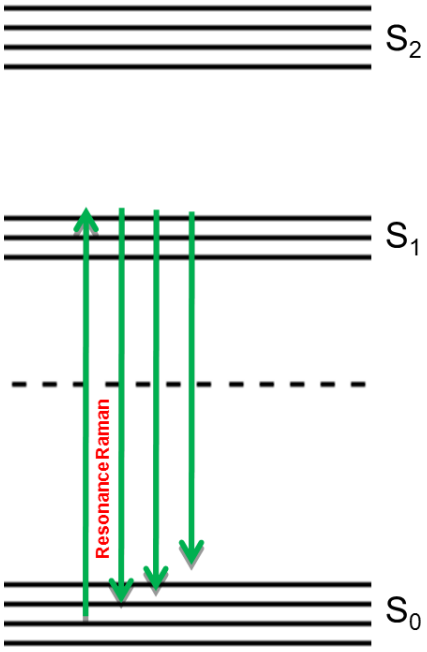

Figure 1.9: Resonant Raman scattering diagram

Raman signal intensity ***I*** for any normal vibrational mode is proportional to the laser power intensity $\boldsymbol{I_0}$, the square of α (polarizability) and the fourth power of the frequency $\boldsymbol{\nu_0}$ according to the following formula: [6, 11,12]

$$I \sim I_0 * \nu_0^4 * \alpha^2 \quad (6)$$

It then follows that ***I*** has a strong dependence on the laser light wavelength; e.g, going from 1000 nm to 250 nm, supposing a *4-fold increase in frequency*, ***I*** increases 256 times.[6,11,12] As a result it is preferable to use shorter excitation wavelengths. However, in practice there is a great inconvenience caused by the interference of fluorescence. Even with the use of short excitation wavelengths, the Raman scattering process is of very low probability, as mentioned earlier only a very small portion of the incident photons will be scattered and even a fraction of it will suffer the Raman inelastic scattering process.

The latter is the reason for the slow progress of the RS in the first decades after its discovery. After, with the laser development, the improvement on the speed technique and the use of increasingly sensitive detectors, there was a breakthrough in the field of RS applications, re-emerging new improved variants such as Resonance Raman spectroscopy (RRS), among others. Please note that for a molecule illuminated by the incident excitation wavelength, the polarizability is inversely proportional to the difference between the incident photon energy and the energy of a given electronic transition, $S_i \rightarrow S_0$. In this way the intensity of a Raman line is given for the resonant model by the expression.[10]

$$I \sim I_0 \frac{\nu_0^4}{(\nu_{S_i - S_0} - \nu_0)^2 + \mathbb{\Gamma}^2} \quad (7)$$

where $\mathbb{\Gamma}$ is the width of the electronic transition. This width prevents when $\nu_0 = \nu_{S_i - S_0}$, ie. in a resonance condition, the Raman intensity becomes infinite. As ν_0 tends

to $\nu_{S_i - S_0}$ the denominator decreases significantly and the Raman intensity increases by several orders of magnitude. This process is called Resonance Raman Spectroscopy (RRS).[13] The increased sensitivity in RRS versus non-resonant conditions in RS is compensated with the loss of information because the increase in the sensitivity is selective. In other words, not all signals corresponding to vibrations of the molecule of interest in a matrix are enhanced by RRS, but only some of them with corresponding functional groups or vibration modes completely symmetrical[14] which interact with the resonant state. Despite this limitation, the resonant condition simplifies the spectrum and allows the study of samples and inaccessible processes by other means as discussed below.

Fluorescence is a process approximately 10^6 times more likely than Raman scattering, so that may interfere the Raman intensity significantly. Therefore it can be concluded that interference of fluorescence is one of the biggest problems that RRS presents. However, higher excitation wavelengths are generally used because it eliminates the possible interference of fluorescence, as they have lower photon energies.

Thus, we may mention several important advantages of the resonance Raman spectroscopy in the study of biological molecules, such as: **a)** the increase in the Raman signal intensity which allows the study of very dilute solutions (10^{-3} to 10^{-6} mol / dm^3) characteristics of biopolymers in organisms, **b)** the selectivity in the increased intensity of the vibrations in only one part of the molecule, simplifying the spectrum and allowing the study of the bonds in that region. Normally the coloured functional groups of the molecule are those which have absorption bands in the visible (called chromophores or active sites), and whose absorption wavelengths or frequencies may be

used for excitation to obtain the desired resonant Raman effect. As an example it can be cited the study of a chromophore group or heme active site in hemoglobin and myoglobin[15], **c)** due to Raman inactivity of H_2O molecule, water has become a solvent of biological molecules commonly used in RRS because of its little interference with the Raman signal of the biological sample.

1.4 Transmission Raman Spectroscopy

1.4.1 What is it?

Transmission Raman Spectroscopy (TRS) is a variant of conventional Raman Spectroscopy suitable for probing bulk content of diffuse scattering samples. TRS occurs due to light scatters through turbid media or materials that do not absorb or block light significantly. Similarly to Spatially Offset Raman Spectroscopy (SORS), in the Transmission Raman process the light extends randomly through the entire sample of diffuse scattering. Transmission Raman could be seen as an extreme example of SORS.

SORS is a variant of the conventional RS technique that allows highly accurate chemical analysis of objects beneath obscuring surfaces, such as tissue, coatings and bottles. Examples of applications of SORS include analysis of bone beneath the skin[16], tablets inside plastic bottles[17], and explosives inside containers[18]. SORS was invented and developed by Matousek et al.[19] in Rutherford Apleton Laboratory in England. The method shows that most materials are not completely transparent to light or completely opaque to it, and normally tend to scatter light.

A good example would be the case in which a red laser pointer illuminates the end of a finger-the light scatters throughout the tissue in the finger. Wherever this light goes there will be some inelastic scattering due to Raman effect, so that at some point most parts of the object will generate detectable Raman signals, even those that are not on the surface of the object.

A typical analysis of SORS will perform at least two Raman spectra; one at the surface and the other from a distance of a few millimetres of the illuminated area. The two spectra can be subtracted by using a subtraction scale to produce the spectra representing the subsurface and surface. This geometric configuration of the SORS technique is illustrated further below in Figure 1.10.

In conventional Raman process, photons are created at all points of the sample surface that the light passes through and are collected by optic detectors. These photons can be directed in a back scattering collection mode or in a perpendicular arrangement, where the incident beam over the sample and the optical detector are arranged geometrically at an angle of 180° or in some cases at an angle of 90°, respectively, as is shown in Figure 1.10. By contrast, in Transmission Raman, the photons are created through entire sample and are directed in a forward collection mode where the incident beam on the specimen and the optical detector are arranged geometrically in an angle of 0° (in the same line), as seen in Figure 1.10.

As is well known[20], the light scattering process in conventional Raman Spectroscopy has its limitations, only one in 10^6-10^8 photons scatter, thereby obtaining a weak Raman signal. Besides, the conventional Raman spectroscopy has the limitation

that the signal produced is generally representative of the surface or surface-near the sample, and it is, therefore, a very weak signal.

Furthermore, another of its limitations is the interference of fluorescence in the UV-Visible, whereby a way to eliminate this interference would be the application of greater near infrared excitation wavelengths. Thus the conventional Raman spectroscopy is usually applied to samples which do not exhibit a strong interference of fluorescence. By contrast, in TRS photons are created through the entire sample as mentioned above, thus producing a strong signal.

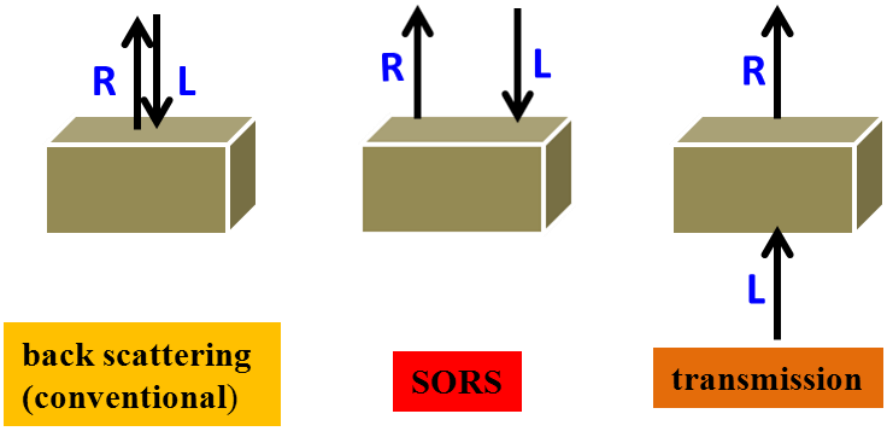

Figure 1.10: Typical geometries of Raman Spectroscopy with respect to the sample. **Left)**conventional back scattering Raman. **Centre:** SORS geometry. **Right:** Transmission Raman geometry. **Legend: R:** Raman light, **L:** laser beam.

As said above, TRS photons are created throughout the sample illuminated by the laser, this phenomenon is directly related to the fact that light scatters through turbid media that do not absorb or block significantly. To better understand this phenomenon it is necessary to consider in detail the theory of propagation or migration of light in diffusely scattering media, such as tissues, developed by Pavel Matousek in 2007.[21]

The main limitation in conventional optical analytical methods for interrogating deep layers of tissue in disease diagnosis is the highly scattering nature of tissue. It is very important to understand the mechanism of propagation of light in diffusely scattering media. Figure 1.11 illustrates the three main components of the light through a diffusely scattering medium.[21] These are ballistic, snake and diffuse, as presented *Alfano et al in 1997*. [22] The "ballistic" light is the part of the light that is not scattered by the medium and its intensity decreases exponentially with depth. Upon propagation through a turbid medium, this component gradually converts to the "snake" light, which in turn becomes the "diffuse" component. The "snake" component is only weakly deviated from its original direction by the scattering events, due to the fact that it only undergoes a small number of scattering events that are, typically, strongly biased towards the forward direction This component also undergoes an exponential decay with depth, although its penetration depth is higher than that of the ballistic component.

Both components can be utilised to form sharp or fuzzy images of objects in these media. This is crucial for applications such as confocal Microscopy, where the passage of light through a confocal aperture serves as a means for depth discrimination of the measured Raman signal. An object seen with ballistic or snake light, would appear transparent or semi-transparent, respectively.

The component penetrating the deepest and therefore the most important for spectroscopic investigations of the deep layers of turbid media, is the diffuse component of light[21.] In tissues it can penetrate to depths of up several centimetres, in the NIR (Near Infrared) region, as opposed to hundreds of micrometres to a few millimetres of

ballistic and snake. An object would appear translucent, when viewed with this type of light.

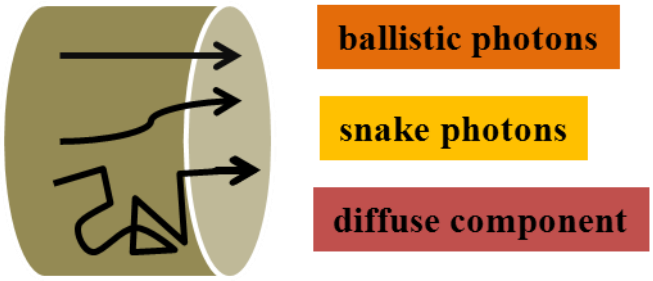

Figure 1.11: Main components of light in turbid media.

Accordingly, in the TRS technique photons are created throughout the sample illuminated by the laser, in particular photons from deeper layers- by the photon propagation or migration- migrate towards the surface layers in picoseconds times and then scatter to reach the detector. In this way more information is obtained from the measured sample since a higher Raman signal is obtained than that of the conventional Raman, providing a signal which is representative to the whole content of the sample and not just to the surface

1.4.2 Background

TRS was invented by Bernhard Schrader along with Bergmann in 1967 who published the seminal article about the first successful use of the TRS in chemical analysis of organic solids.[23] The TRS technique was again re-invented in 2006 by Matousek and Parker,[24,25] who showed the ability of this technique in analyzing tablets and powdered compounds of several millimetres thick. This was a breakthrough in the Pharmaceutical

world, because the TRS technique represents a fast analytical method, for non-invasive pharmaceutical dosage of capsules and tablets. The pharmaceutical traditional testing techniques have various limitations, due to the surface sensitivity (i.e. NIR reflectance), the presence of phase changes due to sample preparation (i.e. liquid chromatography), or sub-sampling (in conventional NIR Raman).[26]

By contrast, the transmission Raman technique is quite insensitive to the surface, requires no sample preparation or phase change and is fast.[24,25] Subsequent investigations by Matousek et al increased the accuracy of this technique and its applicability in the quantification of tablets and powdered compounds of formulation.[27,28]

The application of conventional Raman spectroscopy in the field of medicine has had its limitations due to the problem presented to the surface sensitivity, making impossible to reach hundreds of micrometres depths and remaining only on the surface. By contrast, and because of its mentioned insensitivity to the surface, the technique of TRS has been presented as a technique of high potential for injury diagnosis in breast tissues.

Several studies conducted by Baker et al[29,30] and Matousek and Stone[31] in the area of breast cancer, were carried out by the chemical identification of calcifications in breast cancer lesions by Kerr gated, SORS and TRS techniques, achieving penetration depths 0.9, 8.7 and 16 mm in chicken breast tissues, respectively.

1.5 Objectives and Structure of the Thesis

1.5.1 Transmission Resonance Raman Spectroscopy: The development of a new technique

Transmission Resonance Raman Spectroscopy (TRRS) is the technique that combines Transmission Raman Spectroscopy (TRS) with Resonant Raman Spectroscopy (RRS).[20]As discussed above in paragraphs 1.3 and 1.4 since each of these techniques improves and enhances the Raman signal, one may expect that the symbiosis of both methodologies into an unique technique should provide a higher improvement of the Raman signal compared to that of each technique separately.

To the best of our knowledge, not many studies have been published in which the improved Resonant Raman excitation was combined with the advantages of collecting transmission Raman signal. *Therefore the development of a new technique combining the Resonance Raman with the Transmission Raman operational features was one of the main motivations of the present Doctoral Thesis.* Indeed, in terms of instrumental development one of the most important achievements of this Doctoral Thesis has been the design, building and setting up of a new technique based on Transmission Resonance Raman Spectroscopy (TRRS).

As it will be shown in **Chapter 2** (as well as in a recent publication in Applied *Spectroscopy)* this objective has been successfully achieved. Thus, a significant part of the thesis is focused on the study and analysis of fruits by non-invasive spectroscopic techniques such as TRRS. In particular, the study of certain compounds called

carotenoids found in carrots, such as β-carotene, responsible for pigmentation[20] and involved in physiological processes such as photosynthesis[32] was carried out

Chapter 2 describes the TRRS technique, a methodology that, as mentioned above, provides an increased signal to noise ratio and an improvement in analytical sensitivity. The technique application in the detection and quantification of β-carotene in carrots directly and noninvasively, gave values of β-carotene 17.3 mg / 100g $_{carrot}$ (coincident with the bibliographic records) and allowed the monitoring of carotenoid spatial distribution in fruits. Also the dependence of the Raman signal as a function of sample thickness (carrot slice) was investigated and rationalized using a theoretical model that satisfactorily describes the experimental measurements.

1.5.2 Resonance Raman Spectroscopy to monitor the mechanism of enzymatic reactions

A good example of the simplicity and high sensitivity of Resonance Raman spectroscopy is the study of catalytic reactions induced by enzymes. In **Chapter 3** both the reaction mechanism and the kinetic of some catalytic reactions in proteins were studied by Resonance Raman Spectroscopy (RRS) and UV-visible absorption. This study confirmed and demonstrated how RRS can resolve the intermediates of catalytic reactions (drawing on the cover), that are crucial for understanding the reaction path and therefore, the discovery of potential enzyme inhibitors.

In particular, we studied the catalysis of trans-resveratrol (t-res) induced by the enzyme tyrosinase (ty) by RRS and UV-Vis absorption spectroscopy. This investigation is of great interest for the discovery of potential inhibitors in the melanin synthesis pathway,

which is catalysed by the ty, and nowadays received great attention in melanoma research.

It was shown how in the early stages of the catalytic route[33] the t-res binds to the ty forming the t-res-ty ^{S}P complex with its characteristic O-O bond linked to the two Cu atoms of the ty active site. The resonance feature of this Raman technique makes possible to observe catalytic intermediates non-detectable by other more conventional techniques such as UV-Vis absorption. The study provided a clear evidence that a class of potential inhibitors of tyrosinase can be found in compounds able to bind the two Cu (II) ions of the enzyme bidentate form.

1.5.3. Laser photons and healthy fruit

In Chapters 2 and 3, laser photons are used as an ingredient to implement the distinct analytical Raman spectroscopic techniques. An important part of the Thesis is based on the use of laser photons not as part of the analytical method but as an (abiotic) agent to induce photochemical changes in fruit which ultimately could improve its health status.

It is well known that plants and fruits possess a defence mechanism by which they react to both biotic and abiotic stress generating beneficial substances to health, called secondary metabolites. So, in this part of the Thesis we employed laser light as a way (a) to induce the abiotic stress in table grapes in order to elicitate secondary metabolites such as trans-resveratrol, or carotenoids and (b) to measure their internal enhancement using the Raman techniques described in previous chapters.

This explains the title of this section of the Thesis "Laser photons and healthy fruit". It is constituted by two chapters: **4** and **5**.

First, **chapter 4** deals with the increase of carotenoids in grapes–due to the interest they attract because of their antioxidant capacity[34]– when the fruit is irradiated using UV-B LED light in order to improve their post-harvest quality. For this purpose, a new Transmission Resonance Raman spectrometer (TRR) based on an Ar^+ laser of 514.5 nm excitation wavelength was setup. It also employs a 360° rotating holder where the grapes receive the LED radiation. After the grapes' irradiation, their carotenoid content is analysed as a function of elapsed time. This experimental system is described together with the main experimental finding, that is, a significant increase of β-carotene content in white grape after 24 hours after fruit irradiation.

Chapter 5 describes the same type of studies with table grapes but using a UV laser, instead of UV-B LED, as the photon source to elicitate the trans-resveratrol content in grapes. The choice of trans-resveratrol was due to its high antioxidant activity, anti-fungal, anti-inflammatory, estrogenic, cardioprotective and chemopreventive properties for cancer.[35,36,37,38,39]

Thus, Table grapes were irradiated with laser pulses at two different wavelengths: one selected at 302.1 nm, i.e. resonant with the trans-resveratrol bi-photon absorption band[40], and another selected at 300 nm, that is a non-resonant wavelength where trans-resveratrol two-photon absorption is negligible.

Attenuated Total Reflectance Fourier Transformed Infrared Spectroscopic analyses of the irradiated grapes´ skin showed an enhancement of polyphenols' content when the resonant wavelength was employed. Furthermore, microbiological analysis performed with non-treated (control), non-resonant and resonantly irradiated grapes demonstrated

how the last samples developed a significantly lower number of colony forming units after cultivation in adequate media.

Since the only difference between the two (resonant and non-resonant) irradiation conditions is just a couple of nanometres in the employed UV-B laser wavelengths, the germicidal effect, in principle not as important as if UV-C light had been employed, of both treatments is very similar and, subsequently, the observed difference in the table grape resistance to microbial infection has to be predominantly attributed to a wavelength dependent effect. Several hypotheses are presented and discussed to rationalize these experimental findings but among all then the photochemical explanation by which two-photon resonant absorption enhances significantly the biosynthesis of trans-resveratrol seems to be the most reasonable.

1.5.4 Are photons strictly necessaries for improving the fruit quality?

Chapter 6 continues the investigation focused on the post-harvest fruit improvement, particularly in table grapes. However, a different approach was adopted to get this objective. Rather than using laser photons, controlled atmospheres or chemical pesticides, our investigation used the natural pesticides present in the own plant. Indeed, an important group of secondary metabolites in plants called phytoalexins, known by their anti-fungal and anti-oxidant capacity,[41,42,43] act as defence compounds under stress or attack conditions, increasing their own content. One of these phytoalexins is trans-resveratrol, which is found in several plants and fruits. Therefore in this chapter a study was carried out to assess the capability of trans-resveratrol as natural bio- pesticides to improve the quality of postharvest grapes.

This goal required the preparation of a natural extract from vine leaves in 95% water and 5% ethanol, in which different bunches of grapes were immersed. The same number of bunches received either water or ethanol (5%) treatment, being both used as blank. Remarkably, on the 14th day after the beginning of the treatment the extract treated grapes, always maintained at room temperature, showed no sign of physical deterioration. In contrast, the two blank samples, i.e.: the water or ethanol treated bunches appeared dehydrated, infected and deteriorated.

It was shown that after the use of such natural bio-pesticides there is an increase in phytoalexins and a significant improvement in the grape's natural resistance to microbial infections. To confirm these results, laser desorption and resonant ionization coupled with mass spectrometric techniques, Fourier Transform Infrared Spectroscopy and microbiological analysis methodologies were employed. As a result to increase the postharvest fruit quality laser photons are a good alternative, in particular if resonant absorption bands of the bio pesticide to be elicitated can be excited. If laser photons are not available an interesting alternative are the employment of LED irradiation techniques and, finally, if neither of the two methods can be implemented the use of the own plant extract is of great help as an ultimate resource.

Finally, **Chapter 7** provides a brief summary of the thesis and highlights the most relevant conclusions drawn from the studies conducted over this project.

1.6 References

(1) K. Thyagarajan, A. Ghatak, Lasers: Fundamentals and Applications, Heidelberg, Germany: Springer, (2010).

(2) H. H. Telle, A. González Ureña and R. J. Donovan, Laser Chemistry: Spectroscopy, Dynamics and Applications, Chichester, U.K.: John Wiley & Sons, (2007).

(3) A. Requena, J. Zuñiga, Espectroscopia, Madrid, Spain: Pearson Education, S.A, (2004).

(4) J. Michaell Hollas, Modern Spectroscopy, Chichester, U.K.: John Wiley & Sons, (2004).

(5) I.N. Levine, Fisicoquímica vol.2, Madrid, Spain: Mc Graw Hill, (2005).

(6) W. Demtrõder, Laser Sectroscopy Vol.2 Experimental Techniques, Heidelberg, Germany: Springer, (2008).

(7) H. A. Kramers and W. Z. Heisenberg, "Über die Streuung von Strahlung durch Atome", Z.Phys **31**(1), 681-708 (1925).

(8) C.V. Raman and K.S. Krishnan, "A New Type of Secondary Radiation", Nature **121**, 501-502 (1928).

(9) A. González-Ureña, Cinética Química, Madrid, Spain: Síntesis, (2001).

(10) W. Demtrõder, Laser Sectroscopy Vol.2 Chapter 3 Experimental Techniques, Heidelberg, Germany: Springer, (2008).

(11) E.V. Effremov, "Advances in Analytical Resonance Raman Spectroscopy",Vrije Universiteit, The Netherlands, October (2008).

(12) S. Tardioli, “Optical Methods For Structure Elucidation Of Protein-Ligand Interactions: Fluorescence and Ultraviolet Resonance Raman Spectroscopy”, Vrije Universiteit, The Netherlands, November (2011).

(13) M. Harrand, R. Lennuier, “Exalation de l´intensité raies dans les spectres Raman émis par des corps présentant au voisínage de la raie excitatrice”, Comptes Rendus Academie des Sciences **223**, 356-359 (1946).

(14) H. Takeuchi, I. Harada, “Ultraviolet resonance Raman spectroscopy of X-Proline bonds: A new marker band of hydrogen bonding at the imide C=O site”, J. Raman Spec. **21**, 509-515 (1990).

(15) J.M. Friedman, D. L. Rousseau, and M. R. Ondrias, “Time Resolved Resonance Raman Studies of Hemoglobins” Ann. Rev. Phys. Chem. **33**, 471-491 (1982).

(16) M. V. Schulmerich, K. A. Dooley, M. D. Morris, T. M. Vanasse and S. A. Goldstein, ”Transcutaneous fiber optic Raman spectroscopy of bone using annular illumination and a circular array of collection fibers”, J. Biomed. Opt. **11**(6):060502-1-3, (2006).

(17) C. Eliasson, P. Matousek, "Non-Invasive Authentication of Pharmaceutical Products through Packaging using Spatially Offset Raman Spectroscopy", Anal. Chem. **79** (4), 1696-1701 (2007).

(18) C. Eliasson, N.A. Macleod, and P. Matousek, "Non-invasive Detection of Concealed Liquid Explosives using Laser Spectroscopy". Anal. Chem. **79**(21), 8185-8189 (2007).

(19) P. Matousek, I.P. Clark, E.R.C. Draper, M.D. Morris, A.E. Goodship, N. Everall, M. Towrie, W.F. Finney, and A.W. Parker, " Subsurface Probing in Diffusely Scattering Media Using Spatially Offset Raman Spectroscopy", Appl. Spectrosc. **59**, 393-400 (2005).

(20) A.G. Gonzálvez and A. González-Ureña, "Transmission Resonance Raman Spectroscopy: Experimental Results Vs. Theoretical Model Calculations", Appl. Spectrosc. **66**(10), 1163-1170 (2012).

(21) P. Matousek, "Deep non-invasive Raman spectroscopy of living tissue and powders", Chem.Soc.Rev. **36**, 1292-1304 (2007).

(22) B. B. Das, F. Liu, and R.R. Alfano, "Time-resolved fluorescence and photon migration studies in biomedical and model random media", Rep. Prog. Phys. **60**, 227–292 (1997), and references therein.

(23) B. Schrader, G. Bergmann, Z. Fresenius, "Die Intensitat des Ramanspektrums polykristalliner Substanzen", Anal. Chem. **225**, 230–247 (1967).

(24) P. Matousek and A.W. Parker, "Bulk Raman Analysis of Pharmaceutical Tablets", Appl. Spec. **60**(12), 1353-1357 (2006).

(25) P. Matousek and A.W. Parker, "Non-invasive probing of pharmaceutical capsules using transmission Raman spectroscopy", J. Raman Spec. **38**, 563-567 (2007).

(26) H. Wang, C.K. Mann, T.J. Vickers, "Effect of Powder Properties on the Intensity of Raman Scattering by Crystalline Solids", Appl. Spectrosc. **56**(12), 1538-1544 (2002).

(27) A. Johansson-Sparen, O. Svensson, S. Folestad, and M. Claybourn, "Quantitative transmission Raman spectroscopy of pharmaceutical tablets and capsules", Appl. Spectrosc. **61**(11), 1211-1218 (2007).

(28) C. Eliasson, N.A. Macleod, L.C. Jayes, F.C. Clarke, S.V. Hammond, M. R. Smith, P. Matousek, "Non-invasive quantitative assessment of the content of pharmaceutical capsules using transmission Raman spectroscopy", Journal of Pharmaceutical and Biomedical Analysis **47**(2), 221–229 (2008).

(29) R. Baker, P. Matousek, K.L. Ronayne, A.W. Parker, K. Rogers, and N. Stone, "Depth profiling of calcifications in breast tissue using picosecond Kerr-gated Raman spectroscopy", Analyst **132**, 48–53 (2007).

(30) N. Stone, R. Baker, K. Rogers, A.W. Parker, and P. Matousek, "Future possibilities in the diagnosis of breast cancer by subsurface probing of calcifications with spatially offset Raman spectroscopy (SORS)", Analyst **132**, 899-905 (2007).

(31) P. Matousek and N. Stone,"Prospects for the diagnosis of breast cancer by non-invasive probing of calcifications using transmission Raman spectroscopy", J. Biomed. Opt. **12**(2), 024008 (2007) [doi:10.1117/18934].

(32) A.J. Young, D. Phillipa, A.V. Rubanb, P. Hortonb, and H.A. Frank, "The xanthophyll cycle and carotenoid-mediated dissipation of excess excitation energy in photosynthesis", Pure &Appl. Chern. **69**, 2125-2130 (1997).

(33) A.G. Gonzálvez, A. González-Ureña, R.J. Lewis, and G. van der Zwan, "Spectroscopy and Kinetics of Tyrosinase Catalyzed trans-Resveratrol Oxidation", J. Phys. Chem. B **116**, 2553−2560 (2012).

(34) J.J.Strain and I.F.F. Benzie: Antioxidants/diet and antioxidant Defence in Encyclopedia of Human Nutrition, vol. **1**, pp. 95-106 (M Sadler, JJ Strain and B Caballero, Editors). London: Academic Press (1999).

(35) A. Cassidy, B. Hanlkey, R.M. Lamuela-Raventós, "Isoflavones, lignans and stibenes-origins, metabolism and potential importance to human health", J. Sci. Food Agric. **80**, 1044-1062 (2000).

(36) L. Fremont, "Biological Effects of Resveratrol", Life Sci. **66**, 663-673 (2000).

(37) J.B. German, R.L. Walzem, "The health benefits of Wine", Annu. Rev. Nutr. **20**, 561-593 (2000).

(38) S. Pervaiz, "Chemotherapeutic potential of the chemopreventive phytoalexin resveratrol", Drug. Res. Updates. **7**, 333-344 (2004).

(39) G.J. Soleas, E.P. Diamandis, D.M. Goldberg, "Resveratrol: A Molecule Who's Time Has Come? And Gone", Clin. Biochem. **30**, 91-113 (1997).

(40) J.B. Jiménez Sánchez, E. Crespo Corral, J.M. Orea, M.J. Santos Delgado, A. González-Ureña, "Trans-resveratrol elicitation by laser resonant irradiation of table grapes", Appl. Phys. B. **87**, 559-563 (2007).

(41) Y. Elad, "Responses of plants to infection by Botrytis cinerea andnovel means involved in reducing their susceptibility to infection", Biol Rev. **72**, 381-422 (1997).

(42) X. Dong, "SA, JA, ethylene, and disease resistance in plants", Curr. Opin. Plant. Biol. **1**, 16-23 (1998).

(43) B.J. Feys, J.E. Parker, "Interplay of signalling pathways in plant disease resistance", Trends Genet. **16**, 449-55 (2000).

Chapter 2

Transmission Resonance Raman Spectroscopy: Experimental Results Vs. Theoretical Model Calculations*

Abstract: A laser spectroscopic technique is described which combines transmission and resonance enhanced Raman inelastic scattering together with low laser power (< 30 mW) and good spatial resolution (<200 μm) operational features. The monitoring of the transmitted inelastic scattering provides an increased signal to noise ratio because the low fluorescence background and, on the other hand, the resonant character of the laser excitation leads to an enhanced analytical sensitivity. The spectroscopic technique was applied to investigate the carotenoid content (specifically the β-carotene concentration) of distinct samples including fruits, reaching a detection limit of the order *of hundred picograms per cubic millimetre* in solid samples which is below the level needed for typical food control analysis. Additional features of the present development comprise direct sampling, non-invasive character and fast analysis with no time consuming. From a theoretical point of view, a theoretical model for the Raman signal dependence on the sample thickness is also presented. Essentially, the model considers the sample to be homogeneous and describes the underlying physics using only three parameters; the Raman cross-section, the laser radiation attenuation cross-section and the Raman signal attenuation cross-section. The model was applied successfully to describe the sample size dependence of the Raman signal in both β-carotene standards and carrot roots. The present technique could be useful for direct, fast and non-destructive investigations in food quality control and analytical or physiological studies of animal and human tissues.

* The contents of this chapter have been published as Alicia G. Gonzálvez and Ángel González Ureña in the Applied Spectroscopy Journal **66**(10), 1163-1170 (2012).

2.1 Introduction

As it is well known carotenoids constitute a main group of pigments with important metabolic functions[1] mostly associated to their antioxidant properties. Some of the human benefits[2-4] associated to their consumption are the reduction of the risk of cancer, bone calcification, eye degeneration, and neuronal damages. Due to their limited solubility and instability carotenoids analysis in vegetables requires careful handling and fast response techniques such that degradation and isomerization processes could be minimized.[5-6]

Carotenoid analysis in food products is usually implemented by high-performance liquid chromatography (HPLC) and spectrophotometry.[7] However; spectroscopic techniques are becoming more frequently used since they are faster and easier to perform than the HPLC method. Thus, for example, lycopene and β-carotene content in tomato fruits and related products have been determined using Fourier transform Raman spectroscopy, attenuated total reflectance infrared and near infrared spectroscopy.[8, 9]

On the other hand, it is well known that Raman scattering is a powerful and widely used technique both in molecular spectroscopy and analytical chemistry.[10-16] The interest of Raman spectroscopy in analytical applications stems on various reasons being one of the most important that no special sample preparation is required. Nevertheless, a severe drawback of the Raman technique is its very weak signal as typically only one in every $10^6 - 10^8$ photons is scattered. This serious limitation has driven the development of distinct enhancement techniques as, for example, resonance Raman (RRS) or surface enhanced Raman spectroscopy (SERS).

The achievements in RRS and the importance of its analytical potential have been recently reviewed.[17] In particular carotenoid analysis by Raman spectroscopy has received a great attention in part because they are strong Raman scatters. Thus Raman spectroscopy of carotenoids has been employed in many studies ranging from non-invasive in vivo determination of carotenoid in human skin[9] through the carotenoid content comparison between a healthy and a carcinoma tissue[18] to their quantification in fruits, vegetables and juices[15-16] as well as in extract of marine phytoplankton.[19]

Despite the greater sensitivity associated to the resonance Raman scattering some important drawbacks, inherently present when one employs this methodology, are the intense fluorescence emission produced by the chromophores and the non-negligible scattering produced in high density samples. Normally, interference from fluorescence emission is usually minimized using IR laser excitation.

An elegant method to reduce the inherent disturbing fluorescence produced by the resonant excitation of the illuminated sample surface, particularly when the fluorescence source is a surface component, is the use of transmission Raman spectroscopy (TRS).[10] This is a variant of Raman spectroscopy rediscovered in 2006 where it was shown[10] its capability in analysing tableted or powdered samples of several millimetres of thickness.

Among the many advantages of this new approach one should note the method ability to probe bulk content of powders and tissues rejecting Raman and Fluorescence components produced from the sample surface as well as the absence of sub-sampling. These advantages have converted TRS in a useful technique in pharmaceutical analysis. [20, 21]

To the best of our knowledge, there are not many studies which combine the enhancement of resonant Raman excitation with the advantages of transmission Raman signal collection. This is the motivation of the present work. Here a simple transmission resonance Raman (TRR) spectrometer is described with further applications to carotenoid detection, specifically, β-carotene in carrots. As discussed later in order to enhance the method sensitivity we used the output of a CW laser at 532 nm to resonantly excite the broad absorption band of the β-carotene.

We anticipate that the combination of these two key features allowed detection sensitivities of sub-nanograms of β-carotene in carrots by using a green laser power of a few tens of mW. This high sensitivity confers our spectrometer many possibilities to investigate the presence of carotenoids especially in food and biological samples. In addition, the high spatial resolution of the developed TRR spectroscopy allows determining the analyte distribution in the whole sample volume, a feature that can provide insight to investigate aspects more related with plant and fruits physiological processes, clearly beyond the mere analytical chemistry domain.

A final comment on dense optical media is worthy. It is well known that for high dense optical samples deviation from the limiting Lambert-Beer law and diffusing scattering are expected to prevail (see further below). Nevertheless the present technique is capable of investigate the thickness dependence of the transmitted Raman intensity for a given solid sample, and a few examples are reported in the application section of the present work.

2.2 Experimental Methodology

A schematic layout of the experimental arrangement employed in the present work is depicted in Figure 2.1.

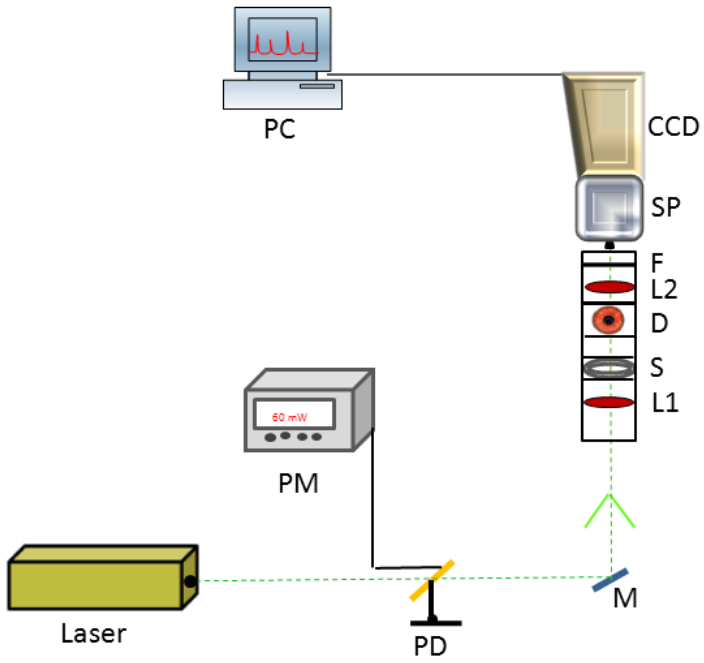

Figure 2.1: Schematic layout of the TRR spectroscopy set up. **L:** a double diode pump green Nd-Yag laser (532nm, cw); **M:** mirror (90º) ; **PM:** power-meter ; **L1:** plane-convex lens f(75mm)(ϕ= 25.4 mm); **S:** XY micrometer sample holder; **D:** Diaphragm; **L2:** plane-convex lens f(25mm)(ϕ = 25.4 mm); **F:** razor-edged filter (Semrock mod.LP03-532RU-25); **SP-CCD:** Andor model: Newton; **PD:** photo-detector; **PC:** Computer.

A diode pump green (λ = 532 nm) cw laser is directed through a cage-system and focused by a one inch diameter, 75 mm focal length plane-convex lens on to the sample. This is typically a 0.2 mm thick 50 mg pellet of KBr containing the carotenoid sample in a concentration range of 2-4 % in weight. The sample is mounted in an XY

micrometer sample holder in a perpendicular plane to the laser beam propagation direction. Typical laser spots at the sample are between 1 or 1.5 mm diameter.

Alternatively, the sample could be a carrot slice of several tenths of millimetre thickness, a green or red grape skin or any other suitable fruit. A diaphragm is situated after the sample to collimate the transmitted light. Furthermore, the scattered light is collected by a plane-convex lens of diameter ϕ = 25.4 mm and focal length of 25 mm. The forward transmitted light is directed through a razor-edged filter (Semrock mod.LP03-532RU-25) which provides a transmission greater than 98% for wavelength higher than 532 nm and less than 10^{-7} below this wavelength and, finally, focussed into the 25-50 μm slit of the CCD detector (Andor model: Newton). Typical operating conditions are 30mW of laser power, a CCD temperature ≤ -90º. Finally every spectrum was taken averaging 66 scans of 10 s each.

2.3 Theory: Attenuation model for Raman transmission signal

The study of light scattering and photon migration in turbid media constitutes nowadays an important research area both in modern spectroscopy and biomedicine. In particular, the dependence of signal on depth in Raman spectroscopy of solid samples or in fluorescence spectroscopy, both in animal and human tissues, has received an increasing attention by several groups.[22-27]

Typically, in these types of studies a Monte Carlo simulation is used in which both the elastically scattered (laser) and inelastically scattered (Raman) photons are individually followed as they propagate through the medium in random-walk like fashion in three- dimensional space. [26-27] The most widely used model for the

transmission Raman Monte Carlo simulation consider the sample to be a homogeneous turbid medium for which the propagation distance over which the photon direction is randomized is approximated by the transport free path, i.e. the average distance photons must travel within the sample maintaining their original direction of propagation.

In this section, a simple theoretical model to analyse the transmission Raman signal as a function of the sample thickness is described. It is a simple ("back-on-an-envelope") theoretical model based on the standard Lambert-Beer formalism which is further extended taking into account (i) the laser radiation attenuation cross-section and (ii) the Raman cross-section attenuation by the homogeneous dense media. The model that incorporates the basic physics and uses only three model parameters reduces to the traditional Lambert-Beer equation in the limit of dilute samples.

We would like to emphasize that the model development here presented is by no means intended to be an alternative to the more rigorous treatments cited above but to provide a few parameter model which could be used by experimentalists with the only support of a pocket calculator.

The developed model can be better understood with the aid of the scheme illustrated in Figure 2.2.

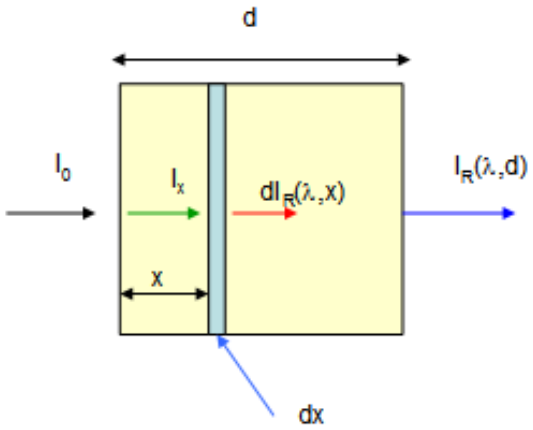

Figure 2.2: Transmission Raman scheme. Simple schematic cross-section to illustrate the distinct incident and transmitted Raman signals relevant to the present model analysis and experiments.

Here a sample of thickness *d* and particle concentration N_s is illuminated by a laser beam of power density P_0. The Raman signal variation $dI_R(\lambda,x)$ produced by the sample element of length *dx* can be expressed in the form:

$$dI_R(\lambda, x) = P(x) \cdot N_S \cdot \sigma_R(\lambda) \cdot dx \quad (1)$$

where $\sigma_R(\lambda)$ stands for the Raman cross-section at a given wavelength λ and $P(x)$ the power density of the laser at *x*.

The total Raman signal collected at *d*, i.e., the transmitted Raman signal $I_R(\lambda,d)$ is obtained by integration of Equation (1).

$$I_R(\lambda \cdot d) = \int_0^d dI_R\ (\lambda, x)dx = \int_0^d P(x)N_s\,\sigma_R(\lambda)dx \quad (2)$$

To perform the integration in equation (2) one needs to know the x-dependence of P(x). For non-optically dense media one can adopt the Lambert-Beer model[14] to describe the laser light attenuation. Thus, we will use the following expression.

$$P(x) = P_0 \cdot e^{-\sigma_a(\lambda_{exc})N_S x} \quad (3)$$

Here $\sigma_a(\lambda_{exc})$ stands for the total laser attenuation cross-section which includes contributions due to resonant absorption, scattering, etc.

Replacing (3) into (2) and performing the integration one gets

$$I_R(\lambda, d) = P_0 \frac{\sigma_R(\lambda)}{\sigma_a(\lambda_{exc})}(1 - e^{-\sigma_a(\lambda_{exc})N_S d}) \quad (4)$$

For very small values of $N_s.d$, i.e. when $N_s.d << 1$, the exponential can be approximated by a linear term of the form:

$$\exp(-\sigma_a(\lambda_{exc})N_s d) \approx 1 - \sigma_a(\lambda_{exc})N_s d \quad (5)$$

This leads to a simple linear function for

$$I_R(\lambda, d) = P_0 \sigma_R(\lambda) N_s d \quad (6)$$

Thus, for optically thin samples the transmitted Raman signal should be linear with the sample concentration for a given sample thickness.

For optically dense media the Lambert-Beer law is not valid and a more realistic model would be needed to describe Raman transmission data. To illustrate the effect of such Lambert-Beer's law deviations we consider in the following the case where the Raman signal is attenuated. To take into account this attenuation we re-write equation (1) in the form:

$$dI_R^a(\lambda, x) = P(x)N_S\sigma_R(\lambda)dx - I_R(\lambda, x)N_S\sigma_R^a(\lambda)dx \quad (7)$$

where the superscript *"a"* stands for attenuation. The first term of the right hand member in (7) is that of equation (1); the second term corresponds to the loss of Raman signal due to the Raman attenuation cross-section $\sigma_R^a(\lambda)$.

Replacing (4) into (7) and integrating over *x* one obtains after some algebra

$$I_R^a(\lambda, x) = P_0 \frac{\sigma_R(\lambda)}{\sigma_a(\lambda_{exc})}\{(1+\gamma)(1-e^{-Bx}) - \gamma Bx\} \quad (8)$$

Where $B = \sigma_a(\lambda_{exc})N_s$ and $\gamma = \sigma_R^a(\lambda) / \sigma_a(\lambda_{exc})$. Equation [8] gives $I_R^a \rightarrow 0$ for $x \rightarrow 0$ and for $x = x^{\infty}$ a limiting value that can be obtained from the condition $(1+\gamma)(1- e^{-Bx^{\infty}}) = \gamma$ Bx^{∞} which reduces to $x^{\infty} = 1/B(1+\gamma/\gamma)$ when $Bx^{\infty} >> 1$. It is interesting to remark that for $Bx << 1$ the exponential e^{-Bx} can be approximated by $e^{-Bx} \sim 1+Bx$. Under these conditions the simple linear form given by equation (6) is recovered. It can be easily shown that for optical densities below 0.1 (e.g. $Bx < 0.1$ the deviation of the linear model represented by equation (6) is less than a 5% with respect to the complete attenuated model.

In addition, Equation (8) has a maximum at $x = x_{max}$ a value that can be deduced by solving the equation.

$$\left(\frac{\partial I_R^a(\lambda,x)}{\partial x}\right)_{x=x_{max}} = 0 \quad (9)$$

This condition is satisfied for

$$x_{max} = \frac{1}{\sigma_a(\lambda_{ex})N_s} \ln(\frac{1+\gamma}{\gamma}) \quad (10)$$

An equation that clearly indicates that for $\sigma_R^a = 0$, i.e. when the Raman signal is not attenuated there is no maximum, since $x_{max} \rightarrow \infty$ for $\gamma = 0$. For a finite γ value the higher the sample concentration or the laser wavelength attenuation cross-section the lower the x_{max} value.

Let us define the reduced x^* and I_R^* as

$$x^* = \frac{x}{x_{max}} \quad (11a)$$

and

$$I_R^* = \frac{I_R^a(\lambda,x)}{(P_0\sigma_R(\lambda)/\sigma_a(\lambda_{exc}))}(\quad (11b)$$

then equation (8) can be cast into the simple form

$$I_R^* = \left\{(1+\gamma)(1-\left(\frac{\gamma}{\gamma+1}\right)^{x^*} - \gamma x^* ln\left(\frac{\gamma}{\gamma+1}\right)\right\} \quad (12)$$

Figure 2.3 illustrates the I_R^* dependence on x^* and γ. Obviously all curves show their maximum at $x^* = 1$ and for a given x^* value the lower the γ the higher the I_R^*.

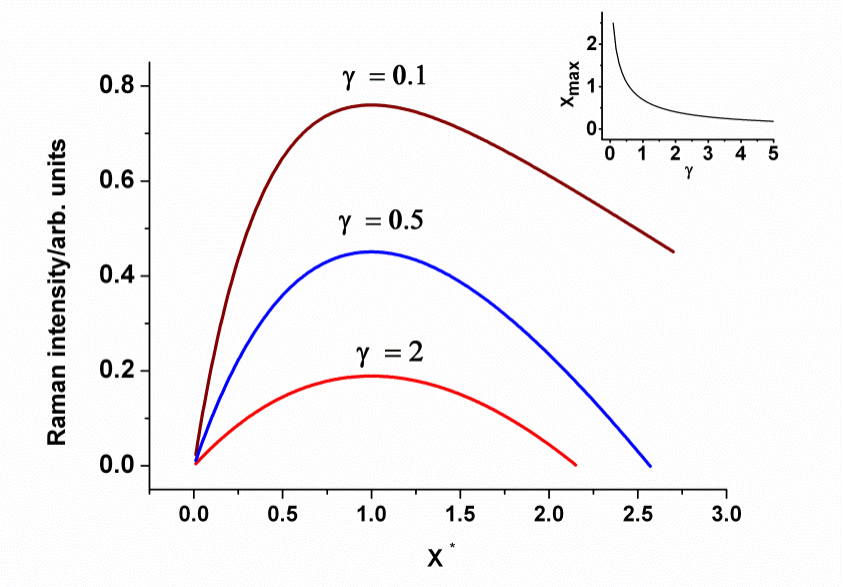

Figure 2.3: I_R*dependence on x* and γ. Note how all curves show their maximum at $x^* = 1$ and for a given x^* value, the lower the γ the higher the I_R^*. The inset shows the x_{max} dependence on γ.

So far, the developed model used N_s as a parameter and x, the thickness, as the variable; however looking at the differential and integral equations (7) and (8), respectively they are symmetrical with respect to these two variables and consequently a similar expression to (8) can be obtained if one uses the thickness as a parameter and the concentration N_s as variable.

In this case the model equation would be

$$(\lambda, Ns) = P_0 \frac{\sigma_R(\lambda)}{\sigma_a(\lambda_{exc})}\left\{(1+\gamma)\left(1-e^{B'N_S}\right)-\gamma B' N_S\right\} \qquad (13)$$

in which B' will be given by $B' = \sigma_a(\lambda_{exc})x$ and $N_s(max)$ will now adopt the form

$$N_s(max) = \frac{1}{\sigma_a(\lambda_{ex})x}\ln\left(\frac{1+\gamma}{\gamma}\right) \quad (14)$$

2.4 Applications

To illustrate the capability of the present technique we have undertaken an investigation of carotenoid and more specifically of β-carotene due to its relevance in the intake of human population. It is well known, that this pigment absorbs in the visible showing a maximum[28] in its absorbance at 451 nm (ε_{451} =139,500 $M^{-1}cm^{-1}$). To avoid the presence of a high fluorescence yield we have used the 2nd harmonic of the Nd: YAG at 532 nm at which the β-carotene still absorbs but moderately[28] (ε_{532} =18110 $M^{-1}cm^{-1}$). In this manner the resonant absorption condition is guaranteed but with low fluorescence yield to optimise the signal to noise ratio. In addition, cw solid state green lasers *(λ= 532nm)* are nowadays commercially available at low cost.

2.4.1 Resonant versus non-resonant Raman scattering

Figure 2.4 displays a typical β-carotene TRR spectrum obtained from a pellet containing 10μg of pure (Sigma-Aldrich) β-carotene diluted in KBr up to 50 mg in weight.

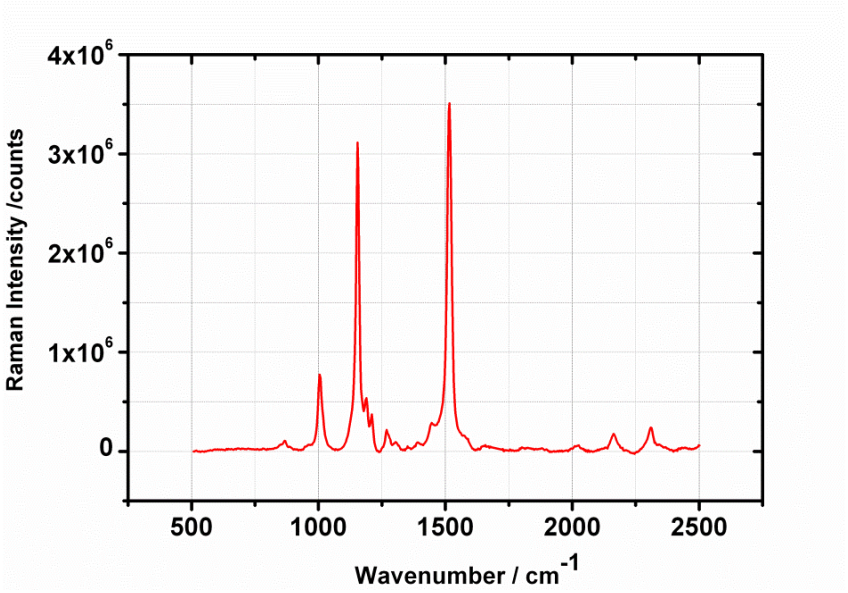

Figure 2.4: TRR Spectra of β-carotene. TRR spectrum of β-carotene standard (10 µg) diluted in KBr up to 50 mg from a 0.2 mm thick pellet. The experimental conditions were: 66 scans of 10 s. each one. The small peaks between 2000 cm^{-1} and 2500 cm^{-1} are understood as experimental artifacts.

Essentially, three carotenoid signals are manifested.[29-30] The bands at 1516 cm^{-1} and 1154 cm^{-1} are typically assigned to the in-phase –C=C-(ν_1) and –C-C (ν_2) stretching vibrations of the β-carotene, respectively. The wavenumber of the first band is generally correlated with the length of the polyene chain. Therefore carotenoids with lower conjugated C=C bonds than the β-carotene (11 double C=C bonds) show characteristic bands at higher wavenumbers.[9,15,29-30] Finally, the in-plane rocking modes of CH_3 bonds coupled with the C-C bonds show a peak of moderate intensity[29-30] at 1007 cm^{-1}.

Working with this sample thickness high level of laser transmission is ensured when pure KBr is used. Consequently, the transmitted Raman signal is entirely associated to the β-carotene contents of the solid sample. Notice the clear presence of the three main Stokes peaks mentioned further above.

In this sub-section a comparison is made between the Raman spectra of the β-carotene and trans-resveratrol. While the former absorbs at 532nm as mentioned earlier the polyphenol shows no absorption at this specific wavelength.[31]

The Transmission Raman spectra of both compounds are depicted in Figure 2.5. Except for the sample concentration, both spectra were taken under identical experimental conditions.

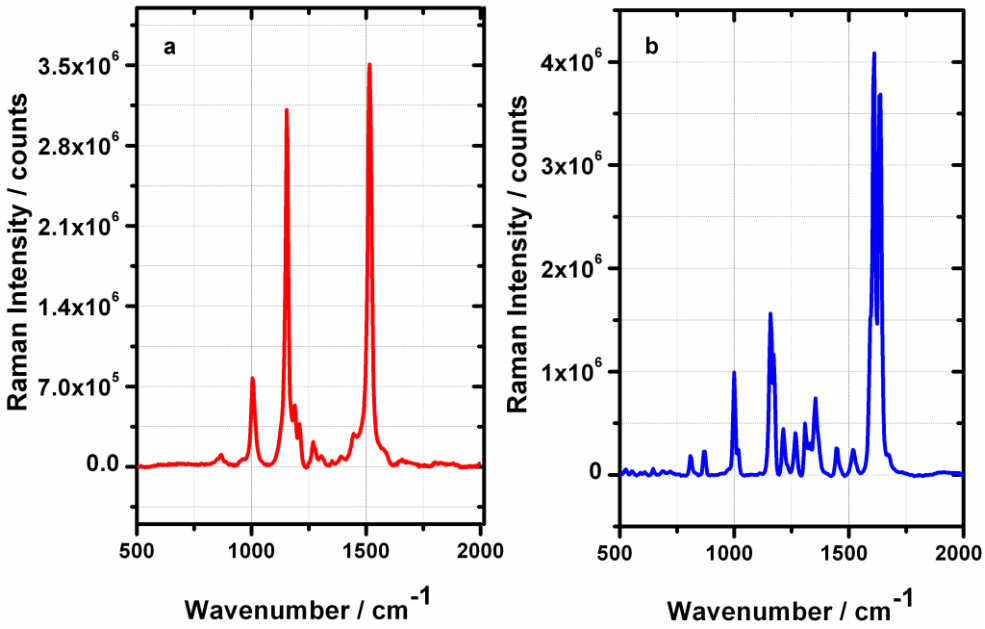

Figure 2.5: Comparison between the transmission Raman spectra of the β-carotene and trans-resveratrol. Except for the molar concentration of the two compounds the spectra were taken under identical conditions. **a)**ß-carotene 0.02µmol; **b)** trans-resveratrol 22 µmol.

In fact the β-carotene spectrum (in red colour) is that of Figure 2.4 which corresponds to a KBr pellet containing 0.01 mg i.e. 0.02 x 10^{-6} mol of pigment. A similar KBr pellet containing 5 mg of tans-resveratrol gives the spectrum shown in the right panel of Figure 2.5. This corresponds to 22 .10^{-6} mol of trans-resveratrol. The comparison between these spectra indicates that a similar number of counts is obtained for the

maximum spectral peak in both samples, but the molar concentration in the β-carotene is *three orders of magnitude lower* than that of trans-resveratrol even though the excitation wavelength is far from the centre of the absorption band of the β-carotene (i.e. $\lambda_{max} \approx 451$ nm). It is therefore evident that by using resonant light the method sensitivity can be enhanced by several orders of magnitude.

2.4.2 Calibration β-carotene for optically thin samples

As one would expect the Raman intensity for a given peak would increase as the beta-carotene concentration does. However, as one further increases the carotenoid concentration, attenuation effect would appear as the optical density of the sample is augmented.

Obviously to guarantee the technique applicability for analytical determinations the most convenient scenario would be that of the linear, Lambert-Beer conditions, described by Equation (6) further above. To illustrate the linear dependence with the concentration and thickness, the 1154 cm^{-1} Stokes signal is displayed as a function of the c*d product, i.e. the concentration β-carotene times the pellet thickness (0.2 mm) in Figure 2.6. A similar linear dependence (not shown) was found for the other Stokes peaks providing that the product *C*d* did not exceed ca. 30 ng / mm^2.

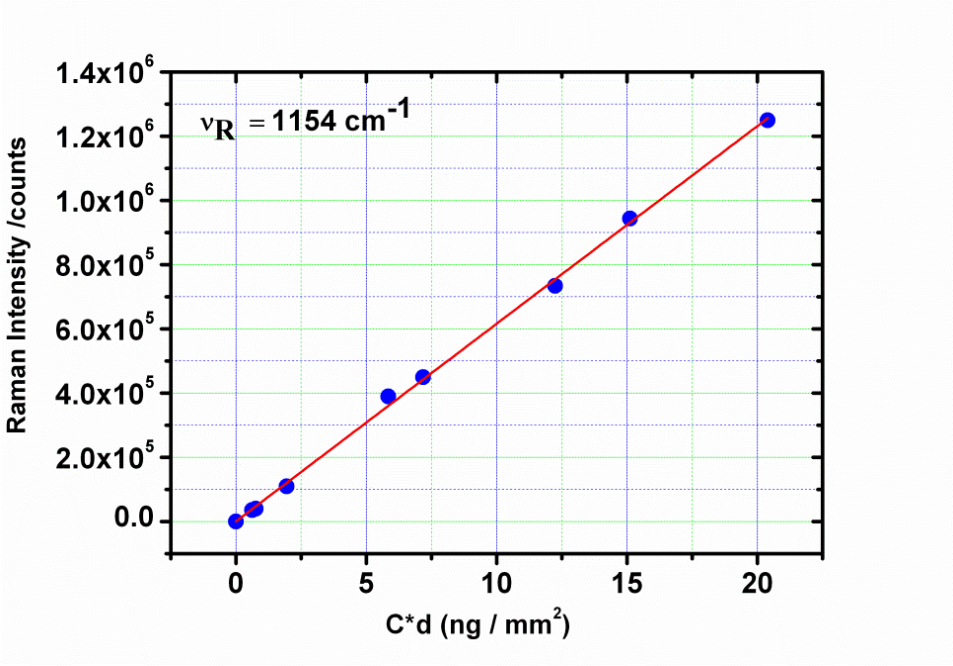

Figure 2.6: Calibration of β-carotene contents using TRR spectroscopy. 1154 cm^{-1} Stokes peak as a function of the β-carotene concentration times 0.2 mm pellet thickness, the units are expressed in ng/ mm^2. Solid red line model fit to equation 6 of the text.

As the matter of fact, Figure 2.6 constitutes a calibration curve for carotene analysis whose best parameters from the linear fit are listed in Table I.

Table I. Calibration Parameters for the TRR spectrometer applied to β-carotene analysis using the 1154 cm^{-1} Stokes line.

Line Intensity (Counts) Equation	1093 + 61552 C*d (ng/mm^2)
Interval (ng/mm^2)	0-25
R^2	0.999
Standard deviation (from the residual sum of squares)	1.37 x10^4
LOD (pg/mm^3)	734
LOQ (ng/mm^3)	2.2

Limit of detection (LOD) and quantification (LOQ) have been estimated following ICH Guideline Q2B[32] via eqs. (15) and (16).

$$LOD = 3.3 \ \sigma/s \tag{15}$$

$$LOQ = 10 \ \sigma/s \tag{16}$$

where σ is the standard deviation of the response and s the slope of the calibration curve. To determine the standard deviation of the response we used the residual standard deviation of the regression line. Using the parameters listed in Table I and samples of 0.2 mm the values obtained for LOD and LOQ were 0.734 ng / mm^3 and 2.2 ng / mm^3, respectively.

Taking into consideration that the typical carrot density is about 1 mg/ mm^3 (see next subsection) the present technique would give a LOD of 0.734 μg / g_{carrot} or equivalently 734 ppb for direct, without sample preparation, carrot analysis. This limit is below the typical carotenoid concentration present in carrots as it would be discussed below.

As it was shown further above, as the beta-carotene increases, not only the Raman signal intensity will increase but also the attenuation effects because the optical density of the sample is augmented. This attenuation effect is shown in Figure 2.7 in which the solid circles represent the 1154 cm^{-1} Stokes signal from a 0.2 mm thick pellet of KBr as a function of the β-carotene concentration.

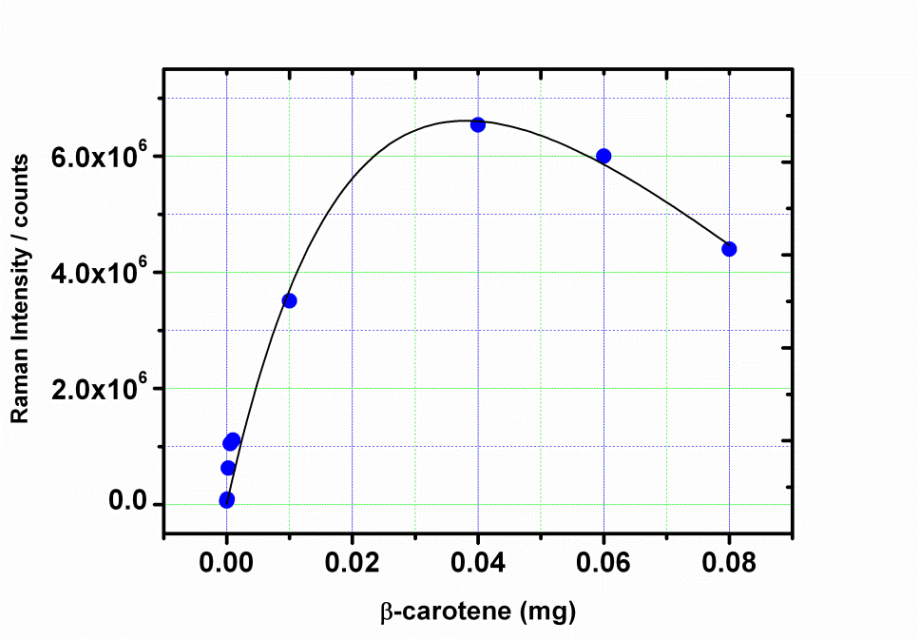

Figure 2.7: TRR signal of β-carotene as a function of its concentration. Solid blue points TRR signal of the 1154 cm^{-1} peak as a function of the β-carotene concentration (mg) in a KBr pellet of 0.2 mm of thickness. Black solid line model fit using equation 13 of the text. Spectra were taken under the same experimental conditions: 66 scans of 10 s. each one.

The solid line is the best fit obtained using equation (13) of the text deduced when one includes the attenuation cross-section. The best fit parameter values where B = 49.26 mm^{-1} and $\gamma = 0.18$. Using equation (14) and the obtained B and γ values one can deduce a σ_a (λ_{exc} = 532 nm) value of 0.18$Å^2$.

It is interesting to note that the β-carotene absorption cross-section that corresponds to the experimental ε (λ=532nm) value is ~ 0.07$Å^2$. This difference with respect to the 0.18$Å^2$ deduced for the total laser attenuation cross-section, seems to be reasonable as the latter contains various contributions as, for example, the β-carotene absorption and scattering cross-section and the KBr absorption and scattering cross-section. It should be noted how this model describes satisfactorily the Raman signal dependence as the β carotene concentration is increased. In fact, it is capable to

describe how the Raman signal increases reaching a maximum at ca.0.034 mg after which it gently decreases.

2.4.3 Carotenoid contents in carrots

Carrot cultivars constitute a very important source of vegetable for human consumption of carotenoid. In this picture optical spectroscopy represents a common technique for both research and control quality of these important compounds. In particular Raman Spectroscopy has become a useful methodology in carotenoid analysis due to its non-destructive identification of distinct components present in plants materials as well as to its high analytical sensitivity.

To prove the analytical capability of our transmission Raman spectrometer in solid food samples the Raman spectrum of a 0.5 mm slice carrot sample is shown in Figure 2.8. The great similarity between this spectrum and that of pure β-carotene displayed in Figure 2.4 should be remarked.

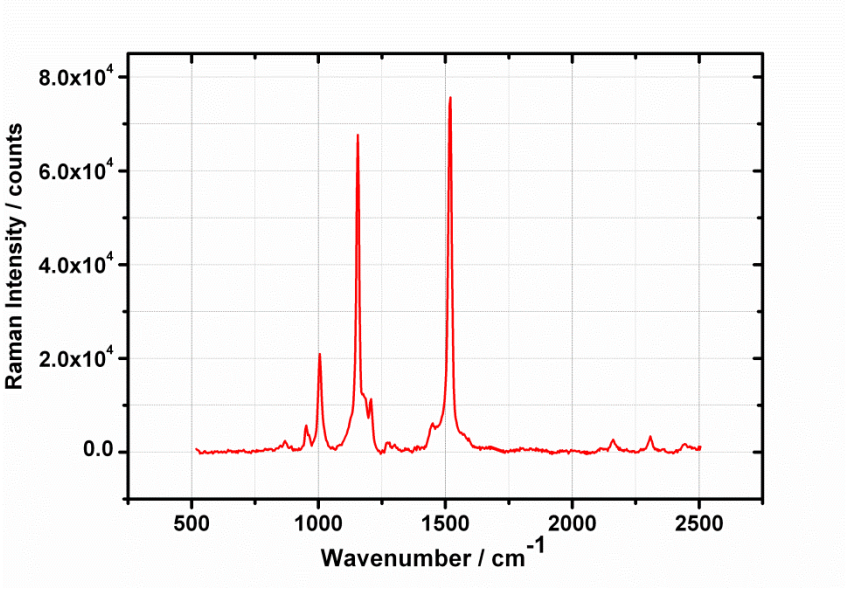

Figure 2.8: TRR of a carrot sample. TRR Spectrum of a 0.5 mm thick carrot slice taken directing the laser spot to the centre of the slice. Notice the close resemblance with the spectrum shown in Figure 2.4 for the β-carotene standard. All measurements were done under the same experimental conditions: 66 scans of 10 s. each one. The small peaks between 2000 cm^{-1} and 2500 cm^{-1} are understood as experimental artifacts.

As it is well known in spectra taken from carotenoids present in plant matrixes as for example in a carrot root, the position of the –C=C- band is shifted to higher wavenumbers[9] and for β-carotene is normally observed[33] at 1520 cm^{-1}. The corresponding peak of Figure 2.8 occurs at 1520 cm^{-1} which indicates that β-carotene is the predominant carotenoid present in the investigated carrot. Likewise the second most prominent peak appears at 1155cm^{-1}.

To guarantee that the measurement was taken in the range of validity of the Lambert-Beer law the evolution of the 1520 cm^{-1}peak intensity was monitored as a function of the slice carrot thickness. Such dependence is displayed in the next sub-section. There, it is shown that Raman intensity measurements for samples thickness below 0.5 mm lie well within the Lambert-Beer behaviour, in other words where a direct and linear dependence should be expected between the Raman signal and β-carotene concentration.

A test of the present technique applicability for β-carotene quantitative analysis in normal food samples was carried out by measuring the Stokes 1155 cm^{-1} signal in carrots. A 0.2 mm thickness slice from a (light) orange carrot bought in the market was prepared and introduced in the sample holder of our Raman spectrometer. The 1155 cm^{-1} Raman peak measured in the carrot cortex gave 2.1 x 10^6 counts, value that corresponds to a C^*d value of 34.1 ng/mm^2 by using the linear regression of the Table I, also represented by the solid red line of Figure 2.6.

Considering that the major contribution to the Stokes 1155 cm^{-1} signal arises from the β-carotene and taken into account the sample thickness of 0.2 mm, a concentration of β-carotene given by c = 171 ng/mm^3 was deduced. By weighing a

known carrot volume its density was determined to be ρ = 0.99 mg/mm^3. Finally, using the latter value the β-carotene concentration was found to be *c* = 173 μg of β-carotene/g_{carrot} or, equivalently, as it is normally expressed c = 17.3 mg of β-carotene/ 100g_{carrot}.

This value compares well with the β-carotene and /or carotenoid content in carrots reported in the literature. In fact our estimated value of 17.3 mg / 100g_{carrot} is consistent with the experimental (17.26 - 24.45) mg / 100g_{carrot} range determined by HPLC and RRS reported in Ref. 33 for light and dark orange carrots, respectively. Therefore, one should note the simplicity and reliability of the presented TRR technique for fast and direct analysis of β-carotene in solid food samples.

2.4.4 Raman signal dependence on sample thickness

A contour map of the TRR data as a function of a carrot slice thickness is displayed in Figure 2.9 over the 0.12 mm-5 mm range. Notice the thickness evolution of the main three peaks discussed earlier. Except for the overall intensity no significant spectral change is noticed as the thickness is increased. For this experiment all measurements were taken directing the laser to the centre of the carrot root.

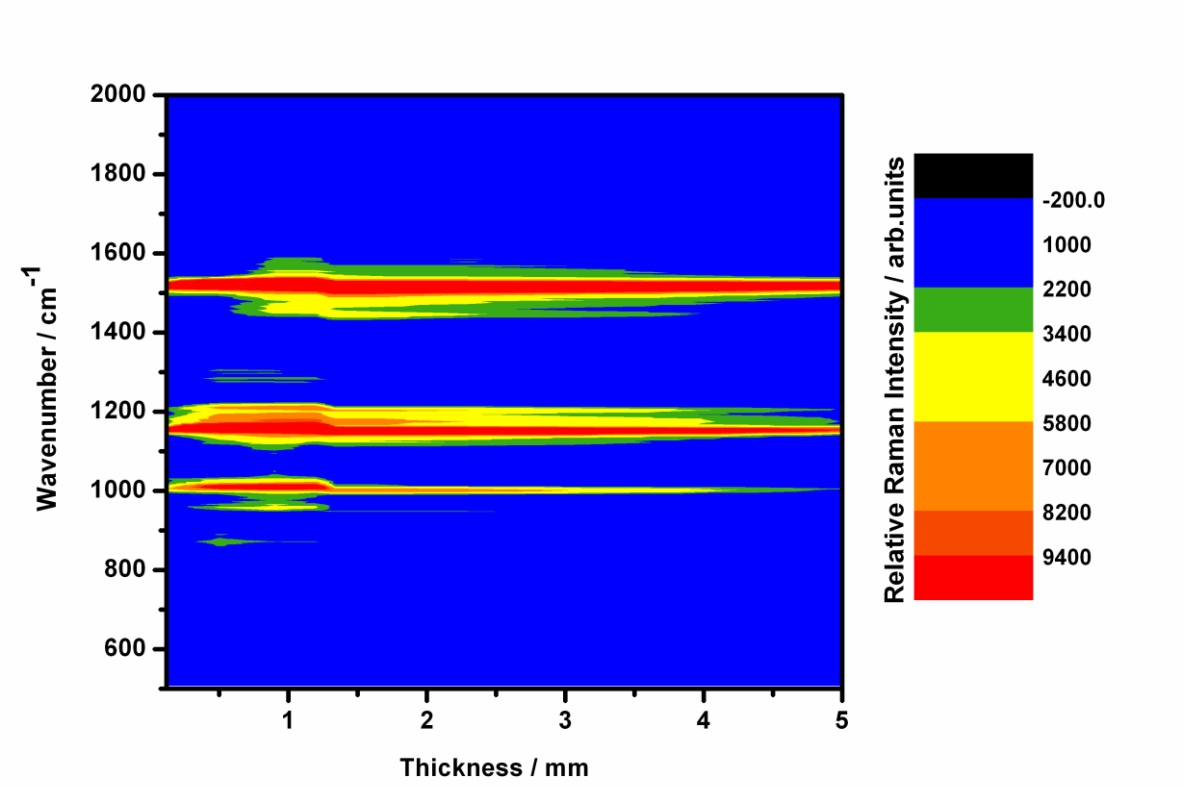

Figure 2.9: Contour map of the TRR data as a function of the carrot slice thickness. Overall, except for the signal intensities no spectral change is noticed as the thickness is varied. Colour relative intensity scale (arb. units) at the right. Notice the signal attenuation as the sample thickness increases. See also Figure 2.10. All TRR spectra were measured under the same experimental conditions: 66 scans of 10 s duration period for each one. See text for comments.

To demonstrate how the Raman signal dependence on the sample thickness does not depend on the specific Stokes lines Figure 2.10 shows the signal from the two more prominent lines e.g. those of the 1520 cm^{-1} and 1155 cm^{-1} as a function of the carrot root thickness.

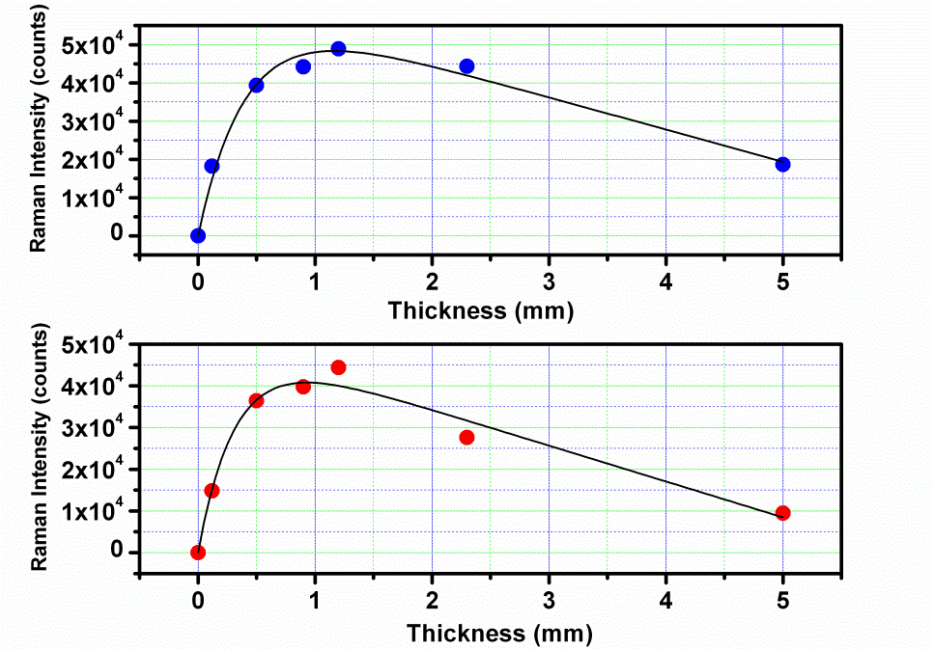

Figure 2.10: TRR signal of a carrot sample as a function of its thickness. For this experiment all measurements were taken directing the laser to the centre of the carrot slice. **Upper panel**: 1520 cm $^{-1}$ signal; solid blue points: experimental data; black solid line: model fit using equation (8) of the text. **Bottom panel**: solid red points 1155 cm^{-1} peak; black solid line model fit using equation 8 of the text. Spectra were taken under the same experimental conditions: 66 scans of 10 s. each one.

As said, except for the signal intensity value, the observed thickness dependence for both Raman lines is similar, as manifested by inspection of the Figure 2.10 and, more specifically, of the *B* and γ values listed in Table II.

Table II. Best fit parameters (B and γ) for the Raman signal dependence of the carrot root thickness.

Raman line (cm^{-1})	**B (mm^{-1})**	**γ**
1520	2.5 ± 0.4	0.06 ± 0.01
1155	3.1 ± 0.6	0.06 ± 0.01

It is interesting to remark that repeating the same sort of calculations made from the best fit of Figure 2.5 data, but now using equation (10) and the Table II parameters one can use the β-carotene concentration of the carrot deduced earlier to get σ_a (λ_{exc}) or vice versa.

If one uses the 17.3mg/100g_{carrot} concentration value deduced further above one gets a σ_a.(λ= 532nm) value of 0.53Å^2 for the laser attenuation cross-section in the light carrot root sample. This value is about three times higher than the one deduced from the β-carotene/ KBr pellet sample mentioned above.

This ratio is consistent with the measured laser transmittance of the two samples under consideration. Indeed, the ratio of the laser signal transmitted by a β-carotene sample (diluted in KBr) and a carrot slice (both samples having the same thickness and similar β-carotene concentration) is 0.31, i.e. a value in good agreement with 3(0.5232 Å^2/0.18 Å^2 = 3), the ratio deduced earlier from the size dependence study. We can therefore conclude that the model, despite its simplicity, is capable not only to fit the sample size dependence of the Raman signal but also to extract optical parameters with a consistent and physical meaning for describing the chemical identity and optical features of the sample under study.

2.5 Conclusions

This paper presented a Raman spectroscopic technique which combines both the transmission and resonance enhanced operational characteristics providing an increased signal to noise ratio and an enhanced analytical sensibility, respectively. Furthermore, the technique uses low CW laser power (~30 mW at the sample), and an unfocussed or

moderately focussed beam spot equal or lower than 1.5mm diameter , experimental features that provide easy and safe operational conditions. Key aspects of the developed technique are the use of direct sampling, a non-invasive character and fast analysis with little time consuming.

Application to β-carotene analysis in standard and carrot samples permitted LOD and LOQ of the *order of hundreds of picograms and a few nanograms per cubic millimetre, re*spectively, for solid samples even though the employed laser wavelength (532 nm) belongs to the red wind of the β-carotene resonant absorption band; features that makes possible the application of the technique in food analysis and animal or human tissues investigations. In addition, the technique allows the mounting of the sample in a XY micrometer sample holder to perform Raman mapping to obtain spatial resolution of the analyte distribution.

The transmission character of the Raman scattering provides important advantages with respect to the back scattering modality as for example the presence of low fluorescence background, and a more accurate analysis because the Raman signal is originated from the entire sample rather than from the surface only.

A simplified model for the Raman signal dependence on the sample thickness was developed in order to account for the deviations from the linear Lambert- Beer regime. Essentially, the model considers the sample to be homogeneous and describes the underlying physics with only three parameters; namely, the Raman cross-section, the laser radiation attenuation cross-section and the Raman signal attenuation cross-section. As one would expect for low optical density samples the latter two contributions can be neglected and the model reduces to the standard Lambert-Beer formalism.

The model was applied to analyze the Raman signal dependence of the β-carotene (i) as a function of its concentration in a constant pellet thickness and (ii) as a function of a carrot slice thickness. It should be expected that due to its simplicity, the presented model cannot be as realistic or as complete as the, normally used, more rigorous, treatments based on Monte Carlo simulation. However, it was shown how the model is capable to fit the experimental data with realistic parameter values that can be used not only to characterise the sample chemical identity but also the optical features of both the compound under analysis and the matrix in which it is embedded.

2.6 References

(1) T. W. Goodwin,"Metabolism, Nutrition, and Function of Carotenoids", Annu. Rev. Nutr. **6,** 273-297 (1986).

(2) I. Cantuti-Castelvetri, B. Shukitt-Hale and J.A. Joseph, "Neurobehavioral aspects of antioxidants and aging", Int. J. Dev. Neurosci. **18**, 367–381 (2000).

(3) L. R. Ferguson, **"**Micronutrients, dietary questionnaires and cancer", Biomed. Pharmacother. **51**, 337-344 (1997).

(4) M. Yamaguchi and S. Uchiyama, "Effect of carotenoid on calcium content and alkaline phosphatase activity in rat femoral tissues in vitro: the unique anabolic effect of beta-cryptoxanthin", Biol. Pharm. Bull. **26**, 1188-1191 (2003).

(5) B. Schoefs, "Chlorophyll and carotenoid analysis in food products. Properties of the pigments and methods of analysis", Trends Food Sci.Technol. **13**, 361–371 (2002).

(6) D. Bicanic, M. Anese, S. Luterotti, D. Dadarlat, J. Gibkes and M. Lubbers, "Accurate and direct determination of total lycopene content in tomato paste", Rev. Sci. Instrum. Part 2 **74** (1), 687-689 (2003).

(7) L. C. Sander, K. E. Sharpless and M. C. Pursch, "C_{30} Stationary phases for the analysis of food by liquid chromatography", J. Chromatogr. **880** (1−2), 189-202 (2000).

(8) H. Schulz, M. Baranska and R. Baranski, "Potential of NIR-FT-Raman spectroscopy in natural carotenoid analysis", Biopolymers **77** (4), 212-221 (2005)

(9) M. Baranska, W. Schutze and H. Schulz, "Determination of Lycopene and β-Carotene Content in Tomato Fruits and Related Products: Comparison of FT-Raman, ATR-IR, and NIR Spectroscopy", Anal. Chem. **78** (24), 8456-8461 (2006).

(10) P. Matousek, "Review of deep non-invasive Raman spectroscopy of living tissue and powders", Chem. Soc. Rev. **36**, 1292-1304 (2007).

(11) M. J. Pelletier, Analytical Applications of Raman Spectroscopy, Oxford. UK: Blackwell Science, 1999.

(12) E. Smith and G. Dent, Modern Raman Spectroscopy: A practical approach, Chichester, U. K: John Wiley & Sons, 2005.

(13) Schrader (Ed.), Infrared and Raman Spectroscopy, New York .USA: VCH, 1995.

(14) H. H. Telle, A. González Ureña and R. J. Donovan, Laser Chemistry: Spectroscopy, Dynamics and Applications. Chichester, U.K.: John Wiley & Sons, 2007.

(15) M.E. Darwin, I. Gersonde, M. Meinke, W. Sterry and J. Lademann, "Non-invasive in vivo determination of the carotenoids beta-carotene and lycopene concentrations in the human skin using the Raman spectroscopic method", J. Phys. D Apply. Phys. **38**, 2696-2700 (2005).

(16) P. Bhosale, I.V. Ermakov, M.R. Ermakova, W. Gellermann and P.S. Bernstein, "Resonance Raman Quantification of Nutritionally Important Carotenoids in Fruits, Vegetables, and Their Juices in Comparison to High-Pressure Liquid Chromatography Analysis", J. Ag. and Food Chemistry **52**, 3281-3285 (2004).

(17) E.V. Efremov, F. Ariese and C. Gooijer, "Achievements in resonance Raman spectroscopy: Review of a technique with a distinct analytical chemistry potential", Anal. Chim. Acta **606** (2), 119-134 (2008).

(18) T.R. Hata, T.A. Scholz, I.V. Ermakov, R.W. McClane, F. Khachick, W. Gellermann and L.K. Pershing, "Non-Invasive Raman Spectroscopy Detection of Carotenoids in Human Skin", J. Invest. Dermatology **115**, 441-448 (2000).

(19) L .C. Hoskins and V. Alexander, "Determination of carotenoid concentrations in marine phytoplankton by resonance Raman spectrometry", Anal. Chem. **49**(6), 695-697 (1977).

(20) K. Buckley and P. Matousek, "Recent advances in the application of transmission Raman spectroscopy to pharmaceutical analysis", J. Pharm. Biomed. Anal. **55**, 645-652 (2011) .

(21) M. Boiret and Y-M. Ginot, "Counterfeit detection of pharmaceutical tablets with transmission Raman spectroscopy", Spect. in Eur. **23** (6), 6-9 (2011).

(22) T. Durduran, R. Choe, W.B. Baker and A.G. Yodh, "Diffuse optics for tissue monitoring and tomography", Rep. Prog. Phys. **73**, 07670 (43pp) (2010).

(23) P. Matousek, M.D. Morris, N. Everall, I.P. Clark, M. Towrie, E. Draper, A. Goodship and A.W. Parker, "Numerical Simulations of Subsurface Probing in Diffusely Scattering Media Using Spatially Offset Raman Spectroscopy", Appl. Spectrosc. **59** (12), 1485-1492 (2005).

(24) B.B. Das, F. Liu and R.R. Alfano, "Time-resolved fluorescence and photon migration studies in biomedical and model random media", Rep. Prog. Phys. **60**, 227-292 (1997).

(25) C.J.H. Brenan and I.W. Hunter, "Volumetric Raman Microscopy through a Turbid Medium", J. Raman Spectrosc. **27** (8), 561-570 (1996).

(26) N. Everall, P. Matuousek, N. Macleod, K.L. Ronayne and I.P. Clark, "Temporal and Spatial Resolution in Transmission Raman Spectroscopy", Appl. Spectrosc. **64** (1), 52-60 (2010).

(27) P. Matousek, N. Everall, D. Littlejohn, A. Nordon and M. Bloomfield, "Dependence of Signal on Depth in Transmission Raman Spectroscopy", Appl. Spectrosc. **65** (7), 724-733 (2011).

(28) H. Du, R. A. Fuh, J. Li, A. Corkan and J. S. Lindsey, "PhotochemCAD: A computer-aided design and research tool in photochemistry", Photochem. and Photobiol. **68**, 141-142 (1998).

(29) N. Tschirner, M. Schenderlein, K. Brose, E. Schlodder and M.A. Mroginski, C. Thomsen and P. Hildebrandt, "Raman spectroscopy of β-carotene and CdSe-based nanocrystals", Phys. Chem. Chem. Phys. **11**, 11471-1178 (2009).

(30) N. Tschirner, M. Schenderlein, K. Brose, E. Schlodder, M.A. Mroginski, P. Hildebrandt and C. Thomsen, "Raman spectroscopy of β-carotene and CdSe-based nanocrystals", Phys. Stat. Sol. (b). **245**, 2225-2228 (2008).

(31) J.M. Orea, C. Montero, J.B. Jimenez and A. González-Ureña, "Analysis of trans-resveratrol by laser desorption coupled with resonant ionization spectrometry. Application to trans-resveratrol content in vine leaves and grape skin", Anal. Chem. **73** (24), 5921-5929 (2001).

(32) IHP Guideline,"Validation of Analytical Procedures: Text and Methodology. Q2B", Fed. Regist. **62**, 27463-27467 (1997).

(33) R. Quilitzch, M. Barauska, H. Schulz and E. Hoberg, "Fast determination of carrot quality by spectroscopy methods in the UV-VIS, NIR and IR range", J. Appl. Botany and Food Quality. **76**, 163-167 (2005).

Chapter 3

Spectroscopy and kinetics of tyrosinase catalyzed *trans*-resveratrol oxidation*

Abstract: The spectroscopy and kinetics of the tyrosinase catalyzed *trans*-resveratrol oxidation were investigated by measuring both UV–VIS absorption spectra over the 200–500nm range and Raman spectra over the 600–1800cm^{-1} region. Room temperature UV–VIS absorption spectra, as a function of time, showed the presence of two isosbestic points located at λ_1 = 270nm and λ_2 = 345.5nm delimiting two different regions: the *reactant region* around 300nm, where the absorption decreased with time, and the *product region* over the low wavelength (λ<260nm) and high wavelength (λ>390nm) wavelength zone in which the absorption increased with time until –in both cases– constant values were achieved. A first-order kinetics was deduced with a rate coefficient of k_1=(0.10±0.001)min^{-1} which turned out to be independent of substrate concentration over the 50μM–5μM range; a feature that was rationalized by invoking the limiting case of the Michaelis–Menten scheme appropriate for substrate concentration much lower than the respective Michaelis constant. The observation of the distinct resonance enhanced Raman lines, specifically those peaking at 830cm^{-1}, 753cm^{-1}, and 642cm^{-1} together with their time evolution permitted us to gain insight into some crucial features and steps of the catalytic reaction. Namely: that the formation of the so-called *trans*-resveratrol and tyrosinase ^{S}P complex with its O–O bridge plays a crucial role in the first steps of this enzymatic reaction; and that the hydroxylation of the ortho C–H bond of the trans-resveratrol OH group occurs *after* O–O bond cleavage in the tyrosinase active site. The present study makes clear that a class of potential inhibitors of tyrosinase can be found in compounds able to bind the two Cu (II) ions of the enzyme bidentate form.

* The contens of this chapter have been published as Alicia G. Gonzálvez, Ángel Gonzalez Ureña, Richard J. Lewis, and Gert van der Zwan in the Journal of Physical Chemistry B **116**, 2553-2560 (2012).

3.1 Introduction

Tyrosinase (EC1.14.18.1) –hereafter denoted by ty– is an important protein in the fields of medicine, agriculture and industry,[1-9] and the cosmetic industry.[2] It is present in fruits, vegetables, and mushrooms and plays an essential role in the fruit browning mechanism as well as in mammalian skin pigmentation, due to its crucial activity in the synthesis of melanin pigments.

The catalytic activity of ty is well documented to be associated with its active site formed of two copper atoms, which is responsible of the hydroxylation of phenols to catechols and the oxidation of catechols to quinones. [1,3,8,9]

The ty enzyme can be found in several isoforms,[3] namely: oxidized (oxyty E_{oxy}), met (metty, E_{met}) and reduced (deoxyty E_{deoxy}); these forms are illustrated in Figure 1.

The oxidized form (E_{oxy}) contains two tetragonal Cu (II) atoms, each coordinated by two strong equatorial and one weaker axial histidine N_{His} ligand while an exogenous oxygen molecule is bound as peroxide bridging the two Cu centres. It was firmly established already in 1938 that E_{deoxy} consists of a bicuprus structure.[4] Finally, the met form (E_{met}), like the oxy form, has two tetragonal copper (II) ions coupled through an endogenous bridge, although hydroxide exogenous ligands other than peroxide are bound to the copper site.[3,8]

Studies of the structure and spectroscopy of copper-dioxygen complexes in general (and that of ty in particular) have attracted much attention in recent years due to their potential relevance to biochemical systems and synthetic catalysis.[3,8] It was not until the experimental determination of their crystallographic structures[1,3,9] that it became amenable to study at the atomic level. Nevertheless, even today a deep knowledge of the reaction mechanisms of ty with many antioxidants remains unclear.

On the other hand, *trans*-resveratrol (3,5,4'-trihydroxystilbene) –hereafter denoted by t-res– is a well-known antioxidant compound naturally produced by vines and other plants as

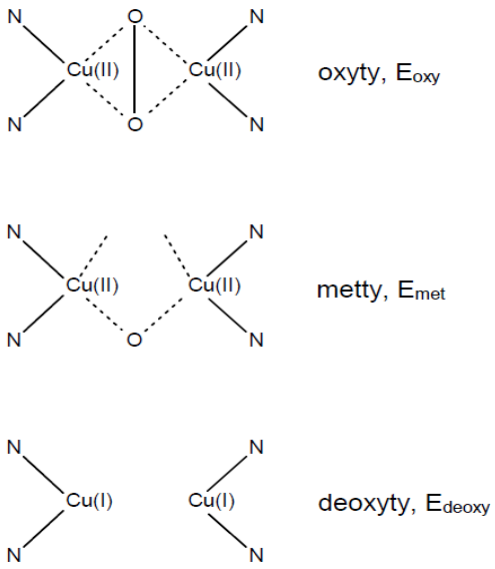

Figure 3.1: Forms of the tyrosinase enzyme ty. Top to bottom: oxidized (Oxy, E_{oxy}), met (Met, E_{met}) and reduced (Deoxy, E_{deoxy}).

self-defence agent acting against pathogenic attack which has recently attracted increased interest as a health-promoting agent due to its anti-platelet, antioxidant, anti-inflammatory, estrogenic, cardioprotective and cancer chemopreventive properties. As such, it has been widely reviewed.[10-16]

The oxidation of phenolic compounds catalyzed by ty was studied extensively by several groups.[1,3,8] Thus, it is well known that ty upon O_2 binding exhibits a characteristic side-on bridging peroxodicopper (II) active centre forming the core of the so–called P intermediate,[1] to which the phenolic substrate binds directly and is, subsequently, hydroxylated via an electrophilic aromatic substitution. While the capability of oxyty to hydroxylate the ortho C–H bond is well documented[1,3,8] to occur

via the mentioned P intermediate, little is known on the intermediates beyond P. *This lack of information constitutes one of the motivations for the present investigation.*

In addition, despite the large number of studies on the catalytic activity of ty with a rich variety of substrates, including phenols, there are very few using t-res. Among them, we can mention the t-res degradation by a novel ty extracted from Carignan grape juice carried out by Gilly et al.,[17] and the ty inhibition by t-res using UV-VIS spectroscopy whose main emphasis was to investigate the t-res potentiality as a bioactive agent for cosmetics.[2] In none of these latter investigations a detailed spectroscopic analysis was presented based on highly sensitive techniques as resonant Raman spectroscopy and, consequently, no detailed assessment on the different reaction steps were experimentally evidenced.

From the kinetic point of view, there is no information on how fast is the t-res oxidation and whether the catalytic reaction occurs via any reaction intermediate. For the latter possibility, it would be interesting to know the structure of such intermediate and the role played by the enzyme active centre and the t-res OH groups.

As the catalytic oxidation reaction requires the presence of O_2, a full understanding of the enzymatic reaction will also require to unravel the particular O_2 binding to the active centre mediating the substrate(t-res) oxidation. In other words, one needs to know if the oxidation reaction proceeds via a peroxide O-O bridge, or any other related structure, bound to the di-copper center of the enzyme. For the latter option, it would be interesting to determine whether the O-O cleavage takes place during or before the hydroxylation of the C-H bond of the t-res.

Even accepting the working hypothesis of the peroxide intermediate formation as the initial configuration of the Ty active centre, this information is insufficient to

fully understand the subsequent mechanistic steps leading to the final oxidation products. Indeed, a proper answer to the above questions would be of a great value not only from a fundamental point of view but, especially, for the design of specific ty inhibitors.

To reach the objectives cited above, the present investigation recorded both UV-visible absorption and Raman spectroscopic data as a function of the time elapsed following ty and t-res mixture under distinct experimental conditions. We anticipate that the observation of the time evolution of several UV-visible absorption and Raman signatures associated to distinct intermediates formed during the catalytic reaction allowed us to unravel the mechanism of this important reaction.

3.2 Experimental Section

3.2.1 Reagents and Standards

Ty extracted from mushrooms and t-res samples were purchased from Sigma Aldrich, both with a stated purity of 99%. Phosphate buffered saline (PBS) of neutral pH was used as the solvent to prepare all samples. The standard samples used in this work were solutions of 1:1 mixtures of 700pM ty and 100μM t-res, as this was determined to be the optimal concentration ratio for both the UV-visible and Raman spectroscopy measurements. In order to investigate the reaction dependence on the t-res concentration, the kinetics was repeated using different substrates, i.e. t-res concentration over the 50μM- 5μM range.

3.2.2 UV-Visible Spectroscopy

The UV-visible spectroscopic measurements were carried out using a Perkin Elmer Lambda 40 spectrophotometer, and the absorption was measured in the range 200-500nm, with one measurement every 30 seconds during a total measurement period of 70 minutes.

3.2.3 Raman Spectroscopy

The Raman spectroscopic measurements were performed using a custom-built Raman microscope in a back-scattering configuration whose main details have been published elsewhere.[18,19] In summary, the Raman microscope consists of a Zeiss D7082 microscope (with a 40× objective, numerical aperture 0.85, and working distance 2mm) coupled to an Andor Shamrock SR-303i single monochromator equipped with a 2400 lines/mm holographic grating and an Andor Newton DU970N CCD camera. A Coherent Innova 300c continuous wave krypton ion (Kr^+) laser with a principal emission wavelength of 413.1nm was employed for excitation, and the Rayleigh scattered light was removed by an Omega Optical Third Millennium long pass edge filter. A 1mm diameter capillary was used to contain the samples, and during all measurements this capillary was kept spinning to minimize local heating.

The standard samples were prepared to a total volume of 100µl and immediately drawn into the capillary. Laser power on the sample was an approximately constant 5mW. One measurement was made every 10 minutes for 70 minutes, with each measurement consisting of the binning of 15 individual 10s exposures. To ensure reproducible results, each measurement was repeated five times.

3.3 Results and Data Analysis

The main body of results presented in this section are divided between the UV-visible absorption and Raman spectroscopic data for individual analysis and discussion. As already mentioned, the data under investigation in each case is presented during a total measurement period of 70 minutes.

3.3.1 UV-Visible Absorption Spectra

Figure 3.2 displays, in contour plot form, the UV-visible absorption in the 200–500nm region as a function of time. Inspection of this figure indicates the presence of two spectral regions showing a different time evolution. While the absorption near 300nm decreases with time, the absorption in the longer wavelength regions at approximately 400nm increases with time. In both cases the absorption approaches steady values for t>50min.

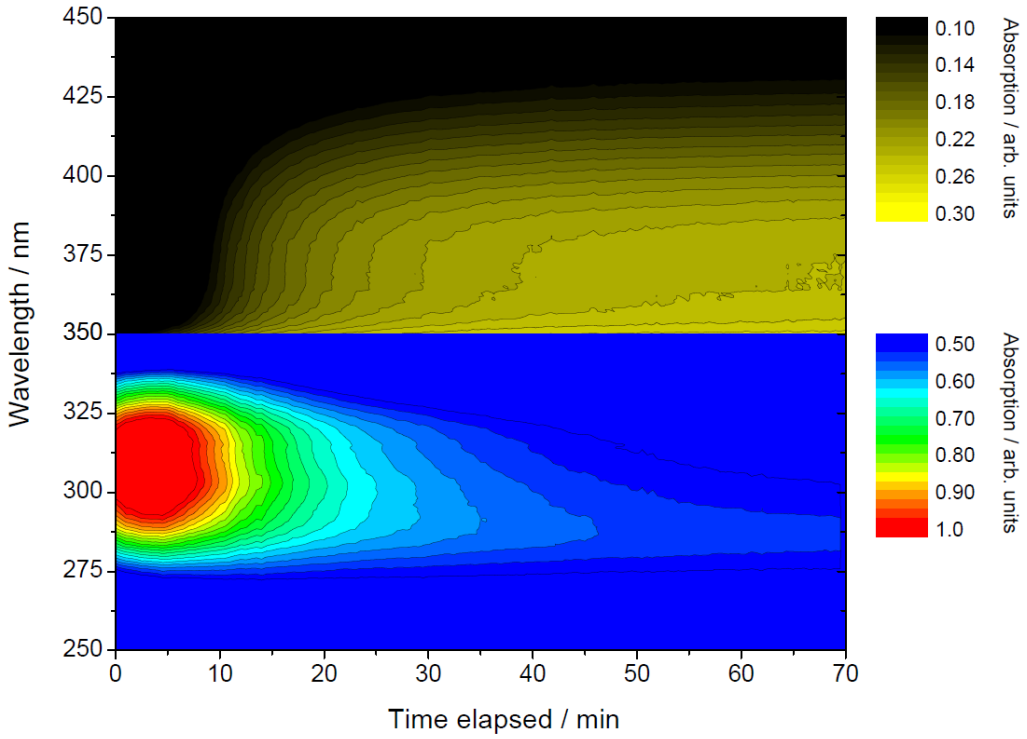

Figure 3.2: Contour Absorption mapping. Contour mapping representation of the Absorption data (arb. Units) measured every thirty seconds of the t-res-ty mixture. Although the absorption signal range for the upper and lower panels are different they use the same arbitrary units.

Repeated scans of the UV-VIS spectral evolution with the reaction time are also shown in the two dimensional plot depicted in Figure 3.3 where, in addition to the mentioned temporal evolution, two isosbestic points (also shown in the respective insets for a better display) and located at $\lambda_1 = 270$nm and $\lambda_2 = 345.5$ are clearly noticed.

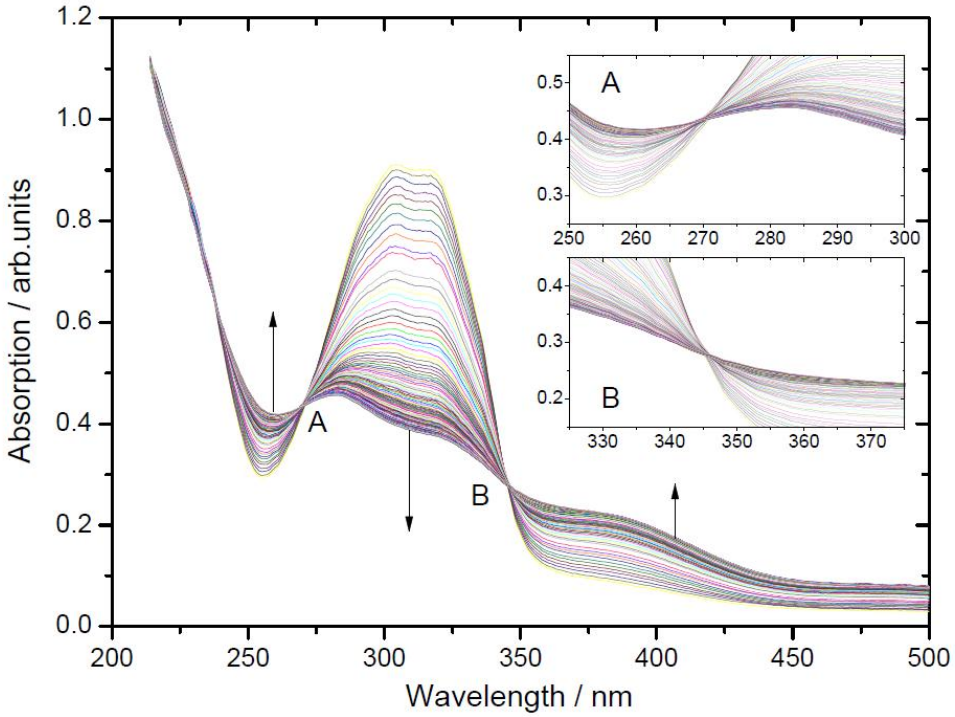

Figure 3.3: Repeated scans of UV-VIS absorption spectra over the 200-500nm range during the measurement period of 70 minutes. Different colours represent the individual measurements taken every 30 seconds, and the arrows indicate the temporal evolution of the indicated regions. Notice the presence of two isosbestic points around 270nm and 345.5nm. Two zoomed insets provide a clearer view of these two points.

Two cross-sections of the absorption contour map at 304 and 400nm are shown in Figure 3.4 to more clearly distinguish the kinetic behaviour. The cut at 304nm represents the time evolution of the t-res consumption, and a simple exponential decay model of the concentration can be fitted to these data, i.e.

$$[\text{t} - \text{res}] = [\text{t} - \text{res}]_0 \exp(-k_1 t)$$

The cut at 400nm represents product (quinone, P) appearance, which can be represented by the particular exponential growth model

$$[\text{P}] = [\text{P}]_0 (1 - \exp(-k_1 t))$$

Note that models use k_1 as the rate coefficient; this is to be expected from the reaction kinetics and the best-fit value was found to be $k_1 = (0.10 \pm 0.01)\text{min}^{-1}$.

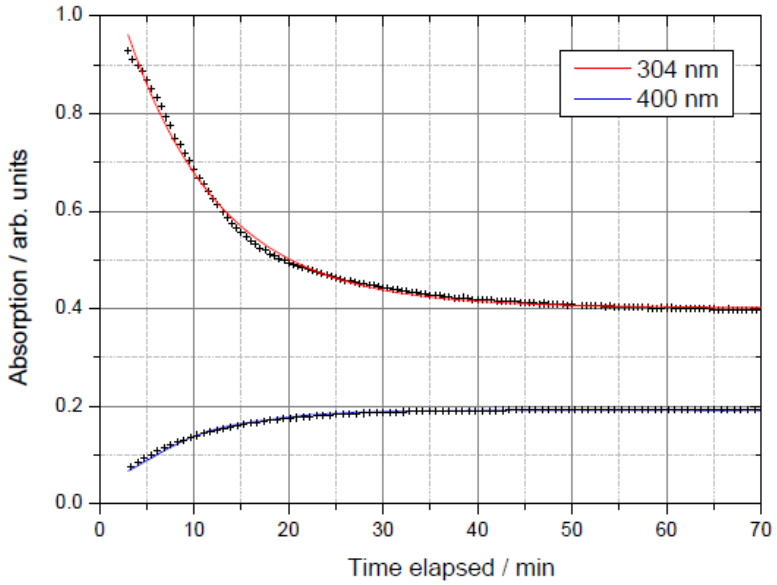

Figure 3.4: Temporal evolution of absorption at 304nm (red, top) and 400nm (blue, bottom). UV visible spectra done every 30 seconds during the measurement period of 70 min. The absorption data is represented in both cases by crosses, and the fitted exponential models as solid coloured lines.

The kinetic experiment was repeated changing the t-res concentration over the 50μM–5μM range. In all cases and even at concentrations as low as 5μM, the temporal evolution of the reactants and product absorption could be fitted by the same exponential law used earlier and, more interesting, within the experimental error of our experiments ε=10%, the same value of k_1 was found. In other words, under the experimental conditions employed in the present study the kinetic of the t-res oxidation can be described by a first order kinetic (see further below for a discussion on this point) with respect to substrate concentration.

3.3.2 Raman Spectra

A contour map of the total Raman signal is displayed in Figure 3.5 as a function of the Stokes Raman shift in the 600 -1800cm^{-1} region and the elapsed time since the reaction mixture was prepared.

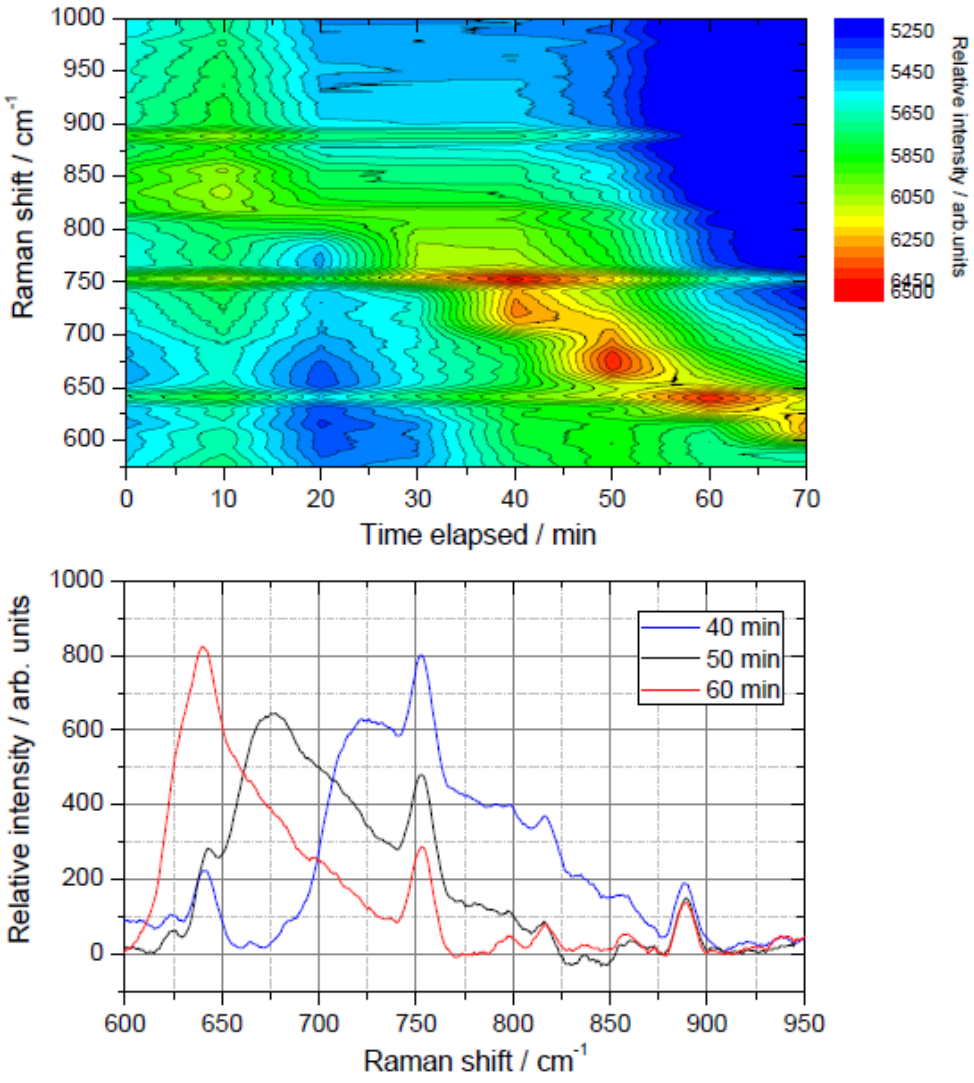

Figure 3.5: Fluorescence and Raman data. **Top:** contour map of the raw data measured every ten minutes of the t-res-ty mixture. **Bottom:** total fluorescence and Raman signal at different times elapsed since the reactants were mixed, as indicated.

Although the two-dimensional representation of the time evolution of the Raman spectrum is instructive, one is hampered in its interpretation due to the fact that the Raman lines are superimposed upon an uneven background of (primarily) fluorescence. In spite of the fact that it is impossible to completely separate the Raman signals from the background, a high degree of separation is nevertheless possible by application of a suitable post-acquisition software filter.

In this study, a modified version of the well-known Rolling Circle Filter (RCF) has been applied. The basic RCF approach was reported in 2006 by Brandt et al.,[20] and in that work the RCF is utilized as a high-pass filter, whereby a rigid circle with a radius larger than the Raman line widths (but less than the fluorescence variation) is "rolled" underneath a spectral trace. The locus of the top of the circle is (after adding the average of the background noise level) used as a model of the background. A simple subtraction of this model then yields a Raman spectrum with a significantly reduced background.

This approach, while simple in concept and application, is insufficient for our purposes since we wish to retain the fluorescence model as well as the Raman spectrum. Further, since the Raman features we are interested in are not much narrower than features in the fluorescence, it is not possible to simply select a circle radius that provides a reliable degree of separation of the fluorescence (the circle "locus") and the Raman features (the "residue").

Our modification is to couple a Savitzky-Golay (SG) smoothing filter to the model of the locus. By coupled we mean that the number of points included in the SG filter window is equal to the radius of the circle rolled underneath the spectral trace. In this way, an appropriate level of smoothing is applied to the locus, which greatly reduces the leakage of Raman features into the model of the fluorescence, and conversely reduces the degree to which the shape of the Raman features themselves are distorted by the circle having rolled into the same features. A third-order polynomial was used for the SG filter model throughout. The contour map of the Raman signal obtained by applying the method briefly described above is shown in Figure 3.6. Comparison of this dataset with the original raw data contour map makes evident the higher degree of separation of the filtered Raman signals from the background which

even permits the identification of a clear series of peaks at different Raman shifts and reaction times.

To reinforce the association of these Raman signals to the induced reaction, a

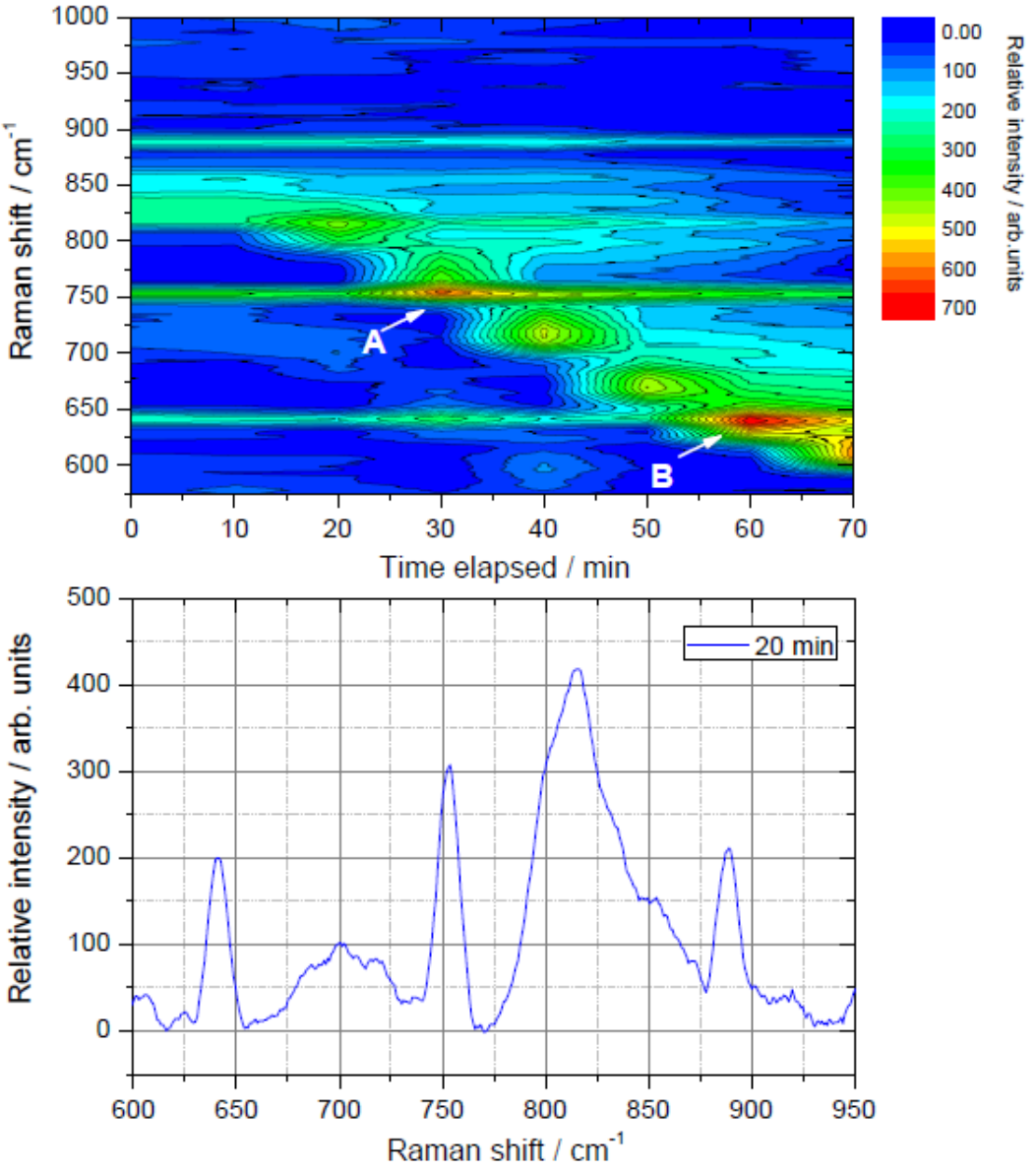

Figure 3.6: Top: contour map of the Stokes Raman spectrum with respect to time. The Raman data was isolated from the background fluorescence by applying the RCF methodology described in the text to the data shown in Figure 3.5. Colour relative intensity scale (arb. units) at the right. Notice the distinct peaks manifested at different wavenumbers and times. The location of the two main reaction intermediates are marked in capital white letters as A and B., See text for a discussion on this matter. **Bottom**: vertical cut of the contour map at 20 minutes. Notice the presence of the four peaks at 889cm^{-1}, 830cm^{-1}, 753cm^{-1} and 642cm^{-1}.

typical Raman spectrum at t = 20min after the ty and t-res mixture was prepared (i.e. a vertical cross-section of Figure 3.6 is shown in the bottom of the figure where several peaks are noticeable, namely at 889cm^{-1}, 830cm^{-1}, 753cm^{-1} and 642cm^{-1}.

Interestingly, these above mentioned Raman lines are absent from spectra of pure t-res, pure ty, ty bubbled with pure oxygen, and a ty and t-res mixture bubbled with pure nitrogen (spectra not shown) which clearly indicates that the Raman signals originate solely from the ty and t-res mixture in presence of oxygen.

As pointed out earlier, a direct analysis of the Raman data depicted in the contour map of Figure 3.6 indicates the presence of several intermediates such as one peaking at 754cm^{-1} and 30min and another peaking at 642cm^{-1} and 50min. The kinetic evolution of these Raman signatures, i.e. the corresponding horizontal cuts, is illustrated in Figure 3.7 and their role in the enzymatic reaction mechanism will be discussed in the next section.

3.4 Discussion

The oxidative degradation of t-res catalyzed by lipoxygenase-1 (LOX-1) studied by Pinto et al.[21] showed the presence of two distinct temporal behaviours, a decrease of the absorption near the 300nm region and a continuous increase in absorption at 250nm and in the region of 375–395nm, as well as the occurrence of two isosbestic points at 275nm and 369nm. The latter feature is often interpreted as only two species are involved in the oxidative processes. Nevertheless, one could not rule out the presence of additional products with negligible absorption in the UV-VIS range.

It is then remarkable the overall similarity of the absorption spectra as well as of their time evolution between the present t-res plus ty reaction and the mentioned t-res oxidative degradation catalyzed by LOX-1 which seems to suggest the formation of

similar oxidation products in the course of the catalytic reactions. It is well accepted that o-quinones are the primary products of the enzymatic oxidation of phenolic substrates by ty;[22,23] compounds which, in general, are unstable and can be separated according to their UV-VIS spectra[22] into two main categories: coloured compounds(λ_{max} = 294 - 324nm) and colourless compounds (λ_{max} = 264,280 or 290nm).

The observation (see Figure 3.4) that the absorption at 304nm decreases with time, that beyond 50min remains constant and does not reach a zero value, may be an indication of the formation of these coloured reaction products. Further below, we will see how the presence of these coloured products does not affect the rate coefficient determination of the t-res oxidation.

The fact that both the t-res decay and the product formation data could be fitted by an exponential decay and grow law with the same rate coefficient suggests the presence of a first-order kinetic. Unfortunately, the body of data available is not sufficient to clearly assess the detailed kinetic mechanism of the reaction under study. As described in the supplementary information, under the employed experimental conditions several reaction schemes lead to a first-order rate equation for both product formation and reactant consumption. Among them we like to mention (i.) the consecutive reaction figure $A \rightarrow B \rightarrow C$ providing that the first step is the rate limiting step, i.e. if $k_1 << k_2$ and (ii.) the Michaelis-Menten mechanism given by $E + S \rightarrow ES \rightarrow P + S$, where S stands for substrate (t-res in the present case), E for ty and P for product.

In the supplementary information file (see Eq.14 in the supplement), it is shown that when the substrate concentration is much lower than the Michaelis constant, k_m i.e. $[S] << k_m$, the kinetics are first order in substrate concentration. In the study

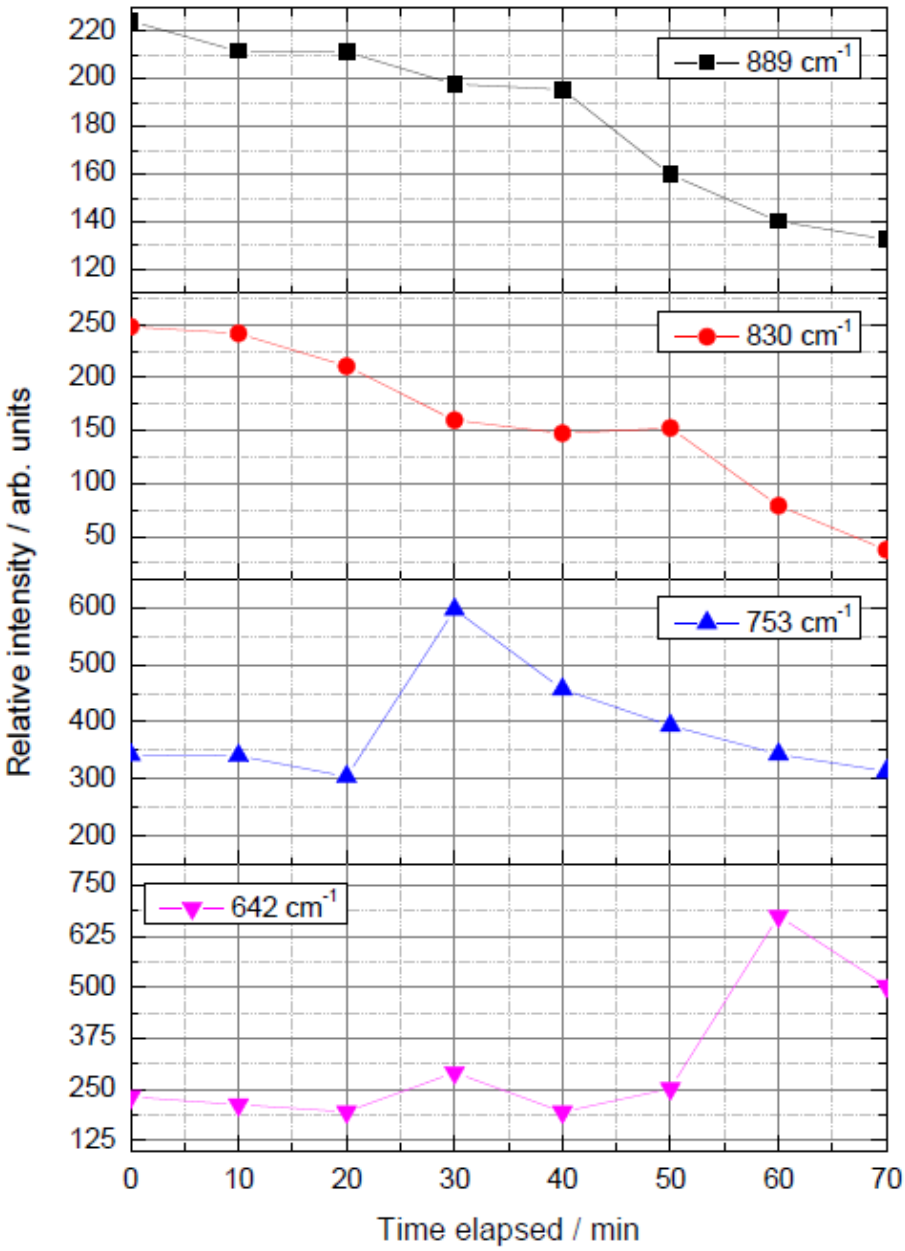

Figure 3.7: Temporal evolution of Raman signal. Horizontal cuts of the Raman data showed in Figure 3.6 at the wave numbers of 889cm^{-1} and 830cm^{-1}, 753cm^{-1} and 642cm^{-1}.

carried out by Gilly et al.[17] it was found that t-res was significantly degraded by a novel ty prepared from Carignan grapes. These authors also reported for the respective reaction a k_m value of 350μM. Although our conditions, especially those concerning the ty origin, are not the same that those used in Ref. 17, we should note that the requirements for first order kinetics are easily obeyed in view of the employed t-res

50μM–5μM concentration range values; clearly lower than that of Michaelis constant cited above.

We would like then to emphasize that the main objective of the present investigation is to gain insight into the distinct intermediates on the titular reaction from both the spectroscopic assignments and the time evolution of the different Raman signatures experimentally observed. This matter is now discussed below.

The four experimental Raman lines observed in the present investigation, at 889cm^{-1}, 830cm^{-1}, 753cm^{-1} and 642cm^{-1}, are compared in Table III with well-known Raman features of 2:1 Cu/O_2 complexes reported in the literature.[1,3]

Table III: Major observed Raman signatures and their spectroscopic assignments; those marked with an asterisk (*) are from the present work, and those marked with a dagger (†) are from specified references. See Figure 3.9 for the structure of radical φ.

Raman shift*/cm^{-1}	Spectroscopic assignments*	Raman shift†/cm^{-1}	Spectroscopic assignments†
889	(Cu-OOH-Cu) unit in hidroxo-peroxo-copper complex formed with t-res and ty (O-O stretching)	889	(Cu-OOH-Cu) unit; other hidroxo-peroxo-copper formed with Ty and different ligands[24]
830	^{T}P complex formed with t-res and ty (O-O stretching)	830	^{T}P ty complexes with different ligands (O-O stretching)[1,8]
753	μ–η^2 :η^2 – peroxodicopper(II) ^{S}P t-res–ty complex (O–O stretching)	730-760	Distinct ^{S}P com-plexes[1]
642	[Cu–O(φ)–Cu] moiety ν_S and ν_{AS} vibra-tional modes	643	[Cu–O(Ph)–Cu] moiety ν_S and ν_{AS} vibrational modes[8,24]

With respect to the moderately intense peak at 889cm^{-1}, it should be noted that this shift has been clearly assigned to the O–O stretching of the hydroperoxo-copper complex by Solomon and co-workers.[3,6] These authors demonstrated how this mode is strongly enhanced by the 25200cm^{-1} absorption band of the [Cu(UN–O–)OOH)](PF$_6$)$_2$ complex.[3,6] Based on these findings, we have assigned the observed 889cm^{-1} line to the Cu(OOH)Cu unit of the ty–t-res complex which likely could be resonantly enhanced by the laser excitation at 24207cm^{-1} (i.e. the Kr^+ laser wavelength of 413.1nm).

On the other hand, it should be noted that the Raman signatures centred at 830cm^{-1}, 740cm^{-1} and 600cm^{-1} are well documented to be associated to the presence of the so-called ^{T}P, ^{S}P, and O 2:1 Cu/O_2 complex intermediates, respectively and whose main structures have been already described in the literature. [1,3,8]

There exist a considerable number of spectroscopic studies of the μ–η^2: η^2–peroxodicopper (II) complexes (the so-called ^{S}P complexes), generally with tetradentate ligands. The most common spectroscopic features of such complexes are directly related to the side-on peroxide binding mode. In general the absorption spectra of these ^{S}P species exhibit[25] a high-energy charge-transfer (CT) band (340–380nm, ε = 18000 − 25000M^{-1} cm^{-1}) and a weaker lower energy CT band (510-560 nm, ε = 1000M^{-1} cm^{-1}). Of relevance to the present investigation is the study carried out by Solomon and co-workers[8] on the reaction of a μ–η^2: η^2–peroxodicopper (II) species with a 2,4-di-tert-butylphenolate. The authors observed several intermediates exhibiting distinct absorption bands, specifically a ~23900 cm^{-1} band (ε = 18000 M^{-1} cm^{-1}), i.e., centred at 418 nm , a wavelength close to the laser principal emission wavelength of 413.1nm employed in the present work. This latter feature together with the use of tyr and t-res (a polyphenol) as reactants provided both the spectroscopic and functional similarities

required for the (resonant) Raman investigation on the enzymatic t-res oxidation performed in the present work.

In general, the resonant Raman (rR) spectra[1,2] of the ^{S}P intermediates show a low-energy O–O stretching vibration at 730–760cm^{-1}. This lower value compared to that of the normal peroxide ion (ca. 830cm^{-1}) is thought to result from back-bonding from Cu (II) orbitals into the orbital σ^{*} of the peroxide ion;[25] an electron transfer that not only weakens the O–O bond but also influences its cleavage.

In this view, the experimentally observed lines at 830cm^{-1}, 753cm^{-1} could be assigned to the enhanced resonant Raman lines of the so-called ^{T}P, ^{S}P 2:1 Cu/O_2 complex intermediates, respectively, formed in the ty–t-res reaction.

Concerning the observed Raman line at 642cm^{-1}, it should be noted that experimental measurements and DFT calculations carried out in the work of Op't Holt[8] showed that vibrations at 648cm^{-1}, 589cm^{-1} and 560cm^{-} correspond to modes of the Cu_2O_2 core. Moreover, a detailed study carried out by Root et al.[24] assigned the 643cm^{-1} peak of Cu_2 (OPh, Ph=Phenyl) complex either to the ν_S (Cu–O(Ph)–Cu) or to the ν_{AS} (Cu–O(Ph)–Cu) vibrational mode. Likewise, based on this analysis we have assigned our experimentally observed 642cm^{-1} peak either to the ν_S (Cu–O(φ)–Cu) or the ν_{AS} (Cu-O(φ)-Cu) vibrational mode. See the representation of the reaction mechanism in Figure 3.8 and Table III for the spectroscopic assignments. See also Figure 3.9 for a definition of the φ radical

In addition to the spectroscopic assignment of the observed Raman signatures, the time evolution of these signatures is of major relevance for the present investigation. As illustrated in Figure 3.7 the following main kinetic features are noticeable: (i.) rather continuous decline with time of both the 889cm^{-1} and 830cm^{-1} signal intensities, and

(ii.) an initial rise and subsequent decline of the 753 and 642cm^{-1} line intensities, peaking at 30min and 60min, respectively.

As for the main reaction pathway of the t-res oxidation catalyzed by the ty, it is important to note that based on the crystal structure of ty as determined by Matoba et al.[9] the catalytic conversion of monophenol to the corresponding quinone through the ortho-diphenol formation is thought to occur via the intermediate formation of a μ–η^2 : η^2–peroxodicopper (II) species.

Following this mechanistic scheme together with the detailed spectroscopic information and time evolution of the observed Raman signatures obtained in the present investigation, the main steps proposed for the ty catalytic oxidation of the t-res are outlined in Figure 3.8. In this scheme, the first step is the action of the peroxide ion, which forms a bridge with two Cu (II) ions featuring the so-called oxy form of ty. This form acts as a base and takes a proton from the phenolic hydroxyl while the phenolate radical binds to Cu^B just at the sixth coordinate site leading to the intermediate named A in Figure 3.6 and 3.8 which represents the ty-t-res ^{S}P complex whose main Raman line peaks at 753 cm^{-1} and 30min.

The next step is the cleavage of the O–O bond. As it is outlined in the reaction mechanism, while an ortho-carbon of the t-res substrate approaches the peroxide ion, one of the two peroxide oxygens is therefore added to the ortho- carbon of the monophenol. As a result the newly generated O atom of the diphenol moiety binds to Cu^A. This intramolecular motion leads to the H54N release from its position that is likely facilitated by the H54N residue flexibility, a dynamical feature evidenced by the crystallographic study conducted by Matoba et al.[9]

Electron rearrangements in the resulting intermediate can finally form both the

quinone and the de-oxy form of ty. It is likely that the quinone formation involves a sequential step in which a C=O bond is formed first. Subsequently, the second C=O bond is produced and the product o-quinone released after ligand displacement and H54N recombination with the Cu^{A}(II) ion, Certainly due to the shorter Cu–Cu distance[1,9] and final H54N recombination, one may expect that the intermediate B- see the reaction scheme- would be stable enough to be detected by the resonant Raman spectroscopic technique . Support to the latter step is provided by the observation of the Raman line at 642cm^{-1} together with its time evolution. Its intensity shows a delayed increase (see Figure 3.7) after the decline of the 753cm^{-1}Raman intensity. This temporal evolution is consistent with the A to B intermediate transformation , as marked in Figure 3.6 and 3.8, whose ν_S (Cu–O(φ)–Cu) or ν_{AS} (Cu-O(φ)-Cu) vibrational modes have been assigned to the observed 642cm^{-1} Stokes line.

The observed Raman signatures observed in the present investigation provides evidence that in the catalytic reaction the hydroxylation of the ortho C–H bond with respect to the t-res OH group *occurs after O–O bond cleavage.* In addition, it provides information about the electronic re-arrangement required for the production of o-quinone which seems to take place in a sequential mode whose final step involves the Cu-O(φ)-Cu core. These mechanistic features of the enzymatic catalysis, we would like to remark, have only been possible to investigate by recording the time evolution of the resonant Raman spectra.

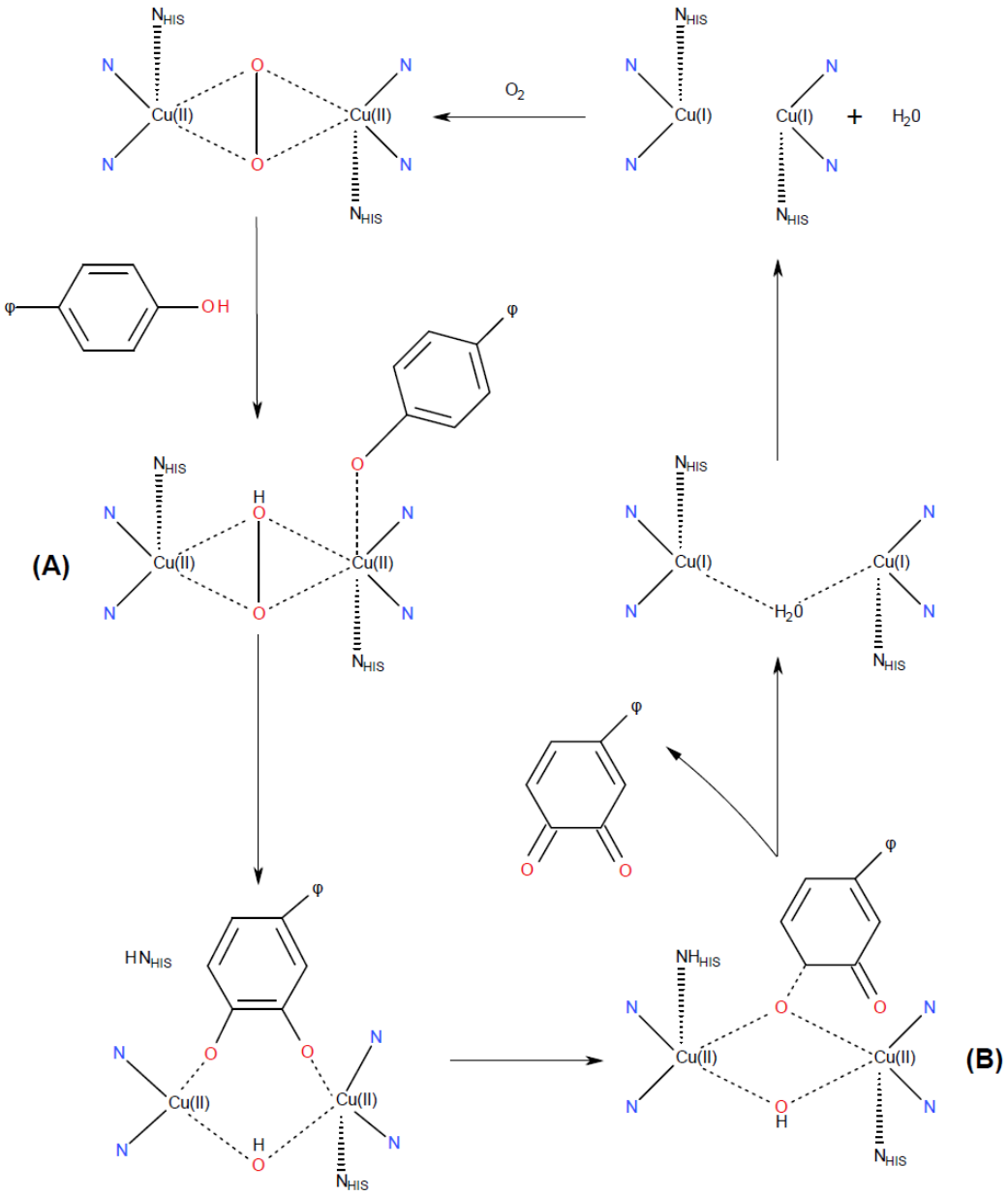

Figure 3.8: Suggested reaction mechanism for the t-res oxidation induced by the ty. The main reaction intermediates are labelled as A and B as also indicated in Figure 3.6. The three histidine groups for each copper atom are denoted by N. To emphasize some reaction steps the histidine groups above and below the equatorial plane are labelled N_{HIS}. See Figure 3.9 for the definition of the radical φ.

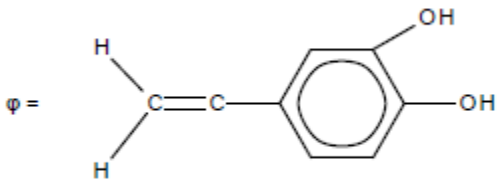

Figure 3.9: Structural diagram of the radical φ used an abbreviation in Figure 3.8.

3.5 Summary and Conclusions

This work centred its attention in the spectroscopy and kinetics of the ty catalyzed t-res oxidation by measuring both UV-VIS absorption, over the 200–500nm range, and Raman spectra over the 600–1800cm^{-1} region in both cases during a period of 70 minutes since the reaction mixture is prepared.

Overall, the full set of UV-VIS absorption spectra as a function of time showed the presence of two isosbestic points located at λ_1 = 270nm and λ_2 = 345.5nm delimiting two different regions, namely (i.) the reactant region around 300nm (i.e. the region between the isosbestic points), where the absorption decreased with time, and (ii.) the product region over the low wavelength (λ<260nm) and high wavelength (λ>390nm) zones in which the absorption increased with time until, in all cases, it approached steady values beyond 50min.

Although no direct chemical analysis was performed to identify the nature of the reaction products it is well known that the phenolic oxidation leads most predominantly to the o-quinone formation. Indeed the absorption spectra observed in the present investigation confirm the presence of the o-quinone absorption bands over 400–430nm

range which is also consistent with the observed isosbestic point at 375nm. As for the kinetics, both the t-res decay and the product formation data could be fitted by an exponential decay and grow law, respectively, with the same rate coefficient suggesting the presence of a first-order kinetics.

The experimentally deduced rate coefficient value was $k_1 = (0.10 \pm 0.01)\text{min}^{-1}$ and, under the employed experimental conditions, turned out to be independent of the substrate concentration over the 50μM–5μM range; a feature that was rationalized by invoking the limiting case of the Michaelis-Menten scheme appropriate when the substrate concentration is much lower than the respective Michaelis constant.

One of the most relevant aspects of the present investigation is the insight gained into the reaction mechanism of the titular reaction, i.e. the main steps and the identification of spectroscopic features associated to the presence of several intermediates that has been only possible by using the powerful resonant Raman technique.

The formation of different reaction intermediates whose absorption bands, most likely associated to charge transfer processes, were resonant or near resonant to the employed laser excitation energy made possible the observation of their enhanced Raman signatures, that otherwise would have been absent . As a result, it led to the vibration mode assignment of the t-res–ty complex intermediate reactive centres formed in the course of the catalytic reaction; a crucial piece of information that was not possible to extract solely from the absorption spectra confirming the great sensitivity of the resonant Raman technique used in the present work.

Indeed, the observation of the distinct Raman lines, specifically those peaking at 830cm^{-1}, 753cm^{-1} and 642cm^{-1} together with their time evolution allowed us to assess

the main features and steps of the catalytic reaction. The time evolution of the Raman signatures observed in the present investigation addresses the dynamical interaction of the enzyme tyrosinase with the anti-oxidant t-res. Thanks to this information it was possible to outline a detailed mechanism for the titular reaction in which the following main steps were established: (i.) the formation of the t-res–ty ^{S}P complex with its O–O bridge plays a crucial role in the first steps of this enzymatic reaction. A reaction intermediate has been observed whose main resonant Raman signature has been observed at 753 cm^{-1} and assigned to the weakened O-O stretching of a μ–η^2 :η^2–peroxodicopper (II) species featuring the ty-t-res ^{S}P complex (ii) the hydroxylation of the ortho C–H bond of the t-res employs one of the O atoms from the peroxide bridge and occurs *after* O–O bond cleavage in the ty active centre (iii) The final step of the enzymatic reaction which seems to involve an intermediate complex whose resonantly enhanced ν_S (Cu–O(φ)–Cu) or ν_{AS} (Cu-O(φ)-Cu) vibrational modes were assigned to the observed 642cm^{-1} Raman Stokes line.

Finally one should point out the crucial role the bidentate form of the oxyty plays in the catalytic reaction – in particular in the quinone formation. Obviously, potential inhibitors of tyrosinase must be able to bind to the two Cu (II) ions of the bidentate form.

3.6 Suplementary Information

In the first part of this supplement we consider the consecutive elementary reaction scheme when the first step is the rate limiting step.

For the consecutive unimolecular reaction

$$R \overset{k_1}{\rightarrow} I \overset{k_2}{\rightarrow} P \tag{1}$$

where *R*, *I* and *P* denote the reactant, intermediate and product, respectively. One can write the respective rate equations

$$\frac{d[R]}{dt} = -k_1[R] \tag{2a}$$

$$\frac{d[I]}{dt} = k_1[R] - k_2[I] \tag{2b}$$

$$\frac{d[P]}{dt} = k_2[I] \tag{2c}$$

When the initial intermediate concentration is zero ($[I_0] = 0$), the integrated equations give for $[R]$ and $[P]$ the following expressions

$$[R] = [R_0]\exp(-k_1 t) \tag{3a}$$

$$[P] = \left\{1 + \frac{k_1 \exp(-k_2 t) - k_2 \exp(-k_1 t)}{k_2 - k_1}\right\}[R_0] \tag{3b}$$

in which $[R_0]$ is the initial Reactant concentration. If $k_2 >> k_1$

$$[P] = \{1 - \exp(-k_1 t)\}[R_0] \tag{4}$$

Thus, the comparison between equation Eq. (3a) and Eq. (4) clearly indicates how the temporal evolution of reactant and product concentrations can be fitted by an exponential law with the same rate coefficient k_1.

Next we demonstrate how under the experimental conditions of our investigation, the Michaelis-Menten mechanism of enzyme catalysis leads to a first order kinetic for both reactant consumption and product formation.

According to this mechanism an enzyme-substrate complex, ES, is formed in the first step and subsequently the substrate can be released unchanged or evolve to form products. Schematically

$$E + S \underset{k_2}{\overset{k_1}{\rightleftarrows}} ES \xrightarrow{k_3} P + E \tag{5}$$

where *E*, *S* and *P* stand for enzyme, substrate and product, respectively. Thus the rate equations for *S* and *P* are given by

$$-\frac{d[S]}{dt} = k_1[E][S] - k_2[ES] \tag{6a}$$

$$\frac{d[P]}{dt} = k_3[ES] \tag{6b}$$

The concentration of *ES* can be obtained from the steady-state approximation, e.g.

$$\frac{d[ES]}{dt} = k_1[E][S] - k_2[ES] - k_3[ES] = 0 \tag{7}$$

From whence it follows

$$[ES] = \frac{k_1}{k_2+k_3}[E][S] = \frac{[E][S]}{K_M} \tag{8}$$

where K_M is the so-called Michaelis constant

$$K_M = \frac{k_2+k_3}{k_1} \tag{9}$$

The initial enzyme concentration $[E_0]$ is equal to

$$[E_0] = [E] + [ES] \tag{10}$$

Replacing Eq. (10) into Eq. (8), and after some algebra, one obtains

$$[E_0] = \frac{[E_0][S]}{K_M+[S]} \tag{11}$$

The rate of the catalytic reaction $\nu = \frac{d[P]}{dt} = -\frac{d[S]}{dt}$ is finally obtained by using Eq. (11) inEq. (6a) and Eq. (6b). The result is given by

$$\nu = \frac{d[P]}{dt} = -\frac{d[S]}{dt} = k_3 \frac{[E_0][S]}{K_M+[S]} \tag{12}$$

Only when $[S] << K_M$, the kinetics are first order in substrate concentration since it can be neglected in the denominator in comparison with KM. In other words, the kinetics are then given by

$$\nu = k_3 \frac{[E_0][S]}{K_M} = k'[S] \tag{13}$$

Where

$$k' = k_3 \frac{[E_0]}{K_M} \quad (14)$$

This limiting first order kinetics is not far from what one would expect when $k_3 >> k_1$. Indeed, the rearrangements and steric requirements to be involved in forming the suggested reaction intermediates A and for B (see Figure 6 of the main article and the Discussion section) would be likely absent in the final step, more concerned with the breaking of the t-res-ty complex to form the quinone product.

3.7 References

(1) L. M. Mirica, X. Ottenwaelder, T. D. P. Stack, "Structure and Spectroscopy of Copper−Dioxygen Complexes", Chemical Reviews **104**, 1013–1046 (2004), PMID: 14871148.

(2) B. Bernard, and J. Y. Berthon, "Resveratrol: an original mechanism on tyrosinase inhibition", International Journal of Cosmetic Science **22**, 219–226 (2000).

(3) E. I. Solomon, U. M Sundaram, T. E Machonkin, "Multicopper oxidases and oxygenases", Chemical Reviews **96**, 2563–2606 (1996).

(4) F. Kubowitz, "Spaltung und Resynthese der Polyphenoloxidase und des Hämocyanins", Biochem. Z. **299**, 32–57(1938).

(5) Á. Sánchez-Ferrer, J. N. Rodríguez-López, F. García-Cánovas, F. García-Carmona, "Tyrosinase: a comprehensive review of its mechanism", Biochimica et Biophysica Acta (BBA) **1247**, 1 – 11(1995).

(6) E. Solomon, M. Lowery, "Electronic Sructure Contributions to Function in Bioinorganic Chemistry", Science **259**, 1575–1581(1993).

(7) D. E. Wilcox, A.G. Porras, Y. T. Hwang, K. Lerch, M. E. Winkler, E. I. Solomon, "Substrate analog binding to the coupled binuclear copper active site in tyrosinase", J. Am. Chem. Soc. **107**, 4015–4027 (1985).

(8) B. T. Op't Holt, M. A. Vance, L. M. Mirica, D. E. Heppner, T. D. P. Stack, E.I. Solomon, "Reaction Coordinate of a Functional Model of Tyrosinase: Spectroscopic and Computational Characterization", J. Am. Chem. Soc. **131**, 6421–6438 (2009), PMID: 19368383.

(9) Y. Matoba, T. Kumagai, A. Yamamoto, H. Yoshitsu, M. Sugiyama, "Crystallographic Evidence That the Dinuclear Copper Center of Tyrosinase Is Flexible during Catalysis", J. Biol. Chem. **281**, 8981–8990 (2006).

(10) A. Cassidy, B. Hanley, R.M. Lamuela-Raventos, "Isoflavones, lignans and stilbenes – origins, metabolism and potential importance to human health", Journal of the Science of Food and Agriculture **80**, 1044–1062 (2000).

(11) L. Frémont, "Biological effects of resveratrol", Life Sciences **66**, 663 – 673 (2000).

(12) J. B. German, R. L. Walzem, "The Health Benefits Of Wine", Annurev. Nutr. **20**, 561–593 (2000).

(13) A. González-Ureña, J.M. Orea, C. Montero, J. B. Jiménez, J. L. González, A. Sánchez, M. Dorado, "Use of Trans-Resveratrol to Control Microbial Flora, Prolong Shelf-Life and Preserve Nutritional Quality of Fruit", Journal of Agricultural and Food Chemistry **51**, 82–89 (2003), PMID: 12502389.

(14) S. Pervaiz, "Chemotherapeutic potential of the chemopreventive phytoalexin resveratrol", Drug Resistance Updates **7***,* 333 – 344 (2004).

(15) J. F. Savouret, M. Quesne, "Resveratrol and cancer: a review", Biomedecine & Pharmacotherapy **56***,* 84–87 (2002).

(16) G. J. Soleas, E. P. Diamandis, D. M. Goldberg, "Resveratrol: A Molecule Whose Time Has Come? And Gone? Clinical Biochemistry **30,** 91–113 (1997).

(17) R. Gilly, D. Mara, S. Oded, K. Zohar, "Resveratrol and a Novel Tyrosinase in Carignan Grape Juice", Journal of Agricultural and Food Chemistry **49**, 1479–1485 (2001).

(18) D. Millo, A. Bonifacio, A. Ranieri, M. Borsari, C. Gooijer, G. van der Zwan, "Voltammetric and Surface-Enhanced Resonance Raman Spectroscopic Characterization of Cytochrome c Adsorbed on a 4-Mercaptopyridine Monolayer on Silver Electrodes", Langmuir **23**, 9898–9904 (2007).

(19) A. Bonifacio, D. Millo, P. Keizers, R. Boegschoten, J. Commandeur, N . Vermeulen, C. Gooijer, G. van der Zwan, "Active-site structure, binding and redox activity of the heme-thiolate enzyme CYP2D6 immobilized on coated Ag electrodes: a surface-enhanced resonance Raman scattering study", J. Biol. Inorg. Chem. **13**, 85–96(2008).

(20) N. N. Brandt, O. O. Brovko, A. Y. Chikishev, O. D. Paraschuk, "Optimization of the Rolling-Circle Filter for Raman Background Subtraction", Appl. Spectrosc. **60**, 288–293(2006).

(21) M. Pinto, J. Garcia-Barrado, P. Macias, "Oxidation of Resveratrol Catalyzed by Soybean Lipoxygenase", Journal of Agricultural and Food Chemistry **51**, 1653–1657(2003).

(22) W. Madani, S. Kermasha, A. Versari, "Characterization of Tyrosinase- and Polyphenol Esterase-Catalyzed End Products Using Selected Phenolic Substrates", Journal of Agricultural and Food Chemistry **47,** 2486 –2490 (1999).

(23) F. C. Richard-Forget, M. A. Rouet-Mayer, P. M. Goupy, J. Philippon, J. J. Nicolas, "Oxidation of chlorogenic acid, catechins, and 4-methylcatechol in model solutions by apple polyphenol oxidase," Journal of Agricultural and Food Chemistry **40**, 2114–2122 (1992).

(24) D. E. Root, M. Mahroof-Tahir, K. D. Karlin, E. I. Solomon, "Effect of Protonation on Peroxo-Copper Bonding: Spectroscopic and Electronic Structure Study of $[Cu_2((UN\text{-}O\text{-})(OOH)]^{2+}$ ", Inorganic Chemistry **37**, 4838–4848 (1998).

(25) M. J. Baldwin, D. E. Root, J. E. Pate, K. Fujisawa, N. Kitajima, E. I. Solomon, "Spectroscopic studies of side-on peroxide-bridged binuclear copper(II) model complexes of relevance to oxyhemocyanin and oxytyrosinase", J. Am. Chem. Soc. **114**, 10421–10431 (1992).

“Laser Photons and Healthy Fruit

Chapter 4

Monitoring LED-induced carotenoid enhancement in grapes by Transmission Resonance Raman Spectroscopy*

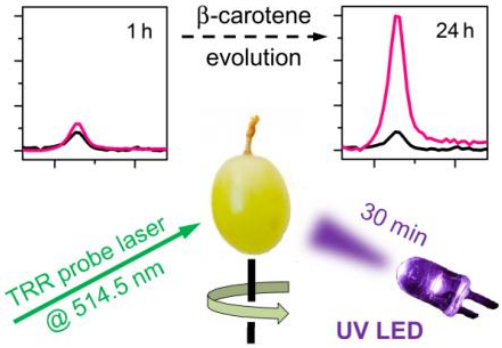

Abstract: Transmission Resonance Raman (TRR) spectroscopy combines increased signal-to-noise ratio with enhanced analytical sensibility. TRR was applied to directly monitor, without any sample preparation, the enhancement of β-carotene content in table grapes when they are irradiated by low power UV-LEDs. It was shown that, with respect to control samples, the carotenoid content in the grapes increased about five-fold, using UV-LED irradiation doses being two orders of magnitude lower than the maximum limit allowed by United States Food and Drug Administration. These promising results may pave the way for the development of easy, non-invasive techniques to improve food quality.

* The contents of this chapter have been submitted for publication as Alicia G. Gonzálvez, Nerea L. Martínez, Helmut H. Telle, and Ángel González Ureña.

4.1 Introduction

Raman Scattering is a widely used technique in Analytical Chemistry due to various reasons, one of the most important being that in many instances no special sample preparation is required.[1-7] This is contrasted by a severe limitation, namely that Raman signals are normally very weak (typically only one in every $10^6 – 10^8$ incident photons is Raman scattered). This drawback has driven the development of distinct enhancement techniques as, for example, Resonance Raman (RR) or Surface Enhanced Raman Spectroscopy (SERS). The achievements in Resonance Raman spectroscopy and the impact on aspects of its analytical potential have been reviewed recently.[8] Although Resonance Raman scattering is associated with greatly improved sensitivity the technique also comes with some fundamental catches, namely that of inherently intense fluorescence emission produced by chromophores in the biological material, and non-negligible diffuse scattering losses in high-density samples.

An elegant method to circumvent the aforementioned disturbing fluorescence, produced by the resonant excitation of the illuminated sample, is to exploit the benefits of a variant technique, Transmission Raman spectroscopy (TRS). While known since the mid-1960s this particular technique was re-discovered for practical use in 2006. Then, researchers demonstrated its capability in analyzing samples in tablet or powder form, up to several millimeters of thickness.[1] Among the many advantages of this approach it is worth mentioning its ability to probe bulk content of powders and tissues, rejecting Raman and fluorescence components produced at the sample surface as well as the absence of just sub-surface sampling. Because of these advantages TRS has evolved into a successful technique for the analysis of pharmaceutical specimen.[9,10]

In recent work from our laboratory a Transmission Resonance Raman (TRR) spectrometer was described, with the particular application to carotenoid detection (specifically β-carotene in carrots); a detection limit of sub-nanograms for β-carotene was reported.[11] That particular study may be placed within the framework of research which increasingly focuses on the nutritional relevance of a series of phytochemicals, such as flavonoids, carotenoids and glucosinates.[12-14] This is not surprising since nowadays plant secondary metabolites are widely used in human health and disease prevention.

The aforementioned carotenoids may be viewed as a representative example of plant secondary metabolites. They are organic pigments mostly found in red-, orange- and yellow-colored fruits and vegetables. Their biosynthesis is attracting a growing interest for a series of reasons, the major one being the fact that vertebrates do not synthesize these pigments. Human beings need the intake of carotenoids to convert them into retinoids, like retinal (the main visual pigment). In addition, all carotenoids containing a β-ring can be converted to retinol, i.e. the precursor of vitamin A. The lack of this vitamin is widespread in developing countries but is equally encountered in the poorest part of the population of developed countries.

The metabolic necessities sketched above raised the interest in the scientific community to search for breakthroughs for the production of secondary metabolites in general, and for metabolic engineering of plant carotenoids in particular.

It is well-known that plant abiotic stress, like UV-irradiation, triggers a plant defense mechanism enhancing the contents of some secondary metabolites, the so-called defense molecules. An example for such a metabolite is trans-resveratrol (e.g. found in

grapes), a compound widely studied because to its beneficial properties for human health. However, despite the many studies of phenolic elicitation in plants induced by UV irradiation, there are few investigations related with this abiotic method to elucidate carotenoids in fruits and plants. In this present work we report on an easy approach to enhance the carotenoid content in fruit using a non-invasive optical method. Specifically, it is shown how a low dose (for its definition see further below) of UV-B irradiation of grapes significantly enhances its β-carotene content.

Probably the key aspect of the present investigation is the use of TRR spectroscopy to monitor the β-carotene content in grapes, without having to resort to any sample preparation or extraction method. This is afforded by the enhanced sensibility of the TRR method to specific molecular compounds, because of the resonant character of the laser excitation (the wavelength is chosen to give access to an electronic transition band). A further, particularly relevant aspect of the present investigation is the use of UV-light from a low power LED. This opens the possibility to implement a simple technique and methodology using low-cost constituent components, which make the method commercially viable.

4.2 Experimental Methodology

In the experiments carried out in this study five assortments of grapes (muscatel variety) were used. These were divided into three sub-groups. Two groups of grapes were irradiated for 30 minutes with light from UV-LEDs, with peak emission at 295nm and 300nm, respectively. The particular devices had radiative power of 20 μW and FWHM of 3 nm (the emission spectra of these two LEDs are shown in the insert in Figure 4.1).

The third group of grapes was used as a control group, i.e. they were not irradiated. After treatment the grapes underwent analysis within our Transmission Resonant Raman spectrometer, whose schematic layout is depicted in Figure 4.1; its main details can be found elsewhere.[14] The TRR excitation wavelength in the experiments was 514.5 nm, which satisfies the resonance conditions for the β-carotene absorption band rather well at its tail end. Consequently, the TRR signal was substantially enhanced, and at the same time contributions from fluorescence were minimized.[1,11]

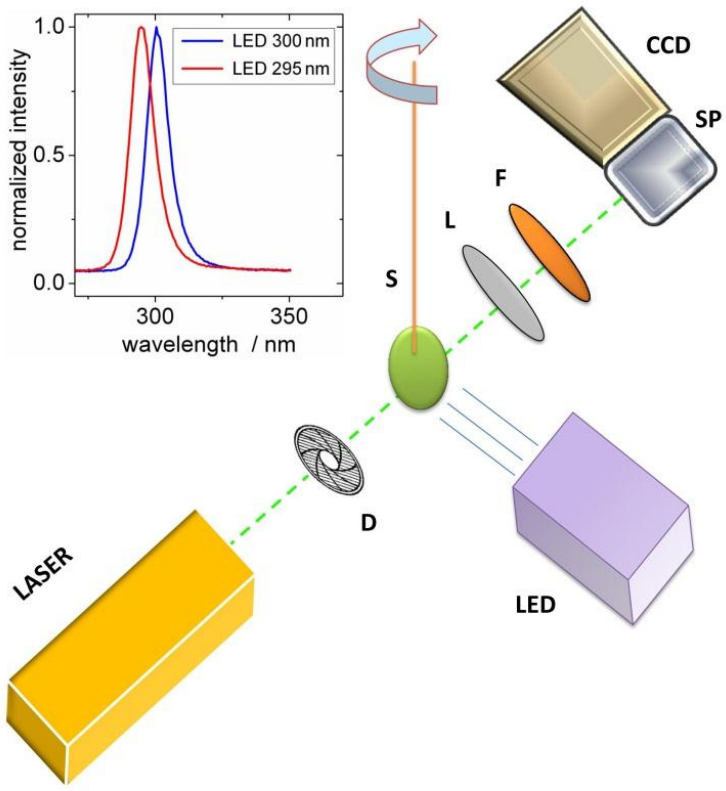

Figure 4.1: Schematic layout of the experimental Transmission Resonant Raman setup; LED irradiation of the grape is at 90º to the β-carotene TRR excitation/observation axis. Laser - cw Ar^+ laser, operating at λ = 514.5 nm; **D** – diaphragm; **S** – (grape) sample mounted in a XY micrometer sample manipulator; **L** - cylindrical lens with f =25 mm; **F** - razor-edged filter (*Semrock* LP03-514RU-25); **SP/CCD**-spectrometer with CCD-array detector. **Insert**: typical emission spectra of the two UV-LEDs used to stimulate secondary metabolites in grapes; (red) solid line - LED λ_{peak} = 295 nm; (blue) dashed line - LED λ_{peak} = 300 nm.

The other conditions for the experiments reported here were as following. The laser beam diameter at the (grape) sample location was of the order 1.0-1.5 mm, with the Ar ion laser power for the 514.5 nm line set to typically 70 mW. The temperature of the CCD detector was kept at below –60 °C to minimize dark current noise. The Raman spectra (as the examples shown in Figure 4.2) were recorded over a period of 660 s, averaging 66 scans of 10 s each. This was required in order not to saturate the detector and to make it easier to eliminate cosmic ray events from the spectra; subsequent to the acquisition and prior to data interpretation spectral background subtraction was performed by advanced rolling circle filtering.[15]

Individual measurement runs constituted a sequence of first irradiating the grapes for 30 minutes with the UV-LED light and, subsequently, Raman spectra were recorded as a function of the time elapsed after having irradiated the grape, in regular intervals from 0 hours up to 53 hours. Note that the Raman measurements were carried out without any sample treatment or preparation, i.e. a direct and online sample spectral monitoring was implemented. This measurement protocol was repeated for all grapes in a set, i.e. five each irradiated by 295 nm and 300 nm UV-LED light, respectively, and five control grapes.

4.3 Results

Typical Raman spectra of the irradiated grapes as well as a non-irradiated control sample are shown in Figure 4.2. The particular spectra shown here were taken 24 hours after the irradiation. All spectra exhibit three main peak features, corresponding to the well-known vibrational bands of beta-carotene. The two most prominent features at about 1160 cm^{-1} and 1525 cm^{-1} can be associated with its

-C-C- (ν_2) and -C=C- (ν_1) stretch vibrations.[16,17] Here, the latter peak was used to follow the time evolution of the β-carotene content in the grapes. Note that the "free" β-carotene ν_1-mode, in the literature tabulated at 1516 cm^{-1}, appears slightly shifted to 1526 cm^{-1} in the grapes, due to matrix effects.[11] Quite noticeable is the apparent, significant enhancement of these peaks for the UV-irradiated samples.

The temporal evolution of β-carotene content in the grapes, after their irradiation with UV light, is plotted in Figure 4.3. The data points in the figure represent the average of the TRR

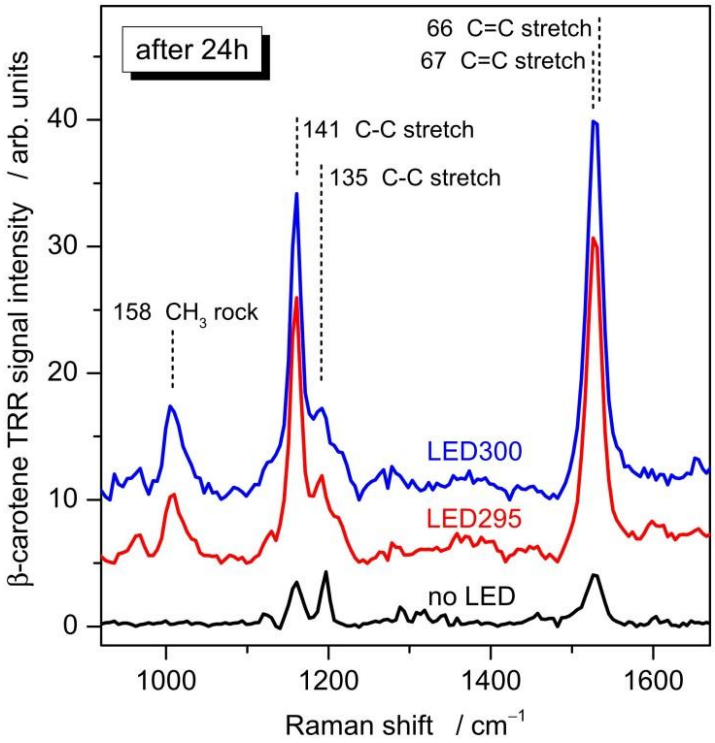

Figure 4.2: TRR spectra of β-carotene in grapes, using 514.5 nm laser stimulation; all spectra were recorded 24h after commencing the individual measurement run. Top trace (blue line) - grape irradiated with LED peaking at 300 nm. Middle trace (red line) - grape irradiated with LED peaking at 295 nm. Bottom trace (black line) - control sample, grape not irradiated. The spectra are offset to each other for clarity. The annotation of β-carotene Raman peaks is according to Tschirner *et al*.[17]

signal associated with the -C=C- ν_1-stretch mode (peak at ~1526 nm). For the irradiated grapes – (blue) square symbols for 300 nm LED, (red) circular symbol for 295 nm LED – the β-carotene content increases dramatically, reaching a maximum after about 24h and then decreasing again, down to about its initial value. For the control group – (blue) triangular symbols – the β-carotene content remains mostly constant. In the maximum the β-carotene content in the irradiated grapes is up to five times higher than in the control (untreated) grapes.

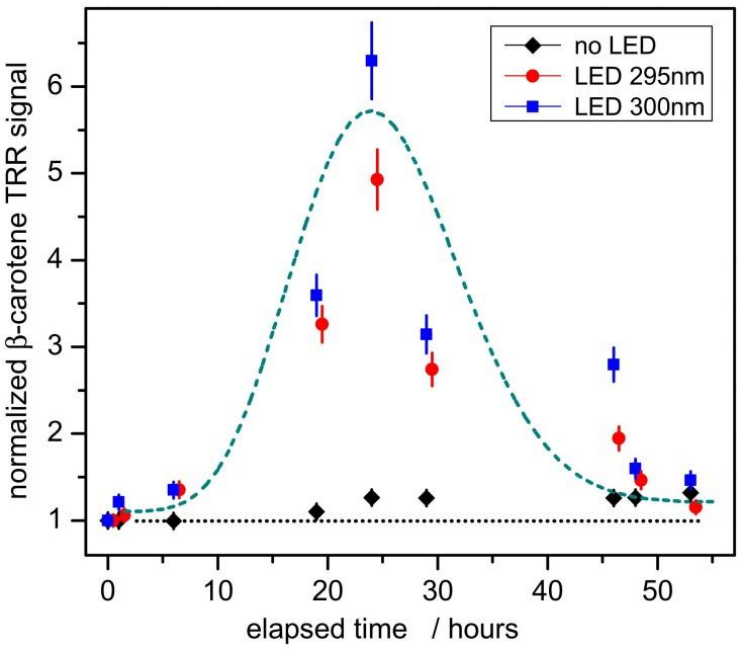

Figure 4.3: Normalized TRR signal for the Raman peak of the C=C stretch mode of β-carotene (1526 cm^{-1}) in grapes, as a function of time elapsed after irradiation with UV LED; (blue) squares – 300 nm LED irradiation; (red) circles – 295 nm LED irradiation; (black) diamonds – control samples, no LED irradiation. The error bars indicate the standard deviation of five repeat measurements for each group of grape samples. The bell-shaped curve (dashed line) serves only to guide the eye, indicating the evolution of β-carotene over time, which for the LED-irradiated samples peaks after about 24h, exhibiting a 5-fold β-carotene increase with respect to the control samples.

4.4 Discussion of β-carotene biosynthesis.

The main steps of the biosynthetic pathway of carotenoids are well described in the literature,[18] and therefore only a few comments are provided here to facilitate the understanding of the results. As illustrated in Figure 4.4, carotenoids – like all isoprenoids – are synthesized in plastids (organelles responsible for photosynthesis).

The sequence basically commences with the 5-carbon compound isopentenyl diphosphate (IDP), which is formed from pyruvate and glyceraldehyde-3-phosphate; subsequently the latter compound undergoes isomerization via the enzyme IDP-isomerase; the sequential addition of three IDPs then produces the 20-carbon molecule geranylgeranyl diphosphate (GGDP).

The head-to-head condensation of two GGDP molecules produces phytoene, the first linear unsaturated chain of 40 carbon atoms, which by introduction of four double bonds converts to lycopene. The cyclization of lycopene leads to β-carotene and its derivatives at the end of the displayed chain. Note that further chemical evolution will take place, which is not shown here, but which it is likely responsible for the observed decline in the β-carotene concentration after 24h.

These complex molecules participate in light-harvesting and photo-protection from excess light energy, thus quenching tissue-damaging free radicals as singlet oxygen species.[19] Although light is well recognized as an important factor that influences fruit carotenegenesis, the role of UV-B radiation on carotenoids is poorly understood and was rarely investigated, except for tomatoes for which several studies have been carried out. For example, Giuntini *et al* [20] found that in some tomato genotypes carotenoid was promoted by UV-B irradiation (280–315 nm).

Lazzeri *et al* [21] carried out a study of carotenoid profiling in the flesh and peel of tomatoes under UV-B depletion; the particular specimen under investigation were a wild-type tomato and a high pigment (hp-1) tomato, a mutant characterized by increased fruit pigmentation. In this latter study it was found that while UV light exerted a negative modulation effect mostly on lycopene synthesis in wild-type tomatoes, it hardly affected carotenoid accumulation in hp-1.

The observed enhancement of the β-carotene content in grapes, induced by low doses of UV-B radiation peaking around 300 nm, suggests the possibility of the photo-activation of distinct steps in the outlined biosynthetic pathway, most likely by resonant absorption in some precursor compound. This speculation seems to be reasonable; in a comprehensive guide to carotenoid analysis in food Rodriguez-Amaya [22] asserts that the carotenoid that precedes ζ-carotene in the de-saturation biosynthetic pathway, phytoene (with three conjugated double bonds), is the only compound whose main absorption band lies within the UV-B range (see Figure 9 in Rodriguez-Amaya [22]).

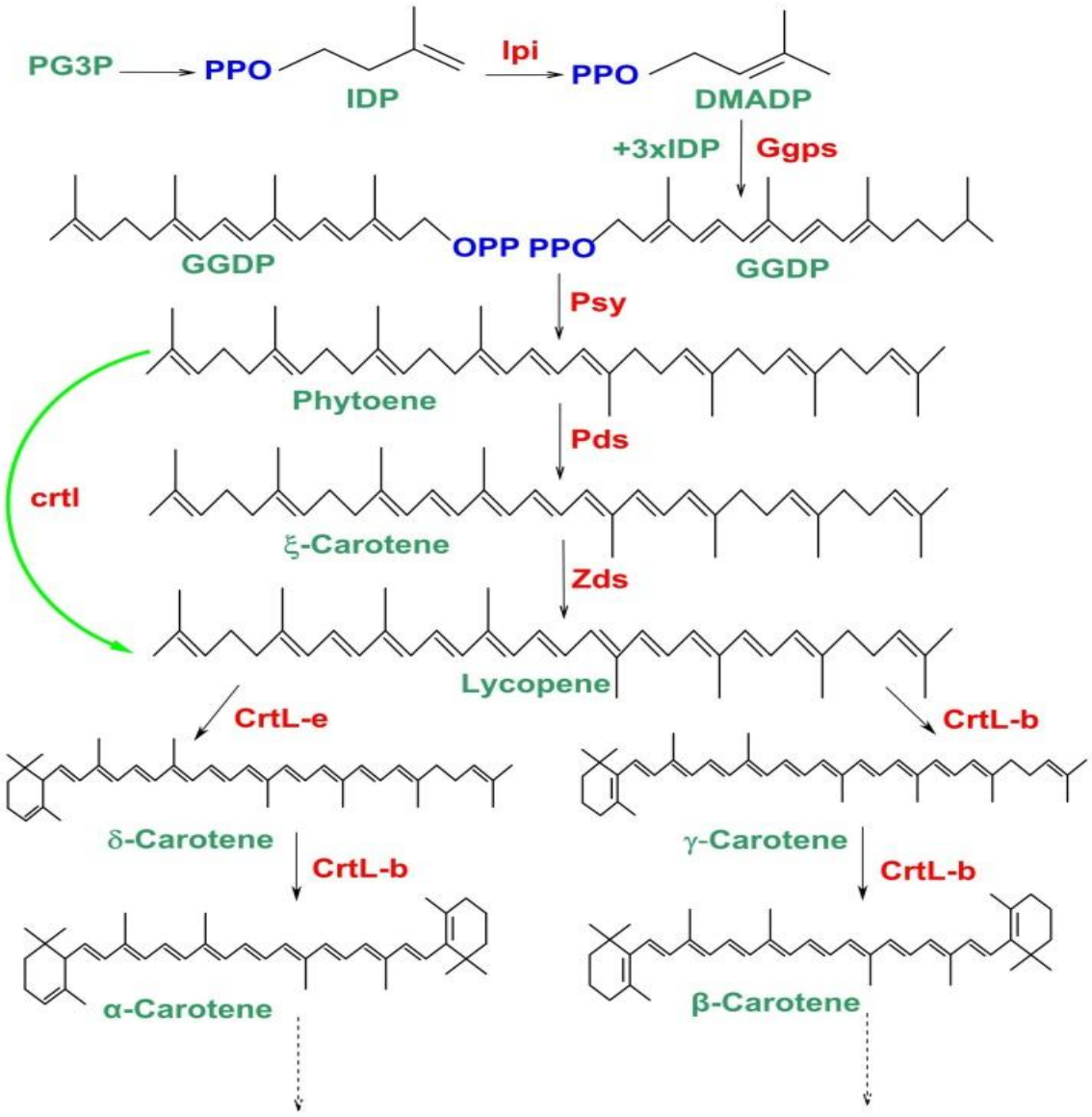

Figure 4.4: Biosynthesis pathway for β-carotene generation in plants. Enzymes are named according to the designation of their genes (for the specific specimen in the chain see "abbreviations" further below).

Following these arguments one may postulate a mechanism which encompasses electronic excitation by resonant UV-B absorption of this β-carotene precursor, which triggers the subsequent addition of double bonds required for highly conjugated carotenoids, such as β-carotene and its derivatives. Although this inference should be taken as a working hypothesis only, requiring further investigation to be fully

confirmed, it is worth noting that exploiting electronic energy excitation is a common practice in laser chemistry if one wishes to enhance chemical reaction yields.[5,23]

Abbreviations

PG3P – Piruvate/Glyceraldehyde 3-Phosphate; IDP – isopentenyl diphosphate; lpi – IDP isomerase; DMADP – Dimethylallyl diphosphate; Ggps – geranylgeranyl diphosphate synthase; GGDP – Geranylgeranyl diphosphate; Psy – phytoene synthase; Pds – phytoene desaturase; Zds – ξ-carotene desaturase; crtl – phytoene desaturase (bacteria type); CrtL-b – lycopene β-cyclase; CrtL-e – lycopene ε-cyclase

4.5 Concluding Remarks

There are three aspects of the present work that we consider to be of major relevance:

(a) In the first place, one finds a remarkable boost of β-carotene in grapes, applying only very low doses of UV-B light. This may become of great important in "functional" food research (such as processed foods or foods fortified with health-promoting additives), supporting the needs of an increasingly health-conscientious society. Furthermore, increased amounts of carotenoids may help to extend the shelf life of agricultural products, thus reducing the substantial losses incurred by excessive ripening or aging.

(b) Secondly, the use of LED technology is quite novel and promises great potential. In particular, it opens the way to potentially implement very low-cost

commercial protocols for post-harvest improvement of fruit, food and vegetable quality.

(c) Last but not least, the third aspect worth noting is the use of Transmission Resonance Raman spectroscopy to monitor the β-carotene content in grapes, without having to resort to any sample preparation or extraction method. This is afforded by the high selectivity and sensitivity of the TRR technique (resonant character of the laser excitation wavelength), but that at the same time interfering fluorescence emission is substantially suppressed.

Clearly, the combined recourse of these factors may well assist in resolving various obstacles in an efficiency-conscious food industry, and in food quality control, irrespective of other, more fundamental-oriented research objectives.

.

4.6 References

(1) P. Matousek, "Review of deep non-invasive Raman spectroscopy of living tissue and powders", Chem. Soc. Rev. **36**, 1292-1304 (2007).

(2) M. J. Pelletier, Analytical Applications of Raman Spectroscopy; Blackwell Science: Oxford, U.K., **1999**.

(3) E. Smith, G. Dent, Modern Raman Spectroscopy: A practical approach; John Wiley & Sons: Chichester, U.K., **2005**.

(4) B. Schrader, (ed). Infrared and Raman Spectroscopy; VCH: Weinheim, Germany, **1995**.

(5) H.H. Telle, A. González-Ureña, R. J. Donovan, Laser Chemistry: Spectroscopy, Dynamics and Applications; John Wiley & Sons: Chichester, U.K., **2007**.

(6) M.E. Darwin, I. Gersonde, M. Meinke, W. Sterry, J. Lademann, "Non-invasive in vivo determination of the carotenoids beta-carotene and lycopene concentrations in the human skin using the Raman spectroscopic method", J. Phys. D Apply. Phys. **38**, 2696-2700 (2005).

(7) P. Bhosale, I.V. Ermakov, M.R. Ermakova, W. Gellermann, P.S. Bernstein, "Resonance Raman Quantification of Nutritionally Important Carotenoids in Fruits, Vegetables, and Their Juices in Comparison to High-Pressure Liquid Chromatography Analysis", J. Agric. Food Chem. **52**, 3281-3285 (2004).

(8) E.V. Efremov, F. Ariese, C. Gooijer, "Achievements in resonance Raman spectroscopy: Review of a technique with a distinct analytical chemistry potential", Anal. Chim. Acta. **606**, 119-134 (2008**)**.

(9) K. Buckley, P. Matousek, "Recent advances in the application of transmission Raman spectroscopy to pharmaceutical analysis", J. Pharm. Biomed. Anal. **55**, 645-652 (2011).

(10) M. Boiret, Y-M. Ginot, "Counterfeit detection of pharmaceutical tablets with transmission Raman spectroscopy", Spectrosc. Eur. **23**(6)**,** 6-9 (2011).

(11) A.G. Gonzálvez, A. González-Ureña, "Transmission Resonance Raman Spectroscopy: Experimental Results vs. Theoretical Model Calculations", Appl. Spectrosc. **66**(10)**,** in press (2012), DOI: 10.1366/12-06632

(12) F. Bourgaud, A. Gravot, S. Milesi, E. Gontier, "Production of Plant Secondary Metabolites: a Historical Perspective", Plant Science **161**, 839-851 (2001).

(13) Y. Nakagawa, S. Fujiwara-Fukuta, T. Yorimitsu, S. Tanaka, R. Minami, L. Shimooka, H. Nakagoshi, "Spatial and temporal requirement of Defective proventriculus activity during Drosophila midgut development", Mech. Dev.**128**, 258-267 (2011).

(14) W. Russell, G. Duthie, "Plant secondary metabolites and gut health: the case for phenolic acids", Proc. Nutr. Soc. **70**, 389-396 (2011) .

(15) A.G. Gonzálvez, Á. González-Ureña, R.J. Lewis, G. van der Zwan, "Spectroscopy and kinetics of tyrosinase catalyzed trans-resveratrol oxidation", J. Phys. Chem. B. **116**, 2553-2560 (2012).

(16) N. Tschirner, M. Schenderlein, K. Brose, E. Schlodder, M.A. Mroginski, P. Hildebrandt, C. Thomsen, "Raman excitation profiles of β-carotene-novel insights into the nature of the ν_1-band", Phys. Stat. Sol. B **245,** 2225–2228 (2008).

(17) N. Tschirner, M. Schenderlein, K. Brose, E. Schlodder, M.A. Mroginski, C. Thomsen, P. Hildebrandt, "Resonance Raman spectra of β-carotene in solution and in photosystems revisited: an experimental and theoretical study", Phys. Chem. Chem. Phys. **11**, 11471-11478 (2009).

(18) J. Hirschberg, "Carotenoid Biosynthesis in Flowering Plants", Curr Opin. Plant Biol . **4**, 210-218 (2001).

(19) G. Giuliano, R. Aquilani, S. Dharmapuri, "Metabolic Engineering of Plant Carotenoids", Trends Plant Sci. **5**, 406-409 (2000).

(20) D. Giuntini, G. Graziani, B. Lercari, V. Fogliano, G.F. Soldatini, A. Ranieri, "Changes in Carotenoid and Ascorbic Contents in Fruits of Different Tomato Genotypes Related to the Depletion of UV-B Radiation", J. Agric. Food Chem. **53**, 3174-3181 (2005).

(21) V. Lazzeri, V. Calvenzani, K. Petroni, Ch. Tonelli, A. Castagna, A. Ranieri, "Carotenoid Profiling and Biosynthetic Gene Expression in Flesh and Peel of Wild-Type and hp-1 Tomato Fruit under UV-B Depletion", J. Agric. Food Chem. **60**, 4960-4969 (2012).

(22) D. Rodriguez-Amaya, A Guide to carotenoid analysis in foods. ILSI Press: Washington, DC, USA, **2001**.

(23) R.D. Levine, Molecular Reaction Dynamics. Cambridge University Press: Cambridge, U.K., **2005**. See Chapter 7.

Chapter 5

Fruit enhanced Resistance to Microbial Infection Induced by Selective Laser Radiation*

Abstract: Table grapes were irradiated with laser pulses at two different wavelengths: one selected at 302.1 nm, i.e. resonant with the trans-resveratrol bi-photon absorption band, and another selected at 300 nm, that is a non-resonant wavelength where trans-resveratrol two-photon absorption is negligible. Attenuated Total Reflectance Fourier Transformed Infrared Spectroscopic analyses of the irradiated grapes´ skin showed an enhancement of polyphenols' content when the resonant wavelength was employed. Furthermore, microbiological analysis performed with non-treated (control), non-resonant and resonantly irradiated grapes demonstrated how the last samples developed a significantly lower number of colony forming units after cultivation in adequate media. Since the only difference between the two (resonant and non-resonant) irradiation conditions is just a couple of nanometres in the employed UV-B laser wavelengths, the germicidal effect, in principle not as important as if UV-C light had been employed, of both treatments is very similar and, subsequently, the observed difference in the table grape resistance to microbial infection has to be predominantly attributed to a wavelength dependent hormetic effect. Finally, the potentiality of this non-invasive method to enhance the postharvest health status of table grapes is remarked.

* The contents of this chapter have been submitted for publication as A.G. Gonzálvez, J.B. Jiménez and A. González Ureña.

5.1 Introduction

Over the past two decades the employment of UV light to improve the quality of fresh fruits and vegetables has received an increased attention[1]and nowadays, it is considered an alternative to chemical approaches because its potential application to control postharvest diseases.[2,1,3,4] Typically, the most widely used UV light is the short-wave UV-C radiation which comprises from 200 nm up to 280 nm. Such an UV-C light when employed at high doses is harmful to living systems but, however, at low doses, it may induce fruit disease resistance, in many cases due hormesis, i.e. due to the elicitation of the so called defence compounds, naturally present in fruits and vegetables.[1]

Table grape is perhaps one of the fruits where UV-C irradiation has been extensively applied. It is well accepted that its resistance to postharvest decay, and specifically to *Botrytis. cinerea* and other pathogens can be enhanced by UV-C induction of phenolic compounds, i.e., phytoalexins like resveratrol, ε-viniferin and α-viniferin.[5,6,7] In addition, the consumption of vegetables and fruits rich in phenolic compounds is an important claim in human dietary habits as these phenolics have shown to be beneficial for the human health. An example of such compound is trans-resveratrol (3, 5, 4'-trihidroxistilbene), a well-known antioxidant compound naturally produced by vine and other plants as self-defence agent acting against pathogens attack.[8] This compound has attracted an increased interest as health promoting agent because its anti-platelet, antioxidant, anti–inflammatory, estrogenic, cardioprotective and cancer chemopreventive properties, as it has been widely reviewed.[9,10,11,12,13]

These facts together with the lack of a proper level of intake of such phenolic compounds in fruits and vegetables, stimulated research oriented to increase the natural content of trans-resveratrol in some fruits, and more specifically, in table grapes, in

order to maintain their post-harvest quality and to develop "functional" foods to overcome the mentioned dietary needs. Thus, significant enhancements of trans-resveratrol content in table grape were reported, for example, by Cantos et al.[14] and Jimenez Sanchez et al.[15], using UV-C and UV-B irradiation, respectively.

In Jimenez Sanchez et al.[15], the wavelength dependence of the trans-resveratrol elicitation was investigated by comparing the elicitation level at two distinct wavelengths. One wavelength was selected right at the maximum of the resonance enhanced two-photon absorption band i.e., at 302.1 nm[16], the resonant wavelength for trans-resveratrol, while the second one was selected at 300 nm, a non-resonant wavelength where trans-resveratrol two-photon absorption is negligible.[16] It was found that the resonant irradiation significantly enhances the grape trans-resveratrol content with respect to that of non-resonant irradiation, with the rest of the conditions being the same. These results demonstrated a wavelength dependent hormic effect at least for table grape irradiation with UV-B photons.

In this context, the present work tries to demonstrate how this wavelength dependent hormic effect increases the table grape post-harvest resistance to microbial infection. That UV irradiation increases such infection resistance and can therefore reduce post-harvest decay of table grapes is a well-known fact.[7] Thus, a good correlation has been reported between trans-resveratrol production (as induced by UV-C elicitation) and gray mould resistance.[17]

Nevertheless, the main question raised by the present study is a distinct one as it tries to investigate whether the resonant UV-B irradiation of grapes induces an additional resistance to microbial infection compared to that of non-resonant irradiation, with the rest of conditions being the same. Since the only difference between the two

irradiation conditions is just a couple of nanometres in the employed UV-B laser wavelengths, a similar germicidal effect, in principle not as important as if UV-C light had been employed, can be expected for both treatments. As a result, any observed difference in the table grape resistance to microbial infection would have to be associated to a *selective wavelength dependent hormetic effect.*

The present investigation shows that changing only a few nanometers the wavelength of the UV-B light employed in the treatment, i.e., changing from resonant to non-resonant conditions with respect to the trans-resveratrol absorption, a significant enhancement of the grape resistance to microbial infection is observed.

We believe it is the first time that the concomitant UV germicidal effect has been decoupled from, in this case, the more intense hormic effect when table grape are irradiated by UV-B light.

5.2 Materials and Methods

5.2.1 Reagents and Standards

Ethanol, from Panreac Química S.A. (Barcelona, Spain), and purified water with a Milli-Q system from Millipore (Milford, MA, USA) were used. Also a trans-resveratrol standard (99%) from Sigma Aldrich Chemie GmbH (Steinheim, Germany) was used.

5.2.2 Samples and Irradiation treatments

Red grapes (*Vitis vinifera*, *Red Globe* variety) were directly purchased from the market at the usual mature ripening stage for commercialization and no additional cleaning was

performed. To minimize effects of different maturity stage between bunches, they were cut in several moieties and each one was incorporated into the groups.

The grapes were removed from the bunch by means of a sharp cutter leaving the peduncle attached to the berry in order to minimize dehydration of the samples. The irradiation protocol was the same as used previously and reported elsewhere[15], thus only a brief description is given here. The output of a dye laser (Continuum ND60) was used to pump an INRAD-AT-III-UV frequency-doubling unit whose (BBO-TST) crystal allows scanning the output from 235 nm up to 365 nm. The employed laser fluence was 0. 141 kJ/m^2 with 5 ns pulses running at a frequency of 10 Hz.

Individual grapes were placed over the external crown of a disc of 30 cm diameter. 24 grapes were uniformly distributed at each run with a separation of 15º between two consecutive samples as is shown in Figure 5.1.

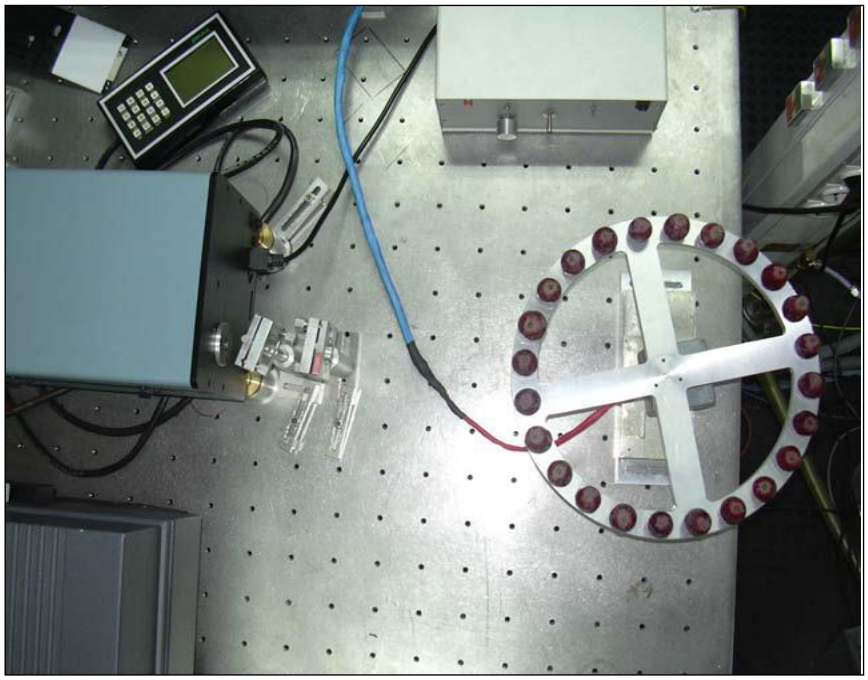

Figure 5.1: Grapes laser irradiation set-up.Individual grapes over an external crown of a disc of 30 cm diameter. Irradiaton was provided through a dye laser (Continuum ND60); which was used to pump an INRAD-AT-III-UV frequency-doubling unit whose (BBO-TST) crystal allows scanning the output from 235 nm up to 365 nm.

Uniform irradiation of samples was guaranteed by turning the disc at 6º / min. All treatments were performed at room temperature. These experimental conditions give irradiation doses of ca 58 J/kg per minute calculated using an average grape diameter of 25 mm and zero reflectivity for the grape skin. Therefore this value should be considered as an upper limit. For the present experiment 10 min of irradiation time was employed which gives irradiation doses of 0.58 kJ/kg i.e. a value lower than the limit of 1 kJ/kg approved by the United States Food and Drug Administration for the preservation and disinfestations of fresh fruits and vegetables.

Two different wavelengths were used for irradiation: 302.1 nm for the resonant wavelength and 300.0 nm for the non-resonant one. The 10 min of irradiation time employed in our experiments proved to be enough to demonstrate the selective enhancement of the health status of the resonantly irradiated grapes. However, no attempt was made in the present investigation to optimize this experimental parameter which may depend on the grape variety. This systematic study will be carried out in our laboratory in the near future. Three replicates of 24 grapes each were obtained for every wavelength by repeating 3 times the whole experiment. Also three replicates of 24 non-irradiated grapes were included in the experiment as a control.

5.2.3 Attenuated Total Reflectance Fourier transformed infrared Spectroscopy (ATR- FTIR)

Single reflection ATR-FTIR measurements were performed to get an overall estimation of the table grape phenolic induction due to resonant radiation. Grape skin extracts were prepared introducing 3 g of grape skin in 30 mL of ethanol, (100mg/ml) i.e. They were stored at 4ºC during 4 weeks with no agitation. After this period of time, 20 μL of each

extract were deposited on the single reflection ZnSe sampling plate in order to carry out the ATR-FTIR analysis.

The spectra were taken by a FTIR Spectrometer (FTIR-8400S from Shimadzu) with a resolution of 4 cm^{-1} and using Happ-Genzel apodization. An ATR spectrum was taken every five minutes until both the spectral shape and band intensities remained unchanged which was then taken as an indication of the complete solvent (ethanol) evaporation. In all cases, a period of time of 30 minutes proved to be enough to get rid of the solvent interferences and, consequently, to assign the ATR spectra to the analyte, i.e. the extracted grape skin components.

This procedure seemed to be adequate to compare the ATR spectrum of the sample produced by the resonant irradiation with that produced by the non-resonant irradiation which, essentially, was the main goal investigated by the ATR technique. In all cases, 50 scans were enough to observe the broad band over the 3000 –3300 cm^{-1} region associated to the presence of multiple OH which is of major relevance for the present work as it will be discussed later.

5.2.4 Microbiological Analysis

Samples were prepared grinding grapes' skin and mixing 3 g of them in 30 mL of a sterile saline solution of NaCl 9%. Successive decimal dilutions were then prepared to enable proper colony quantification. 0.1 ml aliquots of each dilution were incubated on a Petri plate at 37ºC for 48 hours with potato-dextrose-agar (PDA) previously poured in it. PDA was selected because it has proven to be adequate for fungi growth with significant reduction of the escort flora due to the low range of pH values featuring this culture medium.

After the incubation period *colony forming units per gram (cfu/g)* were counted following standard procedures.[17] Accordingly, three samples were prepared; namely: skin from non-irradiated grapes (control), skin from resonantly irradiated grapes and skin from non-resonantly irradiated grapes. This analytical protocol was repeated three times for each sample.

5.3 Results

5.3.1 Polyphenols elicitation monitored by ATR- FTIR

Figure 5.2 top, shows the ATR-FTIR spectra of two samples over the 800 cm^{-1}-3600 cm^{-1} region. Solid black line corresponds to the grape skin sample irradiated with resonant photons. Dashed red line is that of irradiated by non-resonant photons being the rest of conditions the same. The bottom part of the Figure displays the difference between both spectra to emphasize the main changes due to laser irradiation with distinct wavelengths.

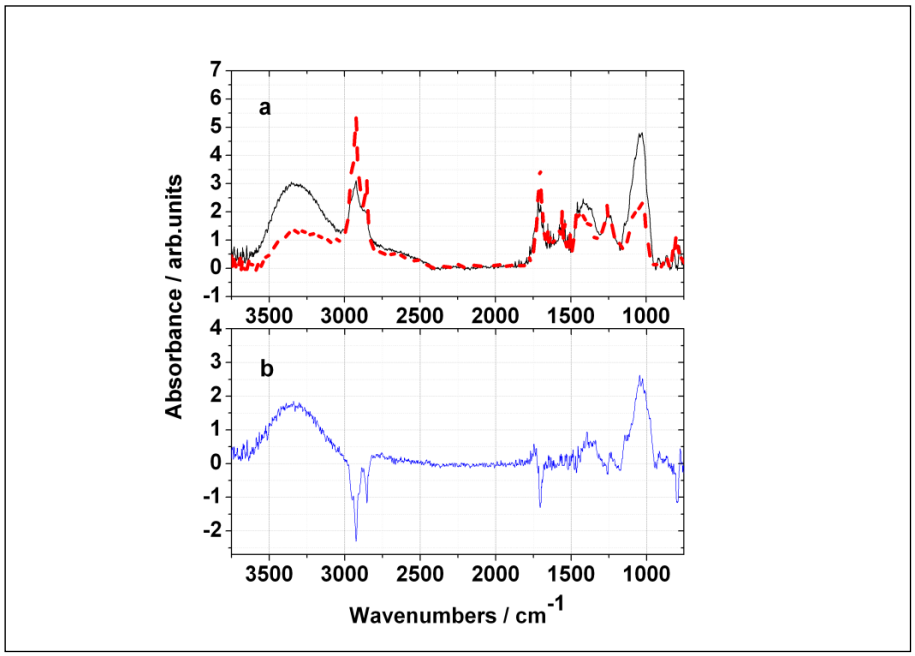

Figure 5.2: ATR – FTIR spectra of resonant and non-resonantly irradiated samples. a) ATR – FTIR spectrum of resonantly irradiated samples (solid black line) vs. non-resonantly irradiated samples (dashed red line). **b)** Difference between the resonant and non-resonant ATR – FTIR spectra (blue line). Notice how the resonant radiation has a bipolar effect. While significant enhancement in the absorbance intensity is observed over the 3000 -3600 cm^{-1} wide band, a significant reduction is observed for other bands as for example those peaking at 2925 cm^{-1}, 2854 cm^{-1} and 1701 cm^{-1}. See text for comments.

As observed in Figure 5.2, several significant changes can be noticed. Two of the most relevant changes correspond to the observed enhancement of the spectral band peaking at 3340 cm^{-1} and 1027 cm^{-1}. In both cases the band intensity of the 302.1 nm irradiated sample (black solid line) is 2 or 3 times more intense than that of 300 nm irradiated one (dashed red line). Furthermore, there are three narrow bands whose intensities diminished after using 302.1 nm laser wavelength for sample irradiation. They correspond to peaks around 1701 cm^{-1}, 2854 cm^{-1} and 2925 cm^{-1}.

5.3.2 Microbiological Results

To demonstrate the improved resistance to infection of the post-harvest grapes when irradiated with resonant photons, a microbiological test was carried out. Following the microbiological analysis protocol described in Material and Section Methods and using the same amount of

grape skin in each experiment, control, resonant and non-resonant treated grape samples were incubated in potato-dextrose-agar for 48 h at 37ºC. After this period of time their colony forming units per gram were counted and the results are plotted in Figure 5.3.

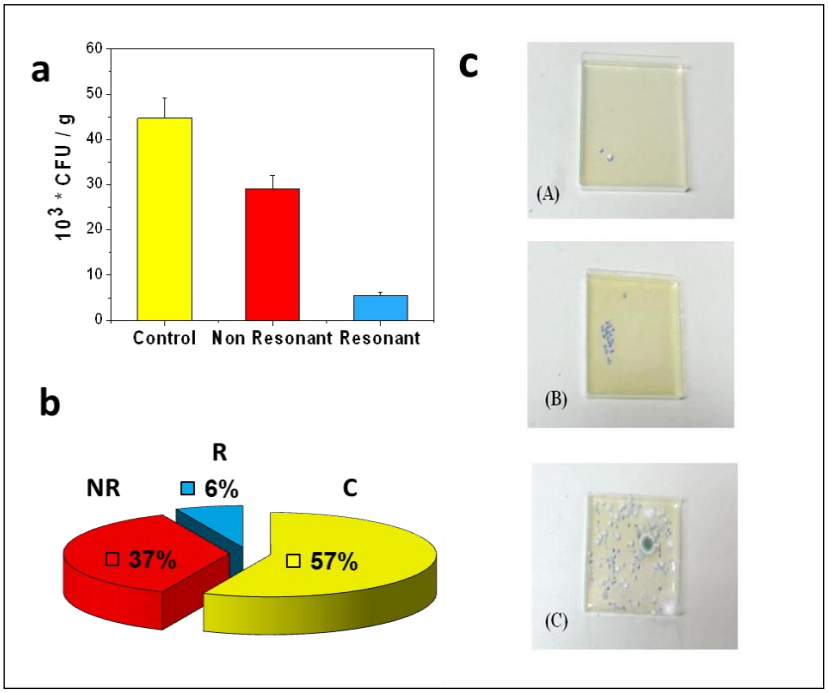

Figure 5.3: a and b) Average *colony forming units per gram (cfu/g)* expressed in bars diagram **(a)** and cheese percentage **(b)** for (R), (NR) and (C) samples, as indicated. Error bars denote the standard deviation. Notice that while the non-resonant sample already developed lower *cfu/g* compared to the control sample, further reduction in the cfu/g is clearly observed in the resonant sample when compared to that of non-resonant one**. c)** Typical pictures of individual Petri plates after incubation in potato-dextrose-agar at 37ºC for 48 h. C, B and A pictures correspond to control, non–resonant and resonantly irradiated grapes, respectively. Notice how the resonant sample shows a significantly lower number (just a very few) of cfu/g in comparison with control and non–resonant samples. (See text for comments).

Figure 5.3a and b depict the average *colony of forming units* per gram expressed in bars diagram and cheese percentage, respectively, for resonant, non- resonant and control samples. For figure 5.3b the total number of colony forming units per gram was normalized to 100. Notice that while the non-resonant sample already developed lower cfu/g compared to the control sample, further reduction in the *cfu/g* is clearly observed in the resonant sample when compared to that of non-resonant one. Figure 5.3c shows

typical pictures of individual Petri plates after incubation in PDA (see further above in Material and Methods).

Essentially, two types of fungi are observed when the Petri plates were analysed under microscope: yeasts of near spherical shape and small size, and rusts of filamentous shape, large size and green colour. After Figure 5.3 results, it is evident how the irradiated samples developed lower number of *cfu/*g than that of control. It is remarkable how the sample which corresponds to grapes irradiated with resonant photons developed a significantly lower number of *cfu /g* than that of non-resonantly irradiated sample.

In other words, the use of resonant UV-B irradiation reduces about six times the cfu/g values in table grape skin with respect to those of the non-resonant UV-B irradiated table grape skin. Since the elcitation of polyphenols, like trans-resveratrol, is the main observed difference in the UV-B irradiation experiment, we can conclude the enhanced table grape resistance to microbial infection is predominantly due to UV-B induced polyphenols.

5.4 Discussion

The main steps of the plant trans-resveratrol synthesis are well described in the literature[13,18,19,20,21] and only a summary is here outlined with the aid of the scheme shown in Figure 5.4, which essentially describes the phenylalanine-polymalonate pathway (see further below). This short recollection is outlined in the following in order to understand the main conclusions subsequently drawn from the selective wavelength resveratrol elicitation.

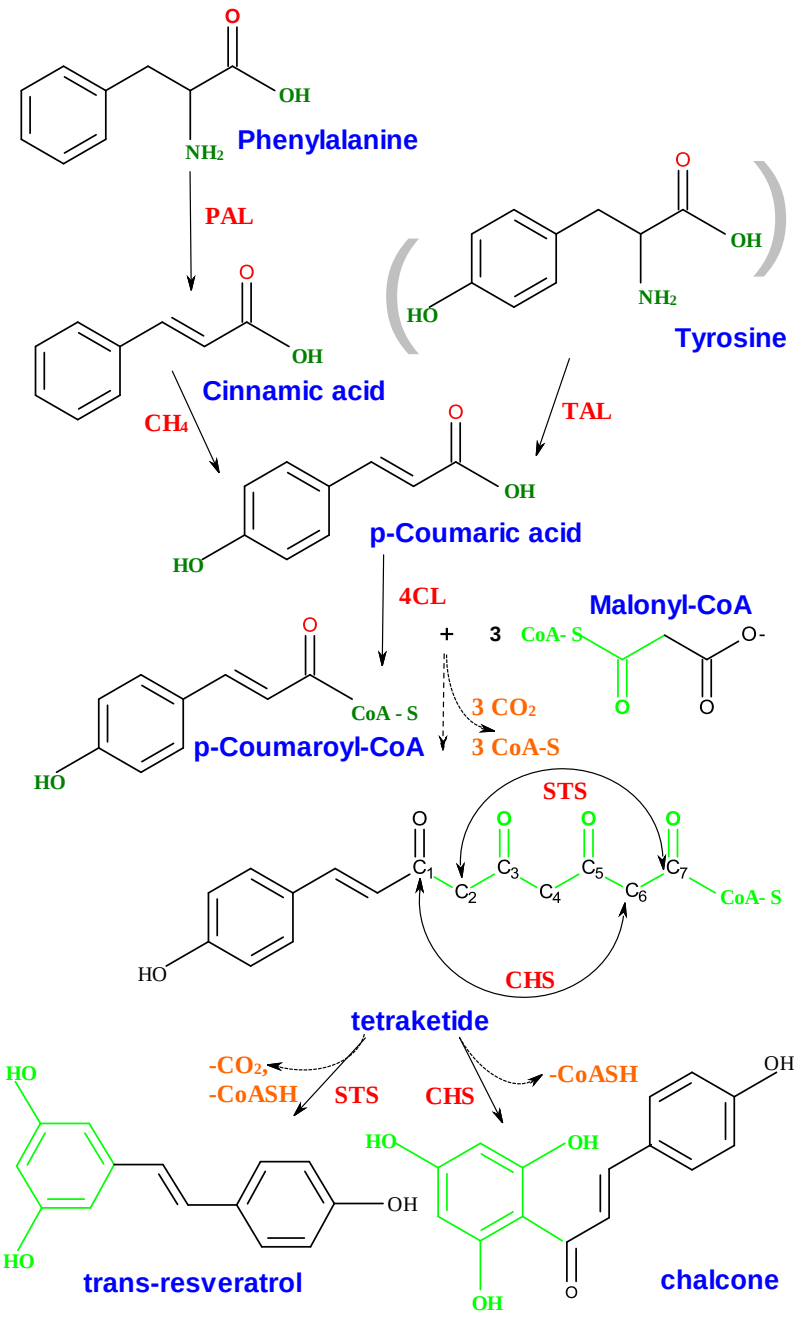

Figure 5.4: Schematic pathway for trans–resveratrol biosynthesis. Adapted from Austin et al. 2004 and Borie et al. 2004. The enzymes involved in the trans-resveratrol biosynthesis are phenylalanine ammonia lyase (PAL), cinnamate-4-hydroxylase (CH4) –which can be substituted by the enzyme tyrosine ammonia lyase (TAL)-, 4coumarate-CoA ligase (4CL) and stilbene synthase (STS). STS and chalcone synthase (CHS) bond the same substrate and produce trans-resveratrol through a C_2-C_7 aldol condensation or chalcone through a C_1-C_6 Claisen condensation, respectively.

It is well known that trans-resveratrol is a phytoalexin whose formation is controlled by stilbene synthase (STS). UV irradiation has been shown to modify the STS activity which was attributed to a genetic response to UV light.[20] This enzyme uses as substrate one p-coumaroyl-CoA and three malonyl–CoA-S. In the formation of the p-coumaric acid as precursor of the p-coumaroyl-CoA two main steps are involved. Firstly, the deamination of the phenylalanine by phenylalanine ammonia-lyase (PAL) leading to cinamic acid would take place. Secondly, further catalysis by cinnamate 4-hydroxylase (CH4) introduces a hydroxyl group in the para position of the phenyl ring.

Afterwards, as sketched in Figure 5.4, an iterative condensation of acetyl units, derived from 3 malonyl-CoA, to p-coumaroyl-CoA forms a tetraketide intermediate which is subsequently used as substrate by the chalcone synthase (CHS) and stilbene synthase (STS) in a competitive manner. Both enzymes use a different cyclization mechanism to produce a distinct end product. While CHS cyclizes the tetraketide intermediate via an intramolecular C6-C1 Claisen condensation to produce chalcone, the STS catalyzes the intramolecular C2-C7 aldol condensation producing trans-resveratrol.[19] A key feature of the STS's tetraketide final step is the spontaneous decarboxylation accompanying the C2-C7 aldol cyclization. In addition to the distinct end product, it should be remarked that a special property of STS catalysis is the terminal carboxyl group elimination as CO_2 (see mechanism in Figure 5.4).

With the scheme of the trans-resveratrol in mind, a few comments on the FTIR spectral features of the resonant and non-resonantly irradiated grapes are necessary to discuss the underlying mechanism behind the observed trans-resveratrol elicitation. In relation with the observed enhancement of the spectral bands peaking at 3340 cm^{-1} and 1027 cm^{-1}following resonant excitation, a previous work from this laboratory[22]

demonstrated the strong and wide 3400 – 3200 cm^{-1} band can be assigned to intermolecular OH interactions arising from a non-free, i.e. associated OH, most likely in the form of a polymer as one would expect for solid trans-resveratrol and other phenolics. Elicitation of these phenolics by resonant laser irradiation is therefore manifested by the increased intensity of this associated OH-band. Furthermore, the enhancement observed in the narrow band peaking at 1027 cm^{-1} can be, in principle, assigned to the C – O – C stretching. This trend could be attributed to a trans-resveratrol glucoside, known as piceid, elicitation. Indeed, piceid biosynthesis has been reported in Napoleon grapes skin[23] after UV irradiation.

The two narrow bands whose intensities diminished after resonant irradiation, peaking at 2925 and 2854 cm^{-1} are well documented to correspond to the CH stretching. The reduction of these narrow bands by resonant irradiation is consistent with the enhancement of the OH and C – O – C bands. Clearly, the induced biosynthesis of the trans-resveratrol and its glucoside by resonant irradiation should involve the consumption of CH groups. Hence an inverse relation between both band intensities could be, in principle, expected.

Before concluding this sub-section, it is worth noting a comment on the reduction of the 1701 cm^{-1} band, also observed upon resonant radiation. This band can be assigned to the carboxylic (─COOH) group. The main trans-resveratrol precursor containing this functional group is the malonyl–CoA which acts as substrate for this polyphenol biosynthesis.

The depletion of the 1701 cm^{-1} band could therefore be originated by this coenzyme reaction with the coumaroyl– CoA. As indicated in the figure 5.4 pathway, the STS catalysis destroys the malonyl–CoA carboxylic groups when the trans-

resveratrol second aromatic group, the one containing two OH, is formed. Now the question arises about the actual mechanism responsible for the observed wavelength dependent trans-resveratrol elicitation.

Langcake and Pryce[7] showed that the biosynthesis of resveratrol by grape wine in response to UV-irradiation in the 220-400 nm spectral zones showed a maximum in the region 260-270 nm suggesting that DNA was the photoreceptor for the response and that the operation of the phenylalanine-polymalonate pathway was the biosynthesis of resveratrol. The same study showed that at wavelengths above 300-310 nm little or no resveratrol production occurred.

The significant wavelength response of the phenolic enhancement observed in our previous[18] and present investigation marked by a clear elicitation at 302.1 nm with little elicitation at 300 nm, being the rest of condition the same, suggests other than the DNA mediated excitation of phenylalanine-polymalonate pathway as responsible for the observed selective transresveratrol enhancement.

A possible alternative could involve two, instead one–photon absorption as the main photochemical step for the polyphenol elicitation. Indeed, in a previous study by our group[24] the resonant two-photon ionization mass spectrometry of trans-resveratrol was investigated over the region 300-308 nm showing an absorption maximum at 302.1 nm and little absorption at 300 nm.

In this picture only resonant two-photon absorption at 302.1 nm could provide enough energy to activate the phenylalanine-polymalonate pathway by energy transfer, a type of mechanism which is common in plant photosynthesis, since one photon excitation is not enough to excite the phenylalanine electronic ground state whose maximum absorption is peaking at 250 nm.[25]

On the same ground, the (electronic and/or vibrational) excitation of the malonyl-CoA by energy transfer from the two-photon excited trans-resveratrol cannot be ruled out by fast intermolecular energy transfer which could also activate the photochemical mechanism of the phenolics biosynthesis.

Likewise in the phenylalanine case the malonyl-CoA UV absorption spectrum has an UV absorption band centred at 256.3 nm with little absorption beyond 290 nm.[26] A closer look at the scheme outlined in Figure 5.4, suggests that this process may well activate the mentioned iterative condensation of acetyl units as well the polyketide synthase decarboxylation, a feature consistent with the 1701 cm^{-1} band depletion mentioned further above. One should bear in mind that electronic or vibrational energy excitation is a common practice to enhance chemical reaction yields.[27,28]

Indeed, the two photon absorption requirement to trigger the biochemical pathway would be supported by the high selectivity of such phenolics´ elicitation, i.e., a simple detuning of a few nanometres in the irradiation wavelength would be enough to inhibit the two-photon trans-resveratrol excitation, and to cancel the energy transfer necessary to produce electronically excited phenylalanine which would have been produced by single photon absorption if UV-C radiation over the 250-270 nm region, instead UV-B photons, had been employed.

It should be noted that although the detailed wavelength dependent photochemical mechanism for trans-resveratrol biosynthesis would need additional work to confirm the suggested two--photon excitation mechanism, the experimental observation of such (wavelength dependent) enhancement of the table grape resistance to microbial infection is by itself an important finding.

Finally, this *selective hormetic effect* observed when table grapes are irradiated with UV-B light instead the more often used UV-C light, may pave the way for future commercial applications without the drawbacks normally associated to the use of the more lethal UV-C radiation. Work is in progress in our laboratory along this direction.

5.5 Concluding Remarks

The main conclusion of the present investigation is that table grapes irradiation with light resonantly absorbed by their polyphenols, as for example trans-resveratrol, not only produces phenolic elicitation but also selectively increases their post-harvest resistance to microbial infection. Indeed, Reverse Phase High Performance Liquid Chromatographic[15] and Attenuated Total Reflectance Fourier Transformed Infrared Spectroscopic analyses demonstrate how resonantly irradiated grapes' skin showed selective enhancement of trans-resveratrol and perhaps other polyphenols. Furthermore, microbiological analysis performed with non-treated (control), non-resonant and resonantly irradiated grapes evidenced how for a given skin sample the higher the polyphenols' content the lower the number of *cfu/g* after culture in PDA.

That food low dose UV-irradiation destroys microbial flora and, therefore, is a well known procedure to preserve its health status is out of the question. Nevertheless, the relevance of the present work relies on the selective character of the employed photons as they are selected to be resonantly absorbed by one or more of the so called defence molecules, as for example - the case here studied- trans-resveratrol. Since this compound has beneficial effects for human health in addition to its antifungal effects, its selective enhancement upon resonant controlled UV- irradiation of the grape skin constitutes a clear example of hormesis using UV-B radiation.

Though the potentiality of this optical method to enhance the health status of fruits is evident and will be further explored in subsequent work, we believe the findings reported in this work could pave the way to design optical non-invasive protocols to improve the post-harvest life of fruits that could be commercially available using low doses of UV-B radiation i.e., without resorting to the more lethal UV-C radiation treatments.

5.6 References

(1) M.T. Charles, and J. Arul, "UV treatment of fresh fruit and vegetables for improvement quality: a status report", Stewart Postharvest Review **3**, 6.1-8 (2007).

(2) J. Arul, J. Mercier, M. T. Charles, M. Baka, and R. Maharaj, "Photochemical treatment for the control of postharvest disease in horticultural crops", In: Physical Methods in plant protection, (eds) C Vinant, B Pameton, F Fleurat-Lessard (Berlin: Springer-Verlag) pp 146-161 (2001).

(3) L. Cisneros-Zevallos, "The use of controlled postharvest abiotic stresses as a tool for enhancing the nutraceutical content and adding-value of fresh fruits and vegetables", Journal of food Science **68**, 1560 -1565 (2003).

(4) G. Shama, "Process challenges in applying low doses of ultraviolet light to fresh produce for eliciting hermetic responses", Postharvest Biology and Technology **44**, 1-8 (2007).

(5) E. Cantos, F.A. Tomás-Barberán, A. Martínez, and J.C. Espín, "Differential stilbene induction susceptibility of seven red wine grape varieties upon postharvest UV-C irradiation", Eur. Food Res. Technol. **217**, 253-258 (2003).

(6) P. Langcake and R.J. Pryce, "The production of resveratrol and the viniferins by grapevines in response to ultraviolet irradiation", Phytochemistry **16**, 1193-1196 (1977).

(7) F. Nigro, A. Ippolito, G. Lima, "Use of UV-C light to reduce Botrytis storage rot of table grapes", Postharvest. Biol. Technol. **13**, 171-181 (1998).

(8) J.B. Jiménez, J.M. Orea, C. Montero, A. González-Ureña, E. Navas, K. Slowing, M.P. Gómez-Serranillos, E. Carretero, and D. De Martinis, "Resveratrol treatment controls microbial flora, prolongs shelf-life, and preserves nutritional quality of fruit", J. of Agric. and Food Chem. **3**, 1526-1530 (2005).

(9) A. Cassidy, B. Hanlkey and R.M. Lamuela-Raventós, "Isoflavones, lignans and stibenes-origins, metabolism and potential importance to human health", J. Sci. Food Agric. **80,** 1044-1062 (2000).

(10) L. Fremont, "Biological Effects of Resveratrol", *Life Sci.* **66,** 663-673 (2000).

(11) J.B. German, R.L. Walzem, "The health benefits of Wine", Annu. Rev. Nutr. **20**, 561-593 (2000).

(12) S. Pervaiz, "Chemotherapeutic potential of the chemopreventive phytoalexin resveratrol", Drug. Res. Updates **7**, 333-344 (2004).

(13) G.J. Soleas, E.P. Diamandis, D.M. Goldberg, "Resveratrol: A Molecule Who's Time Has Come? And Gone", Clin. Biochem. **30**, 91-113 (1997).

(14) E. Cantos, J.C. Espin and F.A Tomas-Barberan, "Postharvest induction modeling method using UV irradiation pulses for obtaining resveratrol-enriched table grapes: A new "functional" fruit?" J. Agric. Food Chem. **49**, 5052-50582001 (2001).

(15) J.B. Jiménez Sánchez, E. Crespo Corral, J.M. Orea, M.J. Santos Delgado, and A. González-Ureña, "Trans-resveratrol elicitation by laser resonant irradiation of table grapes", Appl. Phys. B. **87**, 559-563 (2007).

(16) C. Montero, J.M. Orea, M. Soledad Muñoz, R.F.M Lobo, and A. González-Ureña, "Non-volatile analysis in fruits by laser resonant ionization spectrometry: Application to resveratrol in grapes" Appl. Phys. B **71**, 1-5 (2000).

(17) M. Sbaghi, P. Jeandet , B. Faivre , R. Bessis, and J.C. Fournioux, "Development of methods using phytoalexin (resveratrol) assessment as a selection criterion to screen grapevine in vitro cultures for resistance to grey mould (Botrytis cinerea)", Euphytica **86**, 41-47 (1995).

(18) A. Kodan, H. Kuroda, and F.A. Sakai, "Stilbene synthase from Japanese red pine (Pinus densiflora): Implications for phytoalexin accumulation and down-regulation of flavonoids biosynthesis", Proc. Nat. Acad. Sci USA **99,** 3335-3339 (2002).

(19) M.B. Austin, M.E. Bowman , J.L. Ferrer, J. Schröder, and J.P. Noel, 2004 "An aldol switch discovered in stilbene synthases mediates cyclization specificity of type iii polyketide systhases"; Chemistry & Biology **11,** 1179-1194 (2004) .

(20) B. Borie, P. Jeandent, A. Parize, R. Bessis and M. Adrian, "Resveratrol and stilbene synthase mRNA production in Grapevine Leaves Treated with biotic and abiotic phytoalexin elicitors", Am. J. Enol. Vitic. **55,** 60-64 (2004).

(21) J.L. Ferrer, M.B. Austin, C. Jr. Sterwart, and J.P. Noel, "Structure and function of enzymes involved in the biosynthesis of phenylpropanoids", Plant Physiol. & Biochem. **46,** 356-370 (2008).

(22) J.B. Jiménez Sánchez, J.M. Orea, A.G. Gonzálvez, and A. González-Ureña, "On the use of the own plant's defence compounds to maintain the post-harvest fruit quality", The Open Agricultural Journal **2**, 43-48 (2008).

(23) E. Cantos, C. García-Viguera, S. de Pascual-Teresa, and F.A Tomás-Barberán, "Effect of postharvest ultraviolet irradiation on resveratrol and other phenolics of cv. Napoleon table grapes", J. Agric. Food Chem. **48,** 4606-4612 (2000).

(24) J.M. Orea, C. Montero, J.B. Jiménez, and A. González-Ureña, "Analysis of trans-resveratrol by laser desorption coupled with resonant ionization Spectrometry. Application to trans-resveratrol content in vine leaves and grape skin", Ana.Chem. **73**, 5921-5929 (2001).

(25) B. Kierdaszuk, I. Gryczynski, and J.R. Lakowicz, "Two-photon induced fluorescence of proteins", in Topics in Fluorescence Spectroscopy. Nonlinear and Two-Photon-Induced Fluorescence Vol.5: (ed) J.R Lakowicz (Plenum Press New York) pp. 187-209 (1997).

(26) H. Chen, H.U. Kim, H. Weng , and J. Browse, 2011 "Malonyl-CoA synthetase, encoded by acyl activating enzyme13, is essential for growth and development of Arabidopsis", The plant Cell, **23**, 2247-2262 (2011).

(27) R.D. Levine, Molecular Reaction Dynamics; Cambridge University Press, Cambridge U.K. 2005, See chapter 7.

(28) H.H. Telle, A. González-Ureña, and R.J. Donovan 2007 Laser Chemistry: Spectroscopy, Dynamics and Applications. John Wiley & Sons, Ltd, Chichester. U. K. (2007), See chapter 22.

Chapter 6

On the Use of the Own Plant's Defence Compounds to Maintain the Post-Harvest Fruit Quality*

Abstract: This work demonstrates that the own plant defence compounds, like resveratrol in grapes, can be used as a natural and ecological alternative to chemical pesticides. An extract from vine leaves was used to maintain the quality of post-harvested grapes. Specifically, an extract (95% water and 5% ethanol) of such leaves was prepared and, subsequently, different bunches of grapes were immersed in it. The same number of bunches received either water or ethanol (5%) treatment, being both used as blank. Remarkably, on the 14th day after the beginning of the treatment the extract treated grapes, always maintained at room temperature, showed no sign of physical deterioration. In contrast, the two blank samples, i.e.: the water or ethanol treated bunches appeared dehydrated, infected and deteriorated. Furthermore, the external application of the leaf's extract does not modify sensorial, biochemical and nutritional properties of the fruits. The beneficial effects of trans-resveratrol, such as anticancer, antiviral, neuroprotective, antiaging and anti-inflamatory support further the use of this natural compound instead of hazardous synthetic pesticides. Therefore, this study represents a step towards the development of new protocols to maintain the post-harvest fruit quality without resorting to chemical pesticides.

* The contents of this chapter have been published as J. B. Jiménez Sánchez, J. M. Orea, A. G. Gonzálvez and A. González Ureña in the Open Agricultural Journal **2,** 43-48 (2008).

6.1 Introduction

In most climates, fruits can only be grown and harvested during a small part of the year. Yet, consumption of fruit, and hence demand occurs throughout the year. For this reason, large parts of fruit harvests must be stored for extended periods of time before they are sold to the consumers. Obviously, such storage causes considerable losses due to pathogen attack and natural senescence. The traditional solutions to these problems have been storage under controlled or modified atmospheres and the use of synthetic pesticides. Nevertheless, losses exceeding 20% are not uncommon. With respect to the use of controlled or modified atmospheres, though significant advances have been made over the recent years,[1,2] no general and efficient methodology is yet available.

Despite the wide literature on sustainability and sustainable agriculture, specially since the publication of the Brundtland Report[3] by the UN World Commission on Environment and Development (WCED), there is still no consensus on the definition of "sustainable agriculture"[4]. Although it seems to be a wide consensus on its importance, in practice, there is no single approach to sustainable agriculture due to its multi-dimensional character, including: economics, environmental and social concerns.[5,6,7] In this view, during the lasts decades there is a worldwide trend to find new alternatives to control post-harvest pathogenic diseases in a more environmentally and toxicologically safe manner.

The use of chemical pesticides is nowadays widely accepted as even more dangerous than previously believed[8], and the indiscriminate use of chemicals is generally considered as one of the main undesirable effects of modern agriculture, affecting both human health and wildlife population. The main problems related to the use of chemical pesticides have been identified as: the high frequency of insecticide

resistance developed by many insect species, pest resurgence, acute and chronic health problems, environmental pollution and uneconomic crop production[9]. This situation has encouraged the search for alternatives to significantly reduce the use and application of chemical pesticides.

In this work we explore an alternative to the use of both controlled atmospheres and chemical pesticides. Our approach consists of using the plant own pesticides to improve their natural resistance. Natural products of plant's secondary metabolism have been used in "natural" medicine since the early times of human history. An important group of secondary metabolites are the so-called "phytoalexines": antiphatogenic compounds produced by plants after infection or elicitation by biotic or abiotic agents. Under pathogen attack plants evolve sophisticated systems of detection and response to decipher the pathogen signals and induce appropriate defenses. These systems include specific networks that operate through the action of signaling molecules such as salicylate, jasmonate and ethylene and generate the accumulation of pathogen related proteins, phytoalexins or other phenolic compounds.[10,11,12]

The basic function of these chemicals is to protect the plant from attack. Then, a good strategy would first require the identification of the components of the natural defense response in plants. They can be then used both as early and sensitive indicators for spoilage and to enhance resistance. For the latter a good strategy will be either to enhance the natural content of these defense compounds or to externally apply them to the harvested fruit to improve its natural resistance. In this way, phytoalexines represent a large reservoir of possible natural pesticides to be used for pest control instead of chemicals.[13,14,15,16]

A good example of a compound with demonstrated phytoalexinic character is the trans – resveratrol (3, 5, 4'- trihydroxistilbene） which is an antioxidant compound naturally produced by a huge variety of plants as self-defense agent. Its production occurs in vine plants as response to fungic infections and other kind of stresses (UV radiation, chemicals, climatic conditions, etc.).[17,18,19,20] This compound has shown to be fungitoxic at physiological concentrations against Botrytis cinerea,[21] which is the most destructive of the post-harvest diseases of table grapes. It also enhances the resistance of vineplants to other pathogens as Plasmopara viticola,[22] Phomopsis viticola[23] or Rhizopus stonifer[24]. This rather unspecific antifungal character and its selective accumulation in grape skin[25] makes it a good candidate as a "natural pesticide" against pathogen attack, and therefore, to improve grapes´ natural resistance to fungal infection. Furthermore, trans-resveratrol is known to show important antioxidant properties that could also have positive effects on fruit conservation during storage.[26]

Previous work from our laboratory demonstrated the resveratrol elicitation in grapes after infection with Botrytis cinerea.[27] Moreover, the external application of this compound to the fruits considerably improved their natural resistance to spoilage as much as 70 days for apples or 13 days for grapes at room temperature, i.e. without need for storage at cold temperatures.[28,29] Therefore the starting point of the present work is to collect vine leaves and after dry them to characterize the presence of polyphenols, specifically, trans-resveratrol, which is subsequently extracted for external application to fruits with the aim to improve their natural post-harvest resistance.

6.2 Materials and Methods

6.2.1 FTIR Analysis

Due to versatility and simplicity, we have employed the Fourier transform Infrared Spectroscopy (FTIR) to analyse and characterize the vine leaves. Nevertheless, a more sophisticated laser analytical method[30] (see below for more details) was used to confirm the presence of the compound, though is availability is not necessary for the protocol here developed, as explained below. To prepare the sample for FTIR analysis, vine leaves were dried before grinding them to particle size below 25 μm. Afterwards a mixture with KBr was prepared in a weight percentage of 4% and 96% for sample and KBr components, respectively. Once the prepared mixture was homogeneous 100 mg of it was used for each run of transmission or diffuse reflectance measurements.

The spectra were taken by diffuse reflectance with a FTIR Spectrometer (FTIR-8400S from Shimadzu) with a resolution of 4 cm^{-1} and using Happ-Genzel apodization. In all cases, a few scans were enough to observe the broad band over the 3000 - 3300 cm^{-1} region associated to the presence of multiple OH which is of relevance for the present work as it will be discussed later.

6.2.2 Extracts Preparation and grapes treatment

The experiments here presented were carried out with an ethanolic extract obtained from Aledo vine leaves. This variety was selected because its high concentration of trans-resveratrol (typically 10 ppm). In order to obtain such extract, the leaves were cut in small pieces and filled in a recipient with ethanol. The quantities used were 8 L of

ethanol to extract 3.5 kg of vine leaves. The leaves were maintained in ethanol with no sample agitation and light protected during 7 weeks to ensure the complete extraction of the phenolic compounds. Periodically, a sample was taken and analized by UV-visible and FTIR spectrophotometry to monitor the advance of the polyphenolic compounds extraction.

The treatment was carried out on grapes (*vitis vinifera*, Muscatel variety) directly purchased from the market. In order to minimize effects of different maturity stages between bunches, they were cut in two similar moieties and were incorporated to three different test groups: one group was immersed in water (control), a second group was immersed in a solution of ethanol 5% in water and the third one was immersed in a solution of 5% of the leaves ethanolic extract in water. Each experiment contained 3 half-bunches of approximately the same weigth. The experiments were repeated up to five times to ensure reproducibility of the results.

6.2.3 Laser Desorption and Resonant Ionization Mass Spectrometry

The trans-resveratrol content in the vine leaves was measured using the laser technique developed in our lab which has been widely described elsewhere[25,30] so only a brief report is given here. It is based on the combination of Laser Desorption (LD) with Laser Resonance-Enhanced Multi-Photon Ionisation (REMPI) coupled to Time-of-Flight Mass Spectrometry (TOFMS) detection. A basic feature of the technique is the absence of any separation method for sample preparation, thus, the combination of Laser Desorption followed by REMPI-TOFMS detection can overcome the main error sources, present in the chromatographic methods generally employed for *trans*-resveratrol analysis in complex samples.

6.2.4 Microbiological Analysis

Weighted mixtures of grapes skin (50%) and vine leaves (50%) were ground and diluted in a sterile saline solution of NaCl 9%. Grape skins and leaves were used in the microbiological work for completeness. However, similar results were obtained by employing grape skins or leaves alone. The polyphenols' content *(pc*) of each mixture was monitored by the intensity of the 3300-3000 cm^{-1} band in the respective FTIR spectrum. Two mixtures called A and B were selected such that their pc_A / pc_B ratio was ca. 4. Furthermore, samples were prepared solving 3 g of each mixture in 30 ml of the NaCl solution, and then successive decimal dilutions were prepared to enable proper colony quantification. 0.1ml aliquots of each dilution were incubated on a Petri dish at 37 ºC for 48 hours with potato-dextrose-agar previously poured in it. After this period *colony forming units per gram (cfu/g)* were counted following standard procedures.[31] This protocol was repeated three times for each A and B sample.

6.3 Results and Discussion

Figure 6.1 shows the Fourier Transform infrared Spectrum of different samples: namely, pure stilbene (top panel), pure trans-resveratrol (bottom panel) and vine leaf powder (middle panel). The same percentage of sample (4%) and KBr (96%) was used for each analysis. Due to the presence of the resveratrol in the dried vine leaf, its spectral band shows more similarity to that of pure resveratrol than to that of pure stilbene.

To further confirm the presence of the resveratrol in the dried vine leaf, we have applied our laser analytical technique to the samples; Figure 6.2 shows the mass spectrum obtained with this technique; the peaks corresponding to stilbene (added as internal reference), resveratrol and quercitrin can be noticed. As it is well known, the = C – H stretching in compounds of the form R_1 – CH = CH – R_2 (cis or trans) and R_1 R_2 C = CH – R_3 show vibrational bands in the 3040 – 3010 cm^{-1} region. Furthermore, if the C–H stretching is originated in an aromatic compound it will occur in the 3080 – 3030 cm^{-1} band.

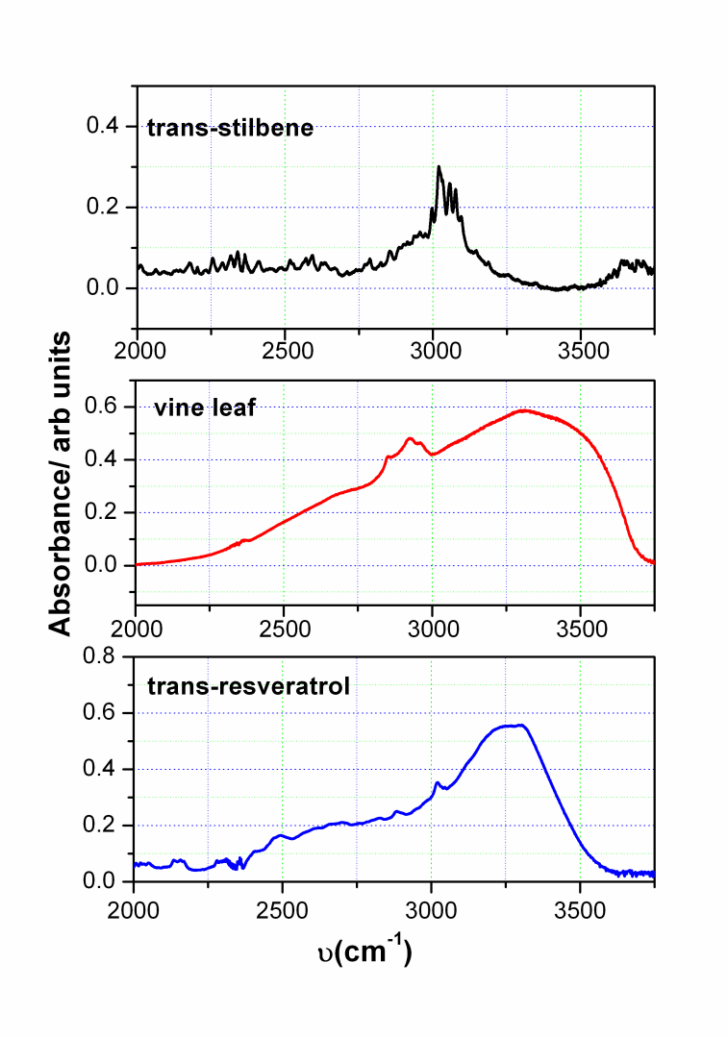

Figure 6.1: Fourier Transform infrared Spectrum of different samples. **Top**: Pure trans-stilbene; **Center**: vine leaf powder; **Bottom**: pure trans-resveratrol. The spectrum is the average of 50 scans.

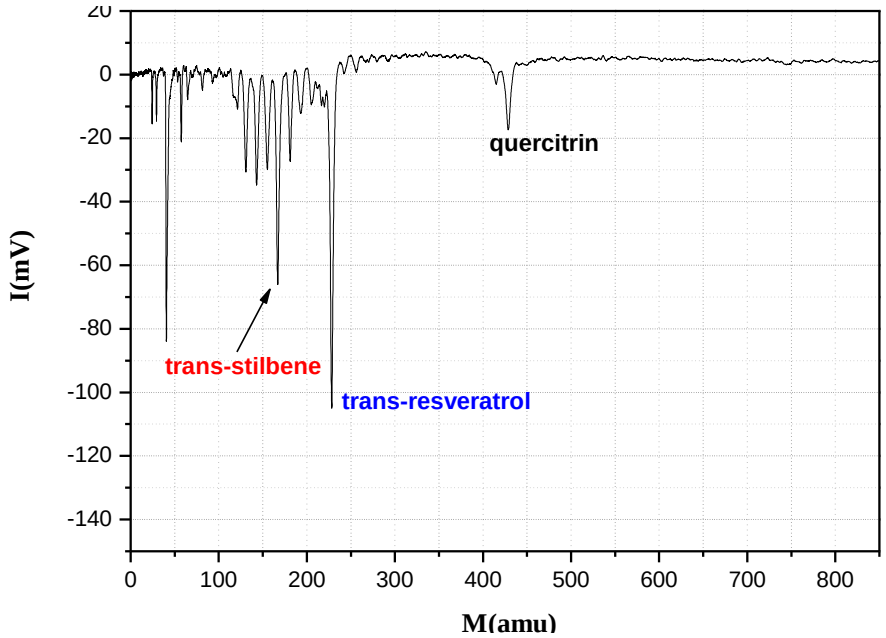

Figure 6.2: Mass spectrum obtained from a sample of vine leave by laser desorption coupled with resonant ionisation spectrometry. The resveratrol peak is indicated. See reference 25 for experimental details.

Comparing the 3500 – 2500 cm^{-1} spectral region of both trans-stilbene and trans-resveratrol (Figure 6.1 top and bottom, respectively) it becomes clear how the trans-resveratrol band is wider than that of trans-stilbene. For example, whereas the absorption intensity decreases sharply toward the blue region after 3000 cm^{-1} in the trans-stilbene, the absorption intensity decreases more gently in the trans-resveratrol reaching even the 3500-3400 cm^{-1} zone with non-negligible values. This feature is clearly manifested by the shift in the maximum band value. These values correspond to 3000 cm^{-1} and 3350 cm^{-1} for the trans-stilbene and trans-resveratrol, respectively.

Since the basic difference between both compounds is the presence of three OH groups in the resveratrol, as can be seen in their structural formula displayed in Figure 6.3, we conclude that the wider band and shift in the maximum value are due to the presence of such associated OH.

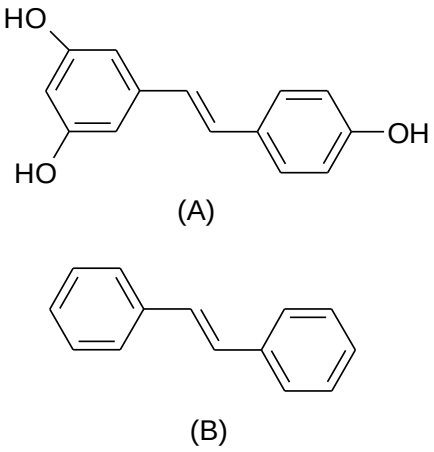

Figure 6.3: Structural formula: (A) trans-resveratrol; (B) trans-stilbene.

Of relevance for the matter under consideration are the expected values of the OH stretching depending on the OH type of interaction as listed in Table IV.[32,33] After inspection of these values, it is evident the observed spectral band of the trans-resveratrol is more consistent with the strong and wide 3400 -3230 cm^{-1} band due to intermolecular OH interaction arising from a non-free i.e. associated OH, most likely in the form of a polymer as one would expect in solid trans-resveratrol.

Table IV. OH – stretching frequencies in cm^{-1} [Adapted from Ref. 32]

OH - Type		*band*	*Shape*	*Intensity*
Free		3670-3580	sharp	variable
Associated	Intermolecular Dimer	3550-3450	sharp	variable
	Intermolecular Polymer	3400-3220	wide	strong
	Intramolecular	3590-3420	sharp	variable
	Coordination Complex / Chelates	3200-1700	wide	weak

It is very interesting to notice how this wide band featuring the presence of non-free OH is also observed in the vine leaf spectrum suggesting the persistence of such associated OH, present in polyphenols, even in the dried leaves, and therefore making possible its extraction and subsequent application as described in the present investigation.

As a result, an ethalonic extract of such leaves was prepared and, subsequently, different bunches of grapes were immersed in this ethanolic extract (95 % water) while the same number of bunches received either water or ethanol 5% treatment. A picture of the three samples is shown in Figure 6.4 corresponding to the 14^{th} day after the beginning of the treatment. It is remarkable to observe how the extract treated grapes maintain a physical aspect with no sign of losses or deterioration.

On the other hand, the water or ethanol treated bunches, appear dehydrated, infected and deteriorated. This experiment was repeated up to five times with similar results.

(A)

(B)

(C)

Figure 6.4: Grapes stored at room temperature during 14 days after different treatments: **(A)** water; **(B)** ethanol 5% and water 95 %; **(C)** leaves extract 5% and water 95 %.

Sensory and biochemical analysis of these samples were implemented following a standard procedure already described elsewhere.[28] The results indicate that the external application of this extract, from the own plant's leaf, does not modify sensorial, biochemical and nutritional properties of the treated fruits compared with those of non-treated, ones.

To demonstrate the improved natural resistance of the post-harvest grapes is due to the antifungic and antimicrobiological character of polyphenols content present in the vine leaves a microbiological test was carry out. Following the microbiological analysis

protocol described in Material and Section Methods and using the same quantity of both A and B samples, the respective colony forming units per gram were counted after sample incubation in potato-dextrose-agar. The resulted *cfu / g* are displayed in Figure 6.5.

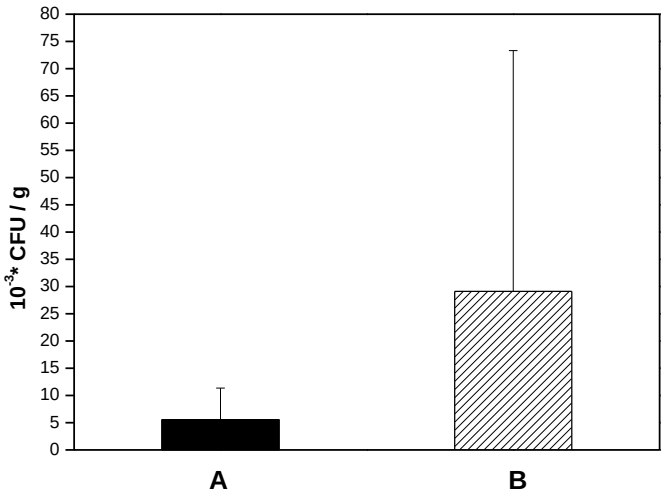

Figure 6.5: Average colony forming units per gram for sample A and B after incubation in potato-dextrosa-agar at 37 ºC for 48 h. Sample A contains 4 times more polyphenols than sample B. See text for further details.

As an example to illustrate the difference observed from the A and B samples the picture enclosed in Figure 6.6 shows the significant difference against the microbiological infection observed in an individual essay. Looking at both Figure 6.5 and 6.6, it is evident how the sample with lower polyphenol-resveratrol content developed a higher number of *cfu / g*

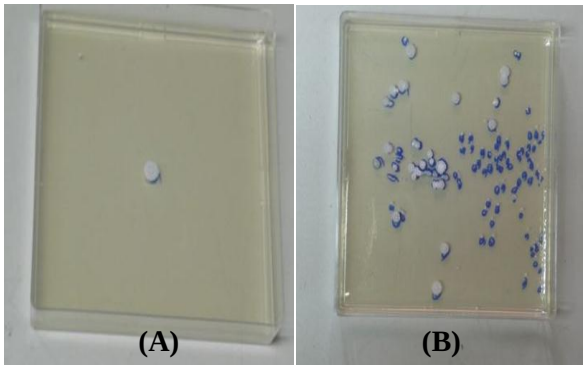

Figure 6.6: Typical picture of individual Petri dishes after incubation in potato-dextrose-agar at 37 ºC for 48 h. Notice how sample shows no presence of colony forming units whereas almost a dozen of them are manifested in sample B. See text for comments.

6.4 Summary and Conclusions

The main conclusion of the present work is the significant improvement of the post-harvest resistance of grapes when these fruits are immersed in a solution formed by 95% water and 5% ethanol vine leaves' extract. Thus, it was remarkable to observe that while at the 14^{th} day of treatment the extract - treated grapes maintained a physical aspect with no sign of deterioration, the two other samples, i.e.: the water or ethanol treated bunches, appeared dehydrated, infected and deteriorated.

The observed positive influence of the natural extracts has been attributed to the presence of polyphenols as monitored by their IR absorption band and demonstrated by specific microbiological analysis. Indeed, analysis performed with these natural samples clearly demonstrated how the higher the content of polyphenols the lower the number of colony forming units after proper cultivation in adequate growing media.

Hence, the results reported in the present investigation may represent a step forward in the use of natural and ecological methods to improve the post-harvest resistance of fruit paving the way to device an alternative to the use of chemical pesticides. Furthermore, this new approach could be of great importance in Agriculture, especially for countries that cannot afford the high cost of chemical pesticides. Interesting aspects of the new methodology are: (i) the added value of the vine leaf which currently is an agriculture sub-product of little, if any, value and (ii): the low cost of the applied protocol. Indeed a simple (low resolution) FTIR is the only equipment required to select the most suitable vine leaves from which to extract the 'natural pesticides'. In addition, the low cost of the leaves as an agriculture sub-product, facilitates the possibility to implement a commercial use of the protocol developed here.

The beneficial effects of trans-resveratrol, such as anticancer, antiviral, neuroprotective, antiaging and anti-inflamatory support further the use of this natural compound instead of hazardous synthetic pesticides. Work is now in progress to apply the ethanolic extract in the form of spray with the objective to develop a more commercial treatment.

6.5 References

(1) F. Artés-Hernández, F. Artés, F.A. Tomás-Barberán, "Quality and enhancement of bioactive phenolics in Cv. Napoleon table grapes exposed to different postharvest gaseous treatments", J. Agric. Food Chem. **51**, 5290-5295 (2003).

(2) M.T. Sánchez Ballesta, J.B. Jiménez , I. Romero , J.M. Orea, R. Maldonado, A. González-Ureña, M.I. Escribano, C. Merodio, "Effect of high CO2 pretreatment on quality, fungal decay and molecular regulation of stilbene phytoalexin biosynthesis in stored table grapes", Postharvest Biol. Technol. **42**, 209-216 (2006).

(3) G. Brundtland, "Our common future: The World Commission on Environment and Development", Oxford, (ed.) Oxford University Press, (1987).

(4) M. Gafsi, B. Legagneux, G. Nguyen, P. Robin, "Towards sustainable farming systems: Effectiveness and deficiency of the French procedure of sustainable agriculture", Agr. Syst. **90**, 226-42 (2006).

(5) C. den Biggelaar, N. Suvedi, "Farmers' Definitions, Goals, and Bottlenecks of Sustainable Agriculture in the North-Ventral Region", Agricult. and Human Val. **17**, 347-58 2000.

(6) N. Shaller, "The concept of agricultural sustainability", Agriculture, Ecosyst. and Env. **46**, 89-97 (1993).

(7) M.J. Kropff, J. Bouma, J.W. Jones, "Systems approaches for the design of sustainable agro-ecosystems", Agr. Syst. **70**, 369-93 (2001).

(8) R. Carson, Silent Spring, Houghton, Miffin, Boston, MA. 1962

(9) M.B. Thomas, "Ecological approaches and the development of "truly integrated" pest management", PNAS USA **96**, 5944-51 (1999).

(10) Y. Elad, "Responses of plants to infection by *Botrytis cinerea* and novel means involved in reducing their susceptibility to infection", Biol. Rev. **72**, 381-422 (1997).

(11) X. Dong, "SA, JA, ethylene, and disease resistance in plants", Curr. Opin. Plant Biol. **1**, 316-23 (1998).

(12) B.J. Feys, J.E. Parker, "Interplay of signalling pathways in plant disease resistance", Trends Genet. **16**, 449-55 (2000).

(13) S.O. Duke, Natural Pesticides from Plant in Advances in New Crops, Janick J. and Simon J.E. Eds., Timber Press, Portland, pp. 511-7 (1990).

(14) T.M. Kutchan, "Ecological Arsenal and Developmental Dispatcher. The Paradigm of Secondary Metabolism", Plant Physiol. **125**, 58-60 (2001).

(15) J. Kuc, "Phytoalexins, Stress Metabolism, and Disease Resistance in Plants", Ann. Rev. Phytopath. **33**, 275-97 (1995).

(16) R. Hammerschmidt, "Phytoalexins: Wath Have We Leearned After 69 Years?", Annu. Rev. Phytopathol. **37**, 285-306 (1999).

(17) M. Barlass, R.M. Miller, T.J. Douglas, "Development of methods for screening gravepines for resistance to downy mildew. II.- Resveratrol production", Am. J. Enol. Vitic. **38**, 65-8 (1987).

(18) P. Jeandet, A.C. Douillet-Breuil, R. Bessis, S. Debord, M. Sbaghi, M. Adrian, "Phytoalexins from the Vitaceae: biosynthesis, phytoalexin gene expressión in transgenic plants, antifungal activity and metabolism", J. Agric. Food Chem. **50**, 2731-41 (2002).

(19) L.L. Creasy, M. Coffee, "Phytoalexin production potential of grape berries", J. Am. Soc. Hortic. Sci. **113**, 230-4 (1988).

(20) P. Langcake, R.J. Pryce, "The production of resveratrol and the viniferins by gravepines in response to ultraviolet irradiation", Phytochem. **16**, 1193-6 (1977).

(21) M. Adrian, P. Jeandet, J. Veneau, L.A. Weston, R. Bessis, "Biological Activity of Resveratrol, a Stilbenic Compound from Grapevines, Against Botrytis Cinerea, the Causal Agent for Gray Mold", J. Chem. Ecol. **23**, 1689-702 (1997).

(22) G.H. Dai, C. Andary, L. Mondolot-Cosson, D. Boubals, "Histochemical Studies on the Interaction between Three Species of grapevine, *Vitis Vinifera, V. rupestris* and *V. rotundifolia* and the downy mildew fungus, Plasmopara viticola", Phys. and Molec. Plant Pathol. **46**, 177-88 (1995).

(23) G. Hoos, R.J. Blaich, "Influence of Resveratrol on Germination of Conidia and Mycelial Growth of Botrytis Cinerea and Phomopsis Viticola", J. Phytopathol. **129**, 102-10 (1990).

(24) P. Sarig, Y. Zutkhi, A. Monjauze, N. Lisker, R. Ben-Arie, "Phytoalexin elicitation in grape berries and their susceptibility to Rhizopus Stolonifer", Phys. and Molec. Plant Pathol. **50**, 337-47(1997).

(25) C. Montero, J.M. Orea, M.S. Muñoz, R.F. Lobo, A. González Ureña, "Non volatile Analysis in Fruits by Laser Resonant Ionization Spectrometry: Application to Resveratrol in Grapes", Appl. Phys. B **71**, 601-5 (2000).

(26) J.M. Orea, A. González Ureña, Measuring and Improving the Natural Resistance of Fruit. In: Jongen w. Ed. Fruit and Vegetable Processing: Maximising Quality, Woodhead Publishing Ltd. Cambridge (UK), pp. 233-266 (2002).

(27) C. Montero, S.M. Cristescu, J.B. Jiménez, J.M. Orea, S. Te Lintel Hekkert, F.J.M. Harren, A. González Ureña, "A Dynamical Study by High-Resolution Laser-Based Techniques", Plant Physiology **131**, 129-38 (2003).

(28) A. González Ureña, J.M. Orea, C. Montero, J.B. Jiménez, J.L. González, A. Sánchez, M. Dorado, "Improving Post-Harvest Resistance in Fruits by External Application of *trans*-Resveratrol" J. Ag. & Food Chem. **51**, 82-9 (2003).

(29) J.B. Jiménez, J.M. Orea, C. Montero, A. González Ureña , E. Navas, K. Slowing, M.P. Gómez-Serranillos, E. Carretero, D. De Martinis, "Resveratrol treatment controls microbial flora, prolongs shelf life, and preserves nutritional quality of fruit", J. Agric. Food Chem. **53,** 1526-302005

(30) J.M. Orea, C. Montero, J.B. Jiménez, A. González Ureña, "Analysis of trans-Resveratrol by Laser Desorption Coupled with Resonant Ionisation Spectrometry. Application to trans-Resveratrol Content in Vine Leaves and Grape Skin", Anal. Chem. **73**, 5921-9 (2001).

(31) *Official Methods of Analysis of AOAC INTERNATIONAL* (2000) 17th Ed., AOAC INTERNATIONAL, Gaithersburg, MD, USA, Official Method 966.23.C

(32) J. Morcillo Rubio, R. Madroñero Pelaez, Aplicaciones Practicas de la Espectroscopia Infrarroja. Facultad de Ciencias. Universidad de Madrid. Madrid 1962. Table 3.

(33) M. Hese, H. Meier, B. Zeeh, Métodos espectroscópicos en Química Orgánica, 2nd Ed. Síntesis, S.A. Madrid, 2005.

Chapter 7

Summary and Conclusions

In all the studies carried out in this Doctoral Thesis, the use of Raman spectroscopic techniques -in particular, Transmission Raman and Resonance Raman or the combination of both– plays a central role. This work has shown the advantages of the Transmission Raman technique respect to conventional Raman due to its geometric configuration and its lack of sensitivity to the sample surface, operational features that increase the signal to noise ratio and reduce the fluorescence background.

Furthermore, it has been demonstrated that the Transmission Raman spectroscopy can be further developed by its combination with the Resonance Raman effect. Indeed, in terms of instrumental development the design, building and setting up of a new technique based on Transmission Resonance Raman Spectroscopy (TRRS), one of the main motivations of the present Doctoral Thesis, was successfully achieved.

The technique, was applied to the carotenoid (mostly β-carotene) analysis in standard and carrot samples, reaching a LOD and LOQ of hundreds of picograms and a few nanograms per cubic millimetre, respectively, and giving β-carotene content values in carrots of 17.3 mg / 100g carrot (consistent with the bibliographic records).

In addition, the developed TRR spectrometer can be also applied to monitor the carotenoid spatial distribution in fruits and the Raman signal dependence on the sample thickness. The latter dependence was rationalized using a theoretical model that satisfactorily describes the experimental measurements.

The reaction mechanism and kinetic of some catalytic reactions in proteins were also studied by Resonance Raman Spectroscopy (RRS) and UV-visible absorption. In particular, we studied the catalysis of trans-resveratrol (t-res) induced by the enzyme tyrosinase (ty) by RRS and UV-Vis absorption spectroscopy.

The UV-Vis absorption permitted to assess first-order kinetics for this reaction. As well the use of Resonance Raman Spectroscopy, allowed the detection of reaction intermediates crucial for the understanding of some key features and steps of the catalytic reaction. This investigation is relevant to the discovery of potential inhibitors in the melanin synthesis pathway, which is catalyzed by the ty, and nowadays received substantial attention in melanoma research.

In the course of this Thesis laser photons have been used not only as part of the analytical method but as an (abiotic) agent to induce photochemical changes in fruit which ultimately could improve its health status. That is, the use of laser light as a way (i) to induce the abiotic stress in table grapes in order to elicitate secondary metabolites such as trans-resveratrol, or carotenoids, and (ii) to measure their internal enhancement using the well-developed TRR technique described earlier. A Transmission Resonance Raman spectrometer based on an Ar+ laser of 514.5 nm excitation wavelength was also setup. The apparatus uses a 360° rotating holder where the grapes receive the UV-B LED radiation. After the grapes' irradiation, their carotenoid content is

analyzed by the TRR spectrometer as a function of elapsed time, noting a significant increase of β-carotene content in white grape after 24 hours of the fruit irradiation.

Furthermore, the same type of studies were carried out with table grapes but using UV laser light, instead of UV-B LED light, as the photon source to elicitate the trans-resveratrol content in grapes. Two different wavelengths were employed, one resonant with the trans-resveratrol bi-photon absorption band at 302.1 nm, and another non resonant at 300 nm. Attenuated Total Reflectance Fourier Transformed Infrared and Microbiological Analysis showed an enhancement of polyphenols' content and an enhanced grape resistance to microbial infection respectively, when the resonant wavelength was employed.

Finally, one of the last studies implemented in the course of the Thesis was focused on the use of natural pesticides present in the own plant to improve the postharvest quality rather than using laser photons, controlled atmospheres or chemical pesticides. This investigation was carried out to assess the capability of trans-resveratrol as natural bio- pesticide to improve the quality of postharvest grapes. For this purpose, a natural extract from vine leaves was prepared. Spectroscopic and microbiological analysis demonstrated how the use of such natural bio-pesticides led to a significant improvement in the grape's natural resistance to microbial infections.

In what follows, a short description of the main conclusions drawn from the present work is outlined:

1. A new Transmission Resonance Raman (TRR) Spectrometer has been set up in our laboratory combining the enhanced sensitivity of Resonance Raman and the

low fluorescence background of the Transmission Raman. The technique is fast, non-invasive and ideal for solid samples showing significant diffuse scattering.

The TRR spectrometer was applied to the analysis of carotenoid in fruit and particularly to the β-carotene content of carrots roots as well as the carotenoid dependence on sample thickness. A detection limit of hundreds of picograms per cubic millimetre was reached which is far below the typical contents of the pigments in fruit. Furthermore, a theoretical model of scattering propagation has been developed which accounts very satisfactorily for the signal dependence on sample thickness.

2. UV-Vis Absorption and Resonance Raman Spectroscopy have been used to monitor the kinetics and mechanism of enzymatic reactions specifically that of t-res-ty catalytic reaction. While the UV-Vis absorption permitted the investigation of the reaction kinetics, suggesting the presence of first-order kinetics, the time evolution of the RRS spectroscopic features revealed the existence of two reaction intermediates in this important enzymatic reaction, which in turn allowed the deciphering of the reaction pathway.

3. Thanks to the information obtained in point **2** it was possible to outline a detailed mechanism for the enzymatic reaction in which the following main steps were established: (i.) the formation of the t-res–ty ^{S}P complex with its O–O bridge playing a crucial role in the first steps. A reaction intermediate has been observed whose main resonant Raman signature was observed at 753 cm^{-1} and assigned to the weakened O-O stretching of a μ–η^2: η^2–peroxodicopper (II) species featuring the ty-t-res ^{S}P complex. (ii) The

hydroxylation of the ortho C–H bond of the t-res employs one of the O atoms from the peroxide bridge and occurs *after* O–O bond cleavage in the ty active centre. (iii) The final step of the enzymatic reaction involves an intermediate complex whose resonantly enhanced ν_S (Cu–O(φ)–Cu) or ν_{AS} (Cu-O(φ)-Cu) vibrational modes were assigned to the observed 642cm^{-1} Raman Stokes line. As a result, one of the main conclusions drawn from this investigation was that potential inhibitors of tyrosinase oxidation must be able to bind to the two Cu (II) ions of the bidentate form.

4. With regard to the research line dedicated to "Laser photons and healthy fruit", UV-B LED photons were employed not only as part of the analytical method, but also as an (abiotic) agent to induce photochemical changes in fruits. Hence the TRRS technique was used to monitor the elicitation of the β-carotene content of UV-B LED irradiated grapes as a function of time elapsed since fruit irradiation. It was found that the β-carotene content in grapes increased five-fold with respect to the grape control (i.e. those that received no irradiation). The relevance of this work relies on the use of low doses of UV-B light, as well as in employment the LED technology, opening the way to develop low cost commercial protocols for postharvest improvement of fruit, food and vegetable quality.

5. With respect to the use of laser photons, table grapes were irradiated with UV light rather than UV-B LED light. Upon resonant controlled UV-irradiation of the grape skin, a selective enhancement of the polyphenols content (trans-resveratrol) was found which was rationalized in terms of the polyphenol enhanced

biosynthesis due to electronic excitation following the precursor two-photon resonant absorption. The relevance of this investigation relies on the selective character of the employed photons as they are selected to be resonantly absorbed by trans-resveratrol. The used of ATR-FTIR and microbiological analysis showed an enhancement of polyphenols' content and of the table grape resistance to microbial infection respectively, when the resonant wavelength was employed.

6. With regards to the question "Are photons strictly necessaries for improving the fruit quality"? The answer is afirmative if one looks for direct and non-invaisve methods. Nevertheless, it should be noted that a significant improvement of the post-harvest resistance of grapes can be obtained by immersing these fruits in a vine leaves' extract. The observed positive influence of natural extracts was attributed to the presence of polyphenols as evidenced by their IR and laser spectroscopy, as well as by their microbiological analysis.

Certainly, the use of natural extracts containing the own plant bio-pesticides improves the fruit quality, but, when available, appropriate laser photons or even UV-B LED light can be a much more efficient, fast and non-invasive method to improve the post-harvest fruit quality. All in all, one could say that appropriate photons and healthy fruit go hand to hand.

Resumen en Español: Introducción, Objetivos, Conclusiones y Aportaciones Fundamentales de la Tesis Doctoral

Cápitulo 8

Introducción: Espectroscopia Raman, Objetivos y Estructura de la Tesis

8.1 Introducción a la Espectroscopia Láser

El láser ha revolucionado el mundo de la ciencia y la tecnología en múltiples de sus campos como, por ejemplo, de la Espectroscopia, área científica de gran relevancia para el estudio de la estructura y dinámica molecular así como para el análisis químico[1,2] . La Espectroscopia[3,4] se basa en la interacción de los átomos y moléculas existentes en la materia con la radiación electromagnética. Esta radiación, es la combinación de un campo eléctrico y magnético oscilante, perpendiculares entre si, que se propaga a través del espacio transportando energía de un lugar a otro. La radiación electromagnética se extiende a toda una serie de regiones del espectro, como por ejemplo, la radiación infrarroja, luz visible (radiación visible), rayos X o rayos gamma.

La radiación electromagnética se caracteriza por la **longitud de onda** λ o la **frecuencia** ν. La **longitud de onda** es la distancia entre crestas sucesivas. Un **ciclo** es la parte de una onda que hay entre dos crestas sucesivas (o entre otros dos puntos cualesquiera sucesivos que tengan la misma fase). La **frecuencia** es el número de ciclos que pasan por un punto dado en la unidad de tiempo[5].

Estas magnitudes se describen en la Figura 8.1 y están relacionadas entre sí por la siguiente ecuación:

$$\nu \cdot \lambda = c \qquad (1)$$

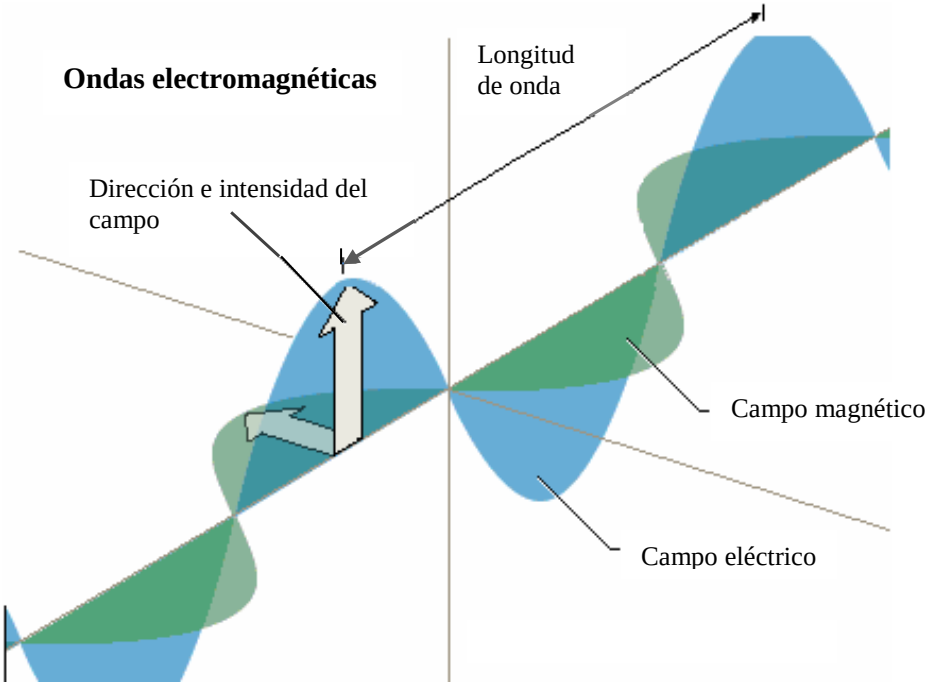

Figura 8.1: Diagrama representativo de la propagación de una onda electromagnética. Adaptada de http://www.google.es/search?q=radiación+electromagnetica

dónde c es la **velocidad de la luz** (en el vacío c = 2,997928·10^8 m·s^{-1})**.** Un cuanto de luz (fotón) de frecuencia ν posee una energía, E, dada por:

$$E = h \cdot \nu = \frac{h \cdot c}{\lambda} = h \cdot c \cdot \ddot{\upsilon} \; ; \; \ddot{\upsilon} = \frac{1}{\lambda} \qquad (2)$$

Donde h es la constante de Planck, ν la frecuencia del campo electromagnético oscilante, c la velocidad de la luz, λ la longitud de onda y ῡ es el numero de onda o inverso de λ que generalmente suele medirse en cm^{-1}. Los métodos espectroscópicos hacen uso de la radiación electromagnética utilizando **longitudes de onda λ** comprendidas entre 200 nm hasta unos pocos μm.

Las zonas espectrales de la radiación electromagnética en su totalidad se ilustran en la Figura 8.2.

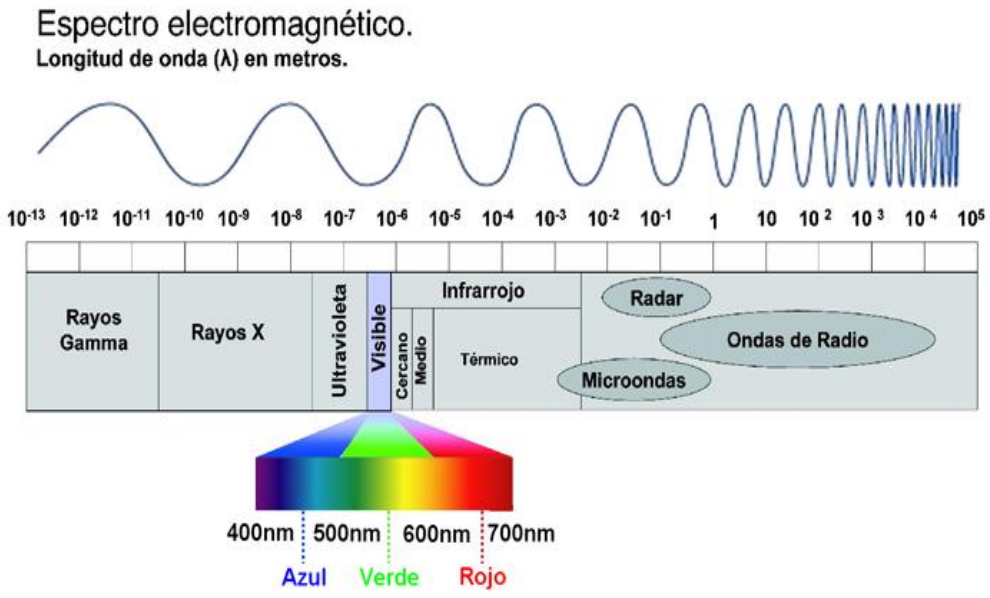

Figura 8.2: Esquema ilustrativo del espectro de la radiación electromagnética. Adaptada de http://www.google.es/search?q=radiacion+electromagnetica

En espectroscopia se estudia la absorción y emisión de radiación electromagnética por la materia. En un sentido más amplio la espectroscopia trata de todas las interacciones de la radiación electromagnética con la materia y por ello contempla también la de la dispersión y transmisión de la radiación. La intensidad de radiación absorbida por una muestra en función de la frecuencia es su **espectro de**

absorción, y en consecuencia, la intensidad de radiación emitida por dicha muestra en función de la frecuencia es su **espectro de emisión**.[3,4] En la espectroscopia láser[2,6] la radiación electromagnética usada procede de un láser. El láser se ha convertido en una herramienta potente en el campo de las ciencias experimentales. Esto es debido a las propiedades específicas de la luz láser: Entre otras podemos citar:

-su brillo

-Su monocromacidad y sintonizabilidad

-Su direccionabilidad.

-Su coherencia temporal y espacial

-Su polarización.

-La capacidad de analizar moléculas usando pulsos ultracortos, como por ejemplo femtosegundos (1 fs $=10^{-15}$s).

El brillo, también llamado radiancia, se define como la potencia emitida por la fuente laser por unidad de superficie emisora y por unidad de ángulo solido. El gran brillo de la luz láser no solo se debe a su escasa divergencia angular sino también a su alta intensidad. Gracias a su gran radiancia la luz laser se puede enfocar con toda su intensidad en zonas de tamaño muy reducido. Ello hace posible aplicaciones industriales como el perforado y mecanizado de materiales o el corte de tejidos en medicina al usarse como un bisturí óptico. En investigación fundamental los láseres de

una alta potencia hacen posible la espectroscopia no lineal produciendo fenómenos de excitación y fragmentación molecular por absorción multifotonica.[2,4,6]

La alta monocromacidad y sintonizabilidad de la luz láser son dos características que hacen posible la alta resolución de la espectroscopia láser. Determinados fenómenos de interacción de radiación láser con moléculas pueden llegar a ser muy selectivos, lo que permite la excitación y análisis de determinados grupos funcionales moleculares y dinámicas de reacción moleculares que absorben radiación láser a longitudes de onda especificas. Uno de los campos donde esta gran pureza espectral de la luz laser tiene mayor aplicación es en química analítica dado de que cada molécula o átomo tiene su espectro de absorción característico a unas determinadas longitudes de onda.

En la mayoría de los láseres la salida de luz láser está polarizada. La radiación electromagnética se puede propagar en múltiples planos de polarización, determinados por dos vectores: uno la dirección de la propagación de la onda electromagnética y otro perpendicular a esta, determinado por el campo eléctrico. Cuando el campo eléctrico esta dirigido verticalmente a la dirección de propagación de la luz se habla de luz polarizada verticalmente. Si esta dirigido perpendicular a la propagación pero formando un plano horizontal con la dirección de propagación, se dice entonces que la luz esta polarizada horizontalmente. Por ultimo si el campo eléctrico esta dirigido perpendicularmente a la dirección de propagación pero a su vez en todas las direcciones dentro de un plano perpendicular al de propagación se habla de luz no polarizada.

Este carácter polarizador le proporciona una característica indispensable para el estudio de la dinámica de las reacciones químicas y sus propiedades vectoriales como

suele estudiarse en Estereodinámica. Asimismo la polarización de las líneas espectroscópicas tanto en Raman como en Infrarrojo constituye una información básica para dilucidar el mecanismo de la interacción radiación materia y la estructura molecular.

La coherencia de la luz laser es una de sus propiedades más notables. Esta propiedad esta directamente relacionada con la monocromaticidad de la luz laser. Si un haz laser es poco monocromático, es decir tiene un gran ancho de banda (si dicho ancho fuese muy grande se convertiría en una lámpara muy potente), las ondas que lo forman acabarían desfasándose unas de otras en poco tiempo y diríamos que su coherencia temporal es muy pequeña.

Si por el contrario el ancho de banda del laser es muy estrecho los fotones emitidos representados por sus respectivas ondas de radiación electromagnética se hallarían en fase, podrían viajar un determinado tiempo sin desfasarse. Se dice entonces que la radiación tiene una coherencia muy grande. Esta coherencia asociada al desfase a lo largo de la dirección de propagación del laser se define como coherencia temporal o longitudinal. Por el contrario la coherencia espacial esta asociada a la fase en la dirección perpendicular a la dirección de propagación de la luz laser.

La coherencia temporal, hace posible la existencia de láseres pulsados, permitiendo el estudio de reacciones ultra-rápidas, utilizando técnicas de excitación láser en escalas de tiempo ínfimas tales como el femtosegundo (10^{-15}s). Estas técnicas permiten estudiar los procesos químicos como la ruptura de un enlace o biológicos como la fotosíntesis en tiempo real .[2,6] Una de las principales aplicaciones de la

coherencia de la luz laser es la holografía, es decir la técnica de producción de imágenes tridimensionales.

8.2 Fundamentos de la Espectroscopia Raman

Durante décadas se han perseguido y han sido de interés universal los misterios e información que nos desvela la luz. Desde que la luz proveniente del Universo alcanza la Tierra, con información de la composición y propiedades de objetos celestiales así como del origen del Universo, se convierte en una de las herramientas más preciadas objeto de estudio e investigación.

Supongamos una colisión entre un fotón con frecuencia ν_0 y una molécula, la mayoría de la luz se transmite, parte es absorbida y otra parte es dispersada. La Espectroscopia Raman (RS) es la ciencia que estudia el fenómeno de la dispersión de la luz. La colisión fotón-molécula puede dispersar el fotón, es decir, puede cambiar la dirección del movimiento del fotón y su energia[5,6]. En esta interacción, se produce una absorción instantánea del fotón el cual es inmediatamente re-emitido. Por ello la molécula puede pasar del estado fundamental S_0 a un estado más energético, denominado estado virtual (línea discontinua en Figura 8.3), ya que no es un estado propio de la molécula y no llega a ser un estado excitado S_1. Inmediatamente después la molécula sufre una desactivación energética y vuelve al estado fundamental S_0. Este fenómeno de dispersión de la luz, se representa en la Figura 8.3.

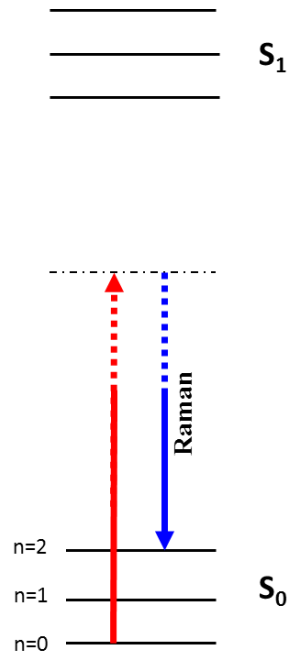

Figura 8.3: Diagrama de Dispersión Raman.

La mayoría de los fotones dispersados tienen la misma frecuencia que la radiación incidente denominándose "dispersión elástica o Rayleight". Sin embargo una pequeña fracción de fotones dispersados intercambian energía con la molécula produciéndose un cambio en su frecuencia. Este fenómeno se denomina efecto "**Raman o dispersión inelástica**", predicha por Kramers and Heisenberg[7] y observado por primera vez por C.V. Raman y K. S. Krishnan[8] en 1928, de ahí el nombre de la espectroscopia y a su descubridor le fue concedido el Premio Nobel de Física 1930. Sea v_0 y v_{disp} las frecuencias del fotón incidente y el fotón Raman dispersado, respectivamente.

El aumento o disminución en su frecuencia (v) da como resultado una variación en ésta, denominada "desplazamiento Raman" o "Raman Shift" representado por $\Delta\nu_R$, objeto de medida en los espectros Raman. En esta variación de la frecuencia Δv_R se obtienen frecuencias menores $\Delta v_R = (v_0 - v_{disp}) > 0$, llamadas Stokes, o mayores $\Delta v_R = (v_0$

- ν_{disp}) < 0, llamadas Anti-Stokes. Tal como se observa en las Figuras 8.4 y 8.5, las líneas Stokes (Anti-Stokes) aparecen a la derecha (izquierda) de la línea de excitación cuando se usa la longitud de onda de la radiación dispersada.

Sean E_a y E_b las energías de las moléculas antes y después de que se disperse el fotón. La conservación de la energía implica,

$$h\nu_0 + E_a = h\nu_{disp} + E_b \text{ , o} \tag{3}$$

$$\Delta E \equiv E_b - E_a \equiv h(\nu_0 - \nu_{disp}) \equiv h\Delta\nu_R \tag{4}$$

La diferencia de energía ΔE es la diferencia entre las energías de dos estados estacionarios de la molécula; por tanto; la medida del **desplazamiento Raman** o **Raman Shift** $\Delta\boldsymbol{\nu_R} \equiv \boldsymbol{\nu_0} - \boldsymbol{\nu_{disp}}$ da los espaciados de niveles energéticos moleculares.

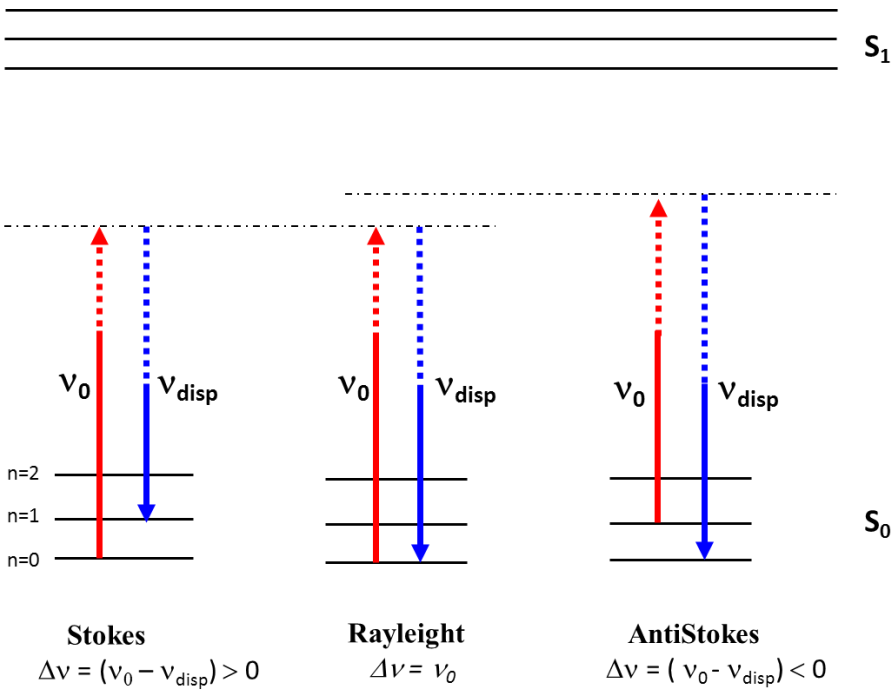

Figura 8.4: Diagrama de nivel de energía de la dispersión Rayleigh, Sokes y Antistokes Raman.

Antes del advenimiento del láser la fuente de radiación era una lámpara y por lo general se usaba una línea de mercurio atómico y la luz dispersada se observaba por medio de una placa fotográfica y tiempos de exposición muy largos.

Dado que las líneas Anti-Stokes parten de un estado vibracionalmente más excitado que el estado inicial, de menor población electrónica, las líneas Antistokes tienen menor intensidad Raman que las Stokes, tal como se ve en la Figura 8.5.

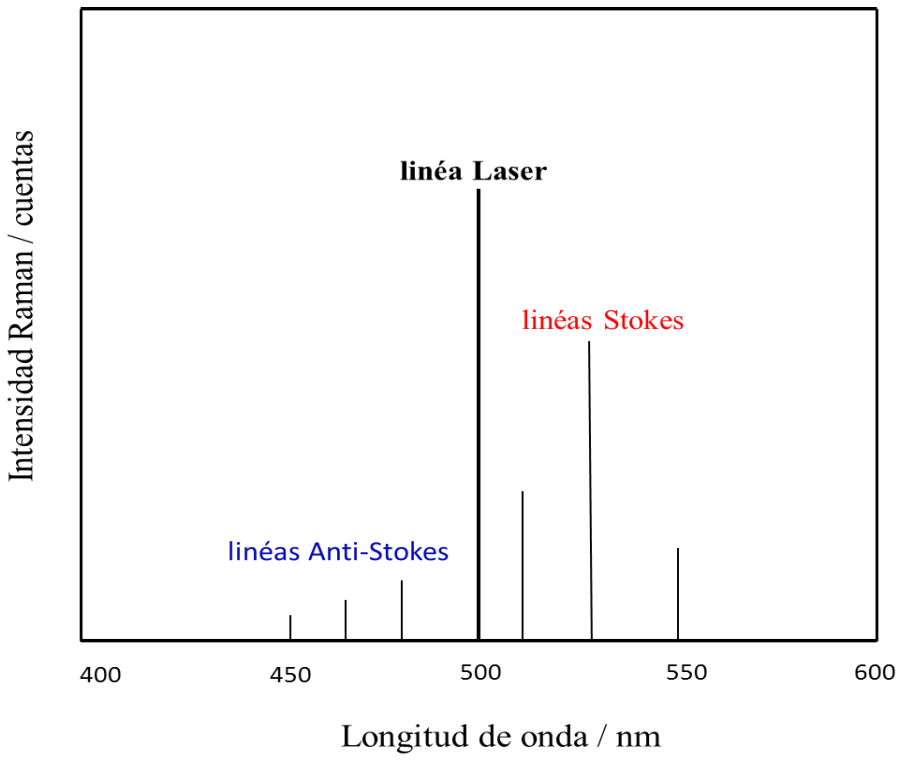

Figura 8.5: Espectro Raman simulado Stokes y Anti-Stokes.

Respecto a las unidades en que viene expresado un espectro Raman, el eje x puede medirse en longitudes de onda (wavelenght, λ, nm), tal como se observa en la Figura 8.5, aunque actualmente se ha impuesto la utilización del desplazamiento Raman $\Delta\bar{\upsilon}_R$ en, cm^{-1}.

Aparte del fenómeno Raman descrito arriba, existen una serie de procesos fotofísicos, que pueden suceder tras la absorción de un fotón por parte de una molécula.

Todos estos procesos se ven reflejados en el **diagrama de Jablonski** indicado en la Figura 8.6 y son de vital importancia en Fotofísica y Fotoquímica.

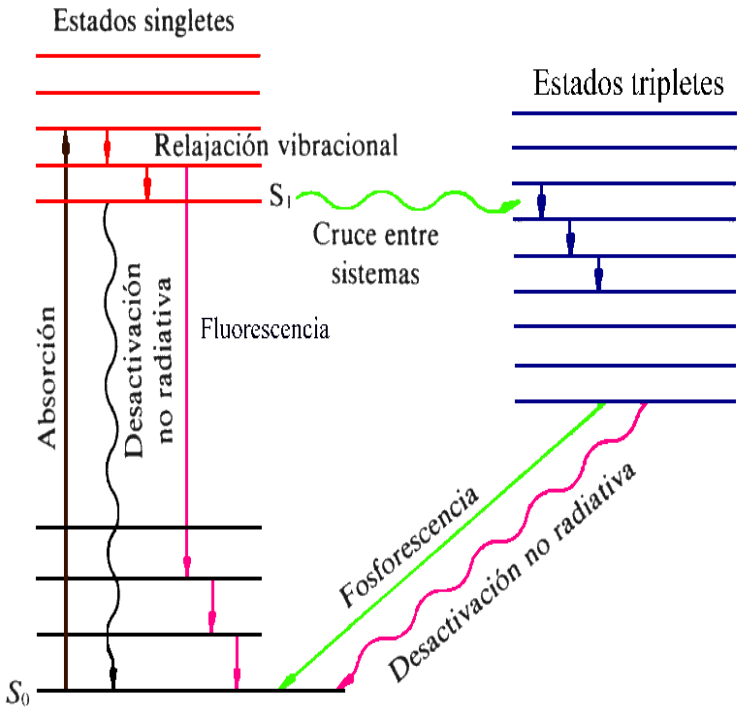

Figura 8.6: Diagrama de Jablonski

En el proceso de **absorción**, durante la interacción fotón-molécula, el fotón es absorbido por la misma pasando del estado fundamental S_0 (estado electrónico denominado singlete fundamental), con todos los espines electrónicos apareados, a un estado electrónico excitado S_1 (singlete excitado) menos poblado. El proceso de absorción se representa por $S_0 + h\nu \rightarrow S_1$. Las transiciones electrónicas en este proceso de absorción tienen un tiempo de vida excesivamente corto de 10^{-15}s como para implicar desplazamientos nucleares significativos según el Principio de Frank-Condon.

Después, el estado excitado S_1 de la molécula puede transferir su energía a otra molécula durante la colisión, volviendo así al estado fundamental S_0, proceso denominado desactivación no radiativa ("quenching"), el cual puede observarse en el diagrama de Jablonski en su parte izquierda mediante una línea ondulada. También

pueden darse colisiones intermoleculares, las cuales transfieren la energía vibracional extra a otras moléculas, dando lugar a que en el estado S_1, la molécula pierda la mayor parte de su energía vibracional hasta alcanzar el estado vibracional más bajo de S_1, proceso llamado **relajación vibracional**[9].

La molécula en el estado $\nu = 0$ de S_1 puede sufrir una transición sin radiación a un estado electrónico diferente. Si ambos estados son singletes por ejemplo si se trata de la transición no radiativa $S_1 \rightarrow S_0$ donde la energía electrónica de este ultimo es inferior a la inicial, entonces debido al principio de conservación de la energía, tendría lugar una conversión de la energía electrónica a energía vibracional. Este proceso se denomina **conversión interna** ($S_1 \rightarrow S_0$) si no hay cambio de multiplicidad. Si por el contrario uno es estado singlete y otro triplete o viceversa, es decir si cambia la multiplicidad, entonces este proceso se llama **cruce entre sistemas.**

El estado excitado S_1 de la molécula puede perder energía electrónica por emisión espontánea de un fotón, cayendo de nuevo a un estado singlete mas bajo del estado fundamental S_0. El proceso que ocurre es: $S_1 \rightarrow S_0 + h\nu$. Produciéndose entonces una emisión de la radiación por una transición electrónica en la cual no cambia su espín total electrónico ($\Delta S = 0$), la cual se denomina **fluorescencia**. El proceso de fluorescencia se ve favorecido en gases a muy baja presión, ya que el tiempo entre colisiones es relativamente largo. Un tiempo de vida típico de un estado S_1 es 10^{-8}s en ausencia de colisiones.

Por otra parte el triplete T puede emitir un fotón y caer al estado fundamental singlete S_0. Este proceso de emisión de radiación $T \rightarrow S_0 + h\nu$ se denomina **fosforescencia**. La fosforescencia viola la regla de selección general de conservación

del espín ΔS=0, por lo que existe una mínima probabilidad de que ocurra. El tiempo de vida del estado triplete excitado más bajo suele ser de 10^{-3} a 1s, en ausencia de colisiones.

El tratamiento clásico de la dispersión Raman (véase referencia 10, capítulo 3) se basa en la inducción de un dipolo eléctrico, con momento ($\boldsymbol{\mu_d}$), por el campo eléctrico de intensidad $\boldsymbol{E}$ de la radiación electromagnética incidente. Este momento dipolar eléctrico inducido viene dado por la relación:

$$\boldsymbol{\mu_d} = \boldsymbol{\alpha} \cdot \boldsymbol{E} \qquad (5)$$

La polarizabilidad molecular, **α,** es una medida del grado en que los electrones en la molécula se pueden desplazar con respecto a los núcleos.[4] En general la polarizabilidad de una molécula, es una propiedad anisotrópica, lo que significa que, a igual distancias desde el centro de la molécula, **α** puede tener diferentes magnitudes cuando se mide en diferentes direcciones. Por ello, por ejemplo, en una superficie dibujada en que la distancia desde el origen a un punto cualquiera en dicha superficie tiene la longitud $\boldsymbol{\alpha}^{-1/2}$, donde α es la polarizabilidad en esa dirección, forma una elipse, presentando secciones transversales elípticas en los planos xz y xy, tal como se ilustra en la Figura 8.7.

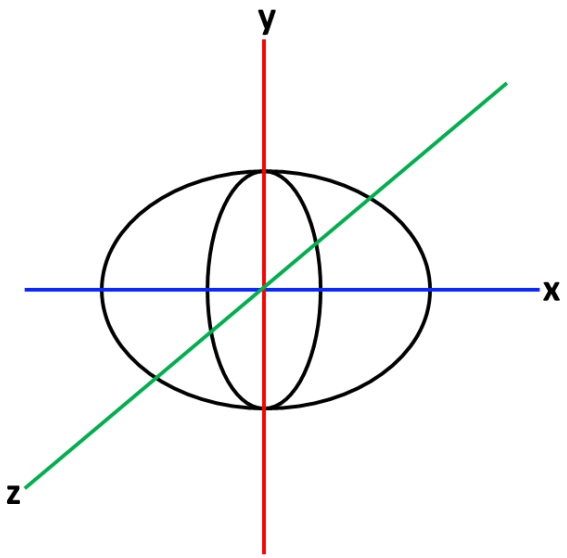

Figura 8.7: Elipse de la Polarizabilidad molecular

De este modelo derivan las reglas de selección particulares de la dispersión Raman; las cuales postulan que cualquier vibración molecular que cambie la polarizabilidad molecular (**α**) será activa en Espectroscopia Raman es decir, podremos verla en el espectro Raman[6,11].

Por el contrario en el caso de la Espectroscopia de Infrarrojo (IR) el modelo difiere, siendo las reglas de selección diferentes, únicamente serán activas aquellas vibraciones moleculares que inducen un cambio en el momento dipolar eléctrico permanente de la molécula (**μ**), apareciendo así en su espectro de IR. En la mayoría de los casos las vibraciones moleculares que son inactivas en Raman son activas en IR y viceversa. Es por ello por lo que se las considera dos técnicas espectroscópicas complementarias.

Según el Principio de exclusión mutua, para una molécula con centro de simetría la misma vibración no puede ser activa en Raman e IR simultáneamente. Así pues, las

vibraciones moleculares simétricas están prohibidas en IR, es decir no son activas, pero si lo son en Raman. Por el contrario las vibraciones moleculares asimétricas son inactivas en Raman pero presentan actividad en IR. Véase ejemplo en la Figura 8.8 donde se señalan dos modos de vibración para la molécula de CO_2.

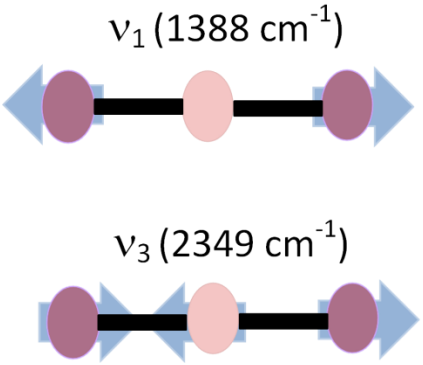

Figura 8.8: Vibraciones ν_1 y ν_3 para el CO_2. Arriba) Vibración de tensión simétrica, no hay cambio en el momento dipolar μ (inactiva en IR, activa en Raman). **Abajo)** Vibración de tensión asimétrica (cambio en el momento dipolar μ, activa en IR, inactiva en Raman).

8.3 Espectroscopia Raman Resonante

La dispersión Raman convencional es un proceso de una muy baja probabilidad (uno de cada 10^7 fotones); pero esta puede verse aumentada en varios ordenes de magnitud si el haz de luz de excitación tiene la misma energía de absorción electrónica de la especie a estudiar. Esto aumenta considerablemente la intensidad de la radiación Raman asociada a los modos vibracionales localizados en la región molecular que es responsable de la absorción electrónica a ν_0. En la figura 8.9 se muestra que en la interacción fotón molécula el fotón es absorbido por la molécula llegando hasta el estado excitado S_1. Por lo que el proceso de dispersión se asocia a los verdaderos estados excitados de la molécula.

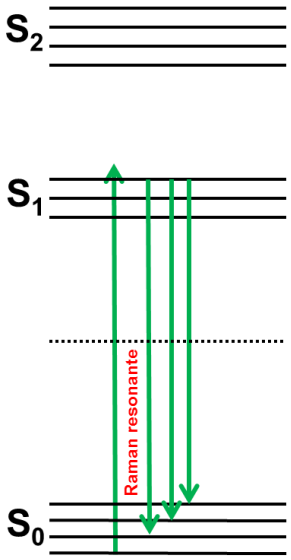

Figura 8.9: Diagrama de dispersión Raman Resonante

La intensidad ***I*** de señal Raman para cualquier modo vibracional normal es proporcional a la intensidad de potencia del laser $\boldsymbol{I_0}$, al cuadrado de $\boldsymbol{\alpha}$ (polarizabilidad) y a la cuarta potencia de la frecuencia $\boldsymbol{\nu_0}$ de acuerdo con la siguiente formula:[6,11,12]

$$I \sim I_0 \ * \ \nu_0^4 * \alpha^2 \qquad (6)$$

De esto se deduce que *I* tiene una relación de fuerte dependencia con la longitud de onda de la luz del laser: al pasar de 1000 nm a 250 nm, su frecuencia ν_0 aumenta 4 veces, por lo que *I* aumenta 256 veces.[6,11,12] Por lo que es preferible el uso de longitudes de onda de excitación cortas. Sin embargo, en la práctica hay un inconveniente causado por la gran interferencia con la fluorescencia. Incluso con el uso de longitudes de onda de excitación cortas, el proceso de dispersión Raman es de muy baja probabilidad, tal y como hemos mencionado anteriormente solo una porción muy pequeña de los fotones

incidentes serán dispersados y una fracción aun minoritaria sufrirá dispersión inelástica o Raman.

Esta es la razón del lento progreso de la RS en las primeras décadas inmediatamente posteriores a su descubrimiento. Después, con el desarrollo del láser, mejora en la rapidez de la técnica y el uso de detectores cada vez más sensibles; tuvo lugar un gran avance en el campo de las aplicaciones de la RS, resurgiendo nuevas variantes mejoradas tales como espectroscopia Raman Resonante (RRS), entre otras. Cabe destacar que para una molécula iluminada por la longitud de onda de excitación incidente, la polarizabilidad **α** es inversamente proporcional a la diferencia entre la energía del fotón incidente y la energía de una transición electrónica determinada, $S_i \rightarrow S_0$. De esta forma la intensidad de una línea Raman viene dada para el modelo resonante por la expresión[10]

$$I \sim I_0 \frac{\nu_0^4}{(\nu_{S_i - S_0} - \nu_0)^2 + \mathbb{\Gamma}^2} \qquad (7)$$

Dónde $\mathbb{\Gamma}$ es la anchura de la transición electrónica. Esta anchura evita que cuando $\nu_0 = \nu_{S_i - S_0}$, es decir en la resonancia, la intensidad Raman se haga infinita. A medida que ν_0 tiende a $\nu_{S_i - S_0}$ el denominador disminuye considerablemente y la intensidad Raman aumenta varios órdenes de magnitud. Este proceso se denomina espectroscopia Raman Resonante (RRS).[13] De esta forma, el aumento de la sensibilidad en RRS frente a las condiciones no resonantes en RS viene compensado con la perdida de información, debido a que el aumento en la sensibilidad es selectivo. De tal forma que no todas las señales correspondientes a las vibraciones de la molécula de interés a estudiar en una

matriz se ven mejoradas por RRS, sino solo algunas de ellas con correspondientes grupos funcionales o modos de vibración totalmente simétricos[14] y que interaccionan con el estado resonante. No obstante ello simplifica el espectro y permite el estudio de muestras y procesos inaccesibles por otros medios como se discutirá más adelante.

La fluorescencia es un proceso aproximadamente 10^6 veces más probable que la dispersión Raman, por lo que puede llegar a interferir la intensidad Raman de una forma muy significativa. Por ello podemos concluir que la interferencia con la Fluorescencia es uno de los mayores problemas que presenta la RRS. Sin embargo longitudes de onda de excitación mayores son utilizadas generalmente debido a que se elimina la posible interferencia de fluorescencia, ya que poseen energías fotónicas menores.

Así pues, podríamos mencionar varias ventajas importantes de la espectroscopia de resonancia Raman en el estudio de moléculas biológicas, tales como: **a**) el aumento de la intensidad de señal Raman lo que permite el estudio de disoluciones muy diluidas (10^{-3} a 10^{-6} mol/dm^3) características de biopolímeros en organismos; **b**) la selectividad en el aumento de la intensidad únicamente en las vibraciones en una parte de la molécula, simplificando el espectro y permitiendo el estudio de los enlaces en esa región. Normalmente suelen ser grupos funcionales de la molécula coloreados que tienen bandas de absorción en el visible (llamados cromóforos o centros activos), cuyas longitudes de onda de absorción o frecuencias pueden utilizarse para la excitación y obtener así el deseado efecto Raman resonante. Podemos citar como ejemplo el estudio del grupo cromóforo o centro activo hemo en la hemoglobina y mioglobina[15]. **c)** debido a la inactividad Raman de la molécula de H_2O, el agua se ha convertido en un

disolvente de moléculas biológicas comúnmente usado en RRS dada su poca interferencia con la señal Raman de la muestra biológica.

8.4 Espectroscopia Raman de Transmisión

8.4.1 ¿Qué es?

La Espectroscopia Raman de Transmisión (TRS) es una variante de la Espectroscopia Raman convencional idónea para investigaciones a granel de muestras de dispersión difusa. La TRS se produce debido a que la luz se dispersa a través de materiales o medios turbios que no absorben o bloquean la luz de manera significativa. De manera similar a la Espectroscopia Raman con Separación Espacial (Spatially Offset Raman Spectroscopy SORS), en el proceso de Transmisión Raman la luz se extiende de forma aleatoria a través de toda la muestra de dispersión difusa. La Transmisión Raman podría considerarse como un ejemplo extremo de SORS.

SORS es una variante de la técnica RS convencional que permite una gran precisión en análisis clínicos de objetos que se encuentran debajo de superficies opacas tales como tejidos, recubrimientos y botellas. Ejemplos de aplicaciones de la técnica SORS son, entre varios, análisis de hueso debajo de la piel[16], comprimidos dentro de botellas de plástico[17] y explosivos dentro de contenedores.[18] La técnica SORS fue inventada y desarrollada por Matousek y colaboradores[19] en el Laboratorio Rutherford Apleton en Ingalterra.

El método pone de manifiesto que la mayoría de los materiales no son completamente transparentes a la luz ni completamente opacos a ésta, y normalmente tienden a dispersar la luz. Un buen ejemplo de ello sería el caso en el que un puntero laser rojo ilumina el final del dedo- la luz se dispersa a través de todo el tejido en el dedo. Donde quiera que vaya esta luz habrá alguna dispersión inelástica debida al efecto Raman, por lo que, en algún momento la mayoría de las partes del objeto generarán señales Raman detectables, incluso las que no se hallan en la superficie de dicho objeto.

Un análisis típico de SORS realizará como mínimo dos espectros Raman; uno en la superficie y otro a una distancia de pocos milímetros de la zona de iluminación. Los dos espectros pueden restarse utilizando una escala de substracción que producirá los espectros que representan la sub-superficie y la superficie. Dicha configuración geométrica de la técnica SORS se ilustra más adelante en la Figura 8.10.

En el proceso Raman convencional los fotones se crean en todos los puntos de la superficie de la muestra que la luz atraviesa y se colectan mediante colectores ópticos (lentes, diafragmas etc.). Estos fotones pueden colectarse mediante una configuración geométrica de dispersión hacia atrás (back scattering) o a veces perpendicular, en el cual el haz incidente sobre la muestra y el detector óptico se hallan dispuestos en un ángulo de 180º o en algunos casos en un ángulo de 90º respectivamente, tal como se muestra en la Figura 8.10. Por el contrario en Transmisión Raman los fotones se crean a través de toda la muestra y se colectan mediante una configuración geométrica distinta, en la cual el haz incidente sobre la muestra y el detector óptico se encuentran dispuestos en un ángulo de 0º (en la misma línea), tal como se observa en la Figura 8.10.

Como es bien sabido[20] el proceso de dispersión de luz en Espectroscopia Raman convencional tiene sus limitaciones, sólo uno de cada 10^6-10^8 fotones se dispersa obteniendo así una señal Raman débil. A su vez la Espectroscopia Raman convencional plantea el problema de que la señal producida suele ser representativa de la superficie o superficie-cercana de la muestra, siendo por ello una señal muy débil.

Por otro lado, otra de sus limitaciones, es la interferencia que presenta con la señal de fluorescencia en la región UV-Visible; por lo cual una forma de eliminar esta interferencia sería la aplicación de longitudes de onda de excitación mayores cercanas al infrarrojo. Así la Espectroscopía Raman convencional suele aplicarse a muestras que no presentan una gran interferencia con la Fluorescencia. Por el contrario en TRS los fotones se crean en toda la muestra atravesada por la luz laser de excitación; produciéndose así una señal muy intensa.

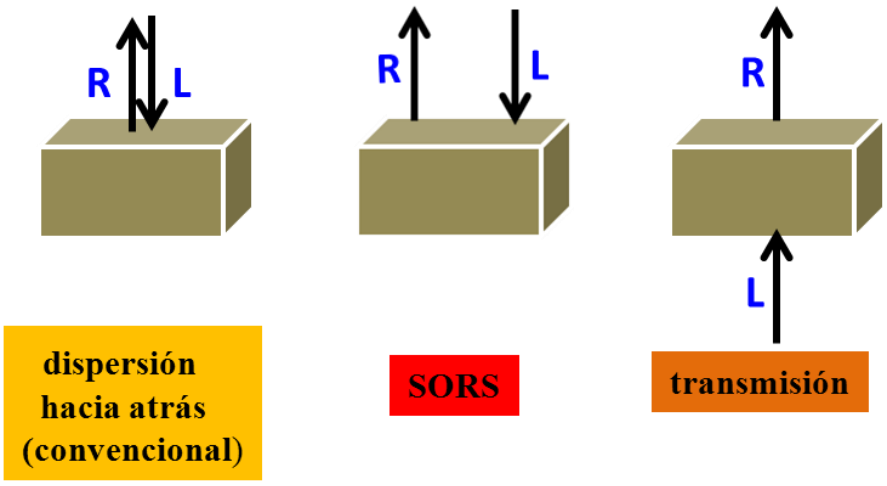

Figura 8.10: Geometrías típicas de Espectroscopia Raman con respecto a la muestra. **Izquierda)** Geometría de dispersión Raman convencional (conventional Raman scattering). **Centro**: Geometría de SORS. **Derecha:** Geometría de Transmisión Raman. **Leyenda**: **R:** luz Raman; **L**: haz laser.

Como ha sido comentado arriba, en TRS los fotones se crean a lo largo de toda la muestra iluminada por el láser, este fenómeno tiene relación directa con el hecho que la luz se dispersa a través de medios turbios que no absorben ni bloquean la luz de manera significativa. Para entender mejor dicho fenómeno es necesario considerar con detalle la teoría de propagación o migración de la luz en medios de dispersión difusa, tales como los tejidos, desarrollada por Pavel Matousek en 2007[21].

La principal barrera existente en métodos analíticos ópticos convencionales para la diagnosis de enfermedades en tejidos, que se hallan en capas más profundas, es la gran dispersión de la luz a través del tejido. Debido a esto es muy importante entender el mecanismo de propagación de la luz en un medio de dispersión difusa. En la Figura 8.11 se puede observar los tres componentes principales de la luz a través de un medio de dispersión difusa.[21] Éstas son balística, serpiente y difusa, tal como presentó *Alfano et al en 1997.*[22] La dispersión formada por fotones "balísticos" es la parte de la luz que no está dispersada por el medio y su intensidad decrece exponencialmente con la profundidad. Después de la propagación a través de un medio turbio, este componente se convierte gradualmente en luz formada por fotones "serpientes", que a su vez se convierte en el componente difuso.

El componente "serpiente" es el único débilmente desviado de su dirección original por los procesos de dispersión, debido al hecho de que sólo se somete a un número pequeño de dichos procesos, los cuales se hallan fuertemente sesgados hacia la dirección de avance. Este componente también decrece exponencialmente con la profundidad, aunque su profundidad de penetración es mayor que en el componente de la luz balística.

Ambos componentes balístico y serpiente pueden ser utilizados para formar imágenes nítidas o borrosas de objetos en estos medios. Esto es crucial para aplicaciones tales como Microscosopía confocal, dónde el paso de la luz a través de una apertura confocal sirve como un medio para la discriminación de la profundidad de la señal Raman. Un objeto visto con luz balística o serpiente, aparecería transparente o semi-transparente respectivamente. El componente penetrante, el más profundo y consecuentemente de mayor importancia para las investigaciones espectroscópicas de las capas profundas de medios turbios, es el componente difuso de la luz[21]. En tejidos puede penetrar diversos centímetros de profundidad, si se usa radiación NIR (Near Infrarred o Infrarrojo cercano), en oposición a los cientos de micrómetros o pocos milímetros en los componentes balístico y serpiente de la luz. Un objeto visto con la luz de dicho componente aparecería translúcido.

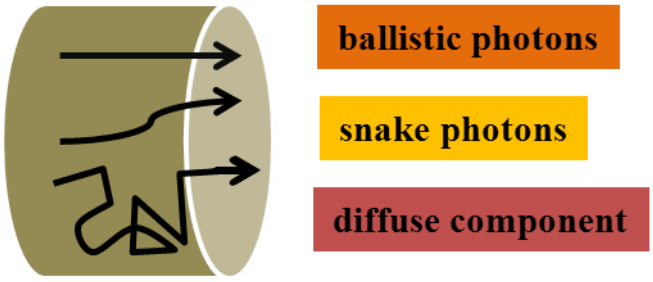

Figura 8.11: Principales componentes de la luz en medios turbios.

En consecuencia, en la técnica de TRS los fotones se crean a través de toda la muestra iluminada por el laser; en particular los fotones de las capas más profundas migran, por la teoría de migración o propagación de la luz, hacia las capas superficiales en tiempos de picosegundos y a continuación se dispersan hasta llegar al detector. De

esta forma se obtiene una mayor información de la muestra a medir debido a que se obtiene una señal Raman mayor que en el Raman convencional, donde la probabilidad de dispersión es de uno de cada 10^6-10^8 fotones, dando una señal que es representativa del contenido de toda la muestra y no solo de la superficie.

8.4.2 Antecedentes

La TRS fue inventada por Bernhard Schrader junto con Bergmann en el año 1967 con el articulo histórico acerca del primer uso exitoso de la TRS en análisis químicos de sólidos orgánicos.[23] La técnica TRS fue de nuevo re-inventada en 2006 por Matousek y Parker,[24,25] quienes mostraron la capacidad de dicha técnica en análisis de comprimidos y compuestos en polvo de varios milímetros de espesor. Ello supuso un avance en el mundo de la Farmacéutica, debido a que la técnica TRS representa un método analítico rápido, no invasivo de dosificación farmacéutica, tales como capsulas y comprimidos. Las técnicas de ensayo farmacéutico tradicionales presentan diversas limitaciones, debidas a la sensibilidad de la superficie (e.j reflectancia en NIR), la presencia de cambios de fase debido a la preparación de la muestra (e.j en cromatografía liquida), o sub-muestreo (en Raman y NIR convencional).[26]

Por el contrario la técnica espectroscópica de Transmisión Raman es bastante insensible a la superficie, no requiere preparación de la muestra ni cambio de fase y es rápida.[24,25] Subsiguientes investigaciones por Matousek y colaboradores aumentaron la precisión de esta técnica y su aplicabilidad en la cuantificación de comprimidos y compuestos en polvo de formulación.[27,28]

La aplicación de la Espectroscopia Raman convencional en el campo de la Medicina ha tenido sus limitaciones debido al problema que presentaba de sensibilidad a la superficie, no pudiendo alcanzar profundidades de cientos de micrómetros y quedándose tan sólo en la superficie. Por el contrario y por su ya mencionada insensibilidad a la superficie se ha podido presentar la técnica de TRS como una técnica de un alto potencial diagnóstico para lesiones en tejidos de mama. Diversos trabajos realizados por Baker et al[29,30] y Matousek y Stone[31] en el área del cáncer de mama, se llevaron a cabo mediante la identificación química de calcificaciones en lesiones de cáncer de mama a través de las técnicas Kerr gated, SORS y TRS, alcanzando profundidades de penetración de 0.9, 8.7 y 16 mm en tejidos de mama de pollos.

8.5 Objetivos y Estructura de la Tesis

8.5.1 Espectroscopia Raman Resonante de Transmisión: Desarrollo de una nueva técnica

La Espectroscopia Raman Resonante de Transmisión (TRRS) es aquella técnica que combina la Espectroscopia Raman de Transmisión (TRS) con la Espectroscopia Raman Resonante (RRS).[20] Como se ha visto anteriormente y por separado en los apartados 8.3 y 8.4, ambas técnicas mejoran y aumentan de forma selectiva y significativa la señal Raman. Por lo que cabe esperar que la simbiosis de ambas de lugar a su vez a un aumento y mejora drásticamente significativa en la señal Raman.

Con el mejor de nuestro conocimiento, hay pocos estudios publicados en el que la mejora de la excitación Raman resonante se combine con las ventajas de colectar la señal Raman de transmisión. Por lo tanto el desarrollo de una nueva técnica que

combina la resonancia Raman con las características operativas de la transmisión Raman fue una de las principales motivaciones de la presente Tesis Doctoral. De hecho, en términos de desarrollo instrumental uno de los logros más importantes de esta Tesis Doctoral ha sido el diseño, construcción y puesta en marcha de una nueva técnica basada en la espectroscopia Raman Resonante de Transmisión (TRRS).

Como se muestra en el **Capítulo 2** (así como en una publicación reciente en Applied Spectroscopy) este objetivo se ha logrado con éxito. Por lo tanto, una parte significativa de la de la tesis se centra en el estudio y análisis de frutos por técnicas espectroscópicas no invasivas, tales como TRRS.[32] En particular, se llevo a cabo el estudio de ciertos compuestos llamados carotenoides que se encuentran en las zanahorias, tales como β-caroteno, responsable de la pigmentation[20] y que participan en procesos fisiológicos tales como la photosynthesis.[32]

En el **Capitulo 2** se describe la técnica TRRS, metodología que, tal como se ha mencionado anteriormente proporciona un aumento en el cociente señal-ruido y una mejora en la sensibilidad analítica respectivamente. La aplicación técnica en la detección y cuantificación de β-caroteno en zanahoria de forma directa y no invasiva, permitió la obtención valores de 17.3 mg β-caroteno / 100 g zanahoria (coincidentes con los bibliográficos), así como la posibilidad de construir mapas de distribución espacial de carotenoides en frutas. También se estudia en este capitulo la dependencia de la señal Raman en función del espesor de la muestra (rodaja de zanahoria) mediante un modelo teórico que describe satisfactoriamente las medidas experimentales.

8.5.2 Espectroscopia Raman Resonante para la determinación del mecanismo de reacciones enzimáticas

Un buen ejemplo de la simplicidad y enorme sensibilidad de la espectroscopia Raman Resonante lo constituye el estudio de las reacciones catalíticas inducidas por enzimas. En el **Capitulo 3** se estudian reacciones catalíticas en proteínas mediante la Técnica de Espectroscopia Raman Resonante (RRS), así como su cinética mediante Absorción UV-Visible. En este estudio se corrobora y pone de manifiesto como, bajo las condiciones de resonancia en Espectroscopia Raman pueden llegar a visualizarse intermedios de reacciones catalíticas (dibujo de la portada), cruciales para el entendimiento de dicha ruta y para el descubrimiento de posibles inhibidores enzimáticos. En particular se estudia la catálisis del trans-resveratrol (t-res) inducida por la enzima tirosinasa (ty) mediante RRS en UV-Vis. Se estudia como el t-res se une a la ty, a través de su centro activo formado por dos átomos de (Cu), formando el complejo *t-res ty SP* con su característico enlace O-O, crucial en los primeros pasos de la ruta catalítica.[33] Por medio de esta técnica se llegan a observar intermedios catalíticos no detectables con otras técnicas más convencionales como Absorción UV-Vis. El presente trabajo deja claro que una clase de inhibidor potencial de la ty podría ser un compuesto capaz de unirse a los dos iones de cobre Cu (II) de la forma bidentada de la enzima. Es bien sabido el gran interés que despierta el descubrimiento de posibles inhibidores en la ruta de síntesis de melanina, la cual cataliza la ty, lo que supondría un gran avance en la investigación del cáncer de melanoma.

8.5.3 Fotones Láser y frutos sanos

En los capítulos anteriores se usan fotones láser especialmente como metodología analítica para desarrollar técnicas espectroscópicas Raman. Una parte importante de nuestro trabajo de Tesis Doctoral ha consistido en el uso de fotones laser no como soporte del método analítico sino como agente inductor de cambios fotoquímicos en frutos. Es conocido que las plantas y frutos ante diversos agentes de estrés tanto bióticos como abióticos- cual seria el caso de la excitación láser -generan sustancias beneficiosas para la salud, los llamamos metabolitos secundarios. Así en esta parte de la Tesis hemos llevado a cabo distintos estudios en uvas de mesa donde hemos empleado la tecnología láser para inducir el aumento de metabolitos secundarios como trans-resveratrol, por una parte, y también para medir dicho aumento, dicha mejora post-cosecha. De hay pues el titulo de esta parte de la Tesis "**Laser photons and healthy fruit**" ("Fotones laser y frutos sanos"). Esta parte esta se halla constituida por los **capítulos 4 y 5.**

Primeramente en el **Capítulo 4** se aborda el estudio e incremento de carotenoides en uvas - debido al interés que éstos despiertan por su capacidad antioxidante[34]- mediante técnicas UV- B LED**,** con el objetivo de mejorar la calidad y post-cosecha de estos frutos. Para este cometido se pasó al desarrollo y puesta a punto de un nuevo sistema experimental basado en un simple espectrómetro Raman Resonante de Transmision (TRR) con el empleo de un laser de Ar^+ a 514.5 nm de longitud de onda de excitación y una superficie rotatoria de 360º dónde la uva recibe radiación UV-B LED. A continuación la uva es analizada en el espectrómetro de TRR en función del tiempo.

Dicho sistema experimental se describe con claridad en este capitulo. En este estudio se observa como tras la exposición de la uva a radiación uv-led (0.58kJ/kg < 1kJ/kg = valor aprobado por la FDA en USA) y mediante su posterior análisis, se visualiza de forma nítida y clara un máximo en el aumento del contenido de β-caroteno en uva blanca a las 24 horas.

En el **Capítulo 5** se procedió al mismo tipo de estudios con uvas de mesa, pero utilizando un laser UV en lugar de UV-B LED como fuente de irradiación de fotones para aumentar la síntesis del contenido de trans-resveratrol en uvas. La elección de este polifenol trans-resveratrol fue debido a su alta actividad antioxidante, anti-fúngica, anti-inflamatoria, estrogénica, cardioprotectora y propiedades quimiopreventivas para el cáncer.[35,36,37,38,39]

Entonces las uvas fueron irradiadas conpulsos laser a dos diferentes longitudes de onda: una seleccionada a 302.1nm resonante con la banda bi-fotónica de absorción del trans-resveratrol[40,] y otra seleccionada a 300 nm, la cual no es resonante y la absorción bi-fotónica del trans-resveratrol es insignificante. specto de una longitud de onda no resonante a 300 nm que solo difiere de la primera en unos nm.

Diversos análisis espectroscópicos de Reflectancia Total Atenuada de Transformada de Fourier Infrarroja muestran un aumento en el contenido de polifenoles en uvas, cuando la longitud de onda resonante fue empleada. Posteriores análisis microbiológicos realizados en uvas control(no-tratadas), irradiadas no resonante y resonantemente mostraron como las ultimas desarrollaron un número significantemente menor de unidades formadoras de colonias después de ser cultivadas en el apropiado medio. Desde que la única diferencia entre las dos condiciones de irradiacion (resonante

y no-resonante) es simplemente un par de nanómetros en las longitudes de onda UV-B empleadas, el efecto germicida, en principio no tan acusado como si se hubiera empleado luz UV-C, en ambos tratamientos es muy similar, y consecuentemente la diferencia observada en la resistencia de las uvas de mesa a infecciones microbianas tiene que ser predominantemente atribuida a un efecto hormético de dependencia de longitud de onda. Diversas hipótesis son presentadas y discutidas para racionalizar estos descubrimientos experimentales pero entre todos ellos la explicación foto-química en la cual la absorción resonante bi-fotónica aumenta significantemente la biosíntesis de trans-resveratrol parece ser la más razonable.

8.5.4 ¿Son los fotones estrictamente necesarios para la mejora de la calidad de los frutos?

En el **Capitulo 6** se continúa el estudio dirigido hacia la mejora de la post-cosecha en frutos, en particular en uvas de mesa. En este capitulo se plantea una alternativa distinta al uso de fotones laser, atmosferas controladas o pesticidas químicos. La investigación consistió en el uso de pesticidas naturales presentes en la planta para mejorar su resistencia natural. Un importante grupo de metabolitos secundarios presentes en las plantas denominados phytoalexenos actúan como compuestos de defensa bajo condiciones de estrés o ataque, aumentando su propio contenido. Se sabe de la capacidad anti-fúngica y antioxidante de dichos compuestos.[41,42,43] Uno de estos phytoalexenos es el trans-resveratrol, el cual se encuentra en diversas plantas y frutas. Por todo ello en este estudio se lleva a cabo el uso de pesticidas naturales, tales como el trans-resveratrol en uva.

Para este cometido se procedió a la preparación de un extracto de hojas de vid en agua al 95% y 5% de etanol, en el que los diferentes racimos de uvas fueron sumergidos. El mismo número de racimos a su vez recibieron los tratamientos bien de agua o etanol disuelto en agua al (5%), siendo ambos utilizados como blanco. Sorprendentemente, en el día 14 después del comienzo del tratamiento de las uvas extracto tratadas, siempre mantenidas a temperatura ambiente, éstas no mostraron ningún signo de deterioro físico. Por el contrario, las dos muestras blanco, es decir: los racimos tratados en agua o etanol aparecieron deshidratados, infectados y deteriorados. Se ha podido demostrar que tras el uso de dichos conservantes naturales hay un aumento en phytoalexenos y mejora significativa en la resistencia natural de la uva a infecciones microbianas. Para la obtención de dichos resultados se usaron las técnicas de Desorción laser e Ionización Resonante acoplada con espectrometría de masas, análisis infrarrojo de Transformada de Fourier y análisis microbiológicos.

Como resultado de mejorar la calidad post-cosecha de los frutos los fotones laser son una buena alternativa, en particular si las bandas resonantes de absorción del bio-pesticida a elicitar (a incrementar su síntesis) pueden ser excitadas. Si los fotones laser no se hallan disponibles una alternativa interesante es el empleo de técnicas de radiación UV-LED, y si finalmente ninguno de los dos métodos puede ser implementado el uso del extracto de la propia planta puede ser de gran ayuda en última estancia

Por último en el **Capitulo 7** (en ingles) **y 9** (en español) se presenta un breve resumen de la Tesis y resaltan las conclusiones más relevantes de los distintos estudios llevados a cabo a lo largo de la misma.

8.6 Bibliografía

(1) K. Thyagarajan, A. Ghatak, Lasers: Fundamentals and Applications, Heidelberg, Germany: Springer, (2010).

(2) H. H. Telle, A. González Ureña and R. J. Donovan, Laser Chemistry: Spectroscopy, Dynamics and Applications, Chichester, U.K.: John Wiley & Sons, (2007).

(3) A. Requena, J. Zuñiga, Espectroscopia, Madrid, Spain: Pearson Education, S.A, (2004)

(4) J. Michaell Hollas, Modern Spectroscopy, Chichester, U.K.: John Wiley & Sons, (2004).

(5) I.N. Levine, Fisicoquímica vol.2, Madrid, Spain: Mc Graw Hill, (2005).

(6) W. Demtrõder, Laser Sectroscopy Vol.2 Experimental Techniques, Heidelberg, Germany: Springer, (2008).

(7) H. A. Kramers and W. Z. Heisenberg, "Über die Streuung von Strahlung durch Atome", *Physik* **31,** 681 -708 (1925).

(8) C.V. Raman and K.S. Krishnan, "A New Type of Secondary Radiation", *Nature* **121,** 501-502 (1928).

(9) A. González-Ureña, Cinética Química, Madrid, Spain: Síntesis, (2001) .

(10) W. Demtrõder, Laser Sectroscopy Vol.2 Chapter 3 Experimental Techniques, Heidelberg, Germany: Springer, (2008).

(11) E.V. Effremov, "Advances in Analytical Resonance Raman Spectroscopy",Vrije Universiteit, The Netherlands, October (2008).

(12) S. Tardioli, “Optical Methods For Structure Elucidation Of Protein-Ligand Interactions: Fluorescence and Ultraviolet Resonance Raman Spectroscopy”, Vrije Universiteit, The Netherlands, November (2011).

(13) M. Harrand, R. Lennuier, “Exalation de l´intensité raies dans les spectres Raman émis par des corps présentant au voisínage de la raie excitatrice”, Comptes Rendus Academie des Sciences **223**, 356-359 (1946).

(14) H. Takeuchi, I. Harada, “Ultraviolet resonance Raman spectroscopy of X-Proline bonds: A new marker band of hydrogen bonding at the imide C=O site”, J. Raman Spec. **21,** 509-515(1990).

(15) J.M. Friedman, D. L. Rousseau, and M. R. Ondrias, “Time Resolved Resonance Raman Studies of Hemoglobins” Ann. Rev. Phys. Chem. **33**, 471-491 (1982).

(16) M. V. Schulmerich, K. A. Dooley, M. D. Morris, T. M. Vanasse and S. A. Goldstein, ″Transcutaneous fiber optic Raman spectroscopy of bone using annular illumination and a circular array of collection fibers”, *J. Biomed. Opt.* **11**, 060502-1-3 (2006).

(17) C. Eliasson, P. Matousek, "Non-Invasive Authentication of Pharmaceutical Products through Packaging using Spatially Offset Raman Spectroscopy", Anal Chem. **79** (4), 1696-1701 (2007).

(18) C. Eliasson, N.A. Macleod, and P. Matousek, "Non-invasive Detection of Concealed Liquid Explosives using Laser Spectroscopy". Anal. Chem. **79**(21), 8185-8189 (2007).

(19) P. Matousek, I.P. Clark, E.R.C. Draper, M.D. Morris, A.E. Goodship, N. Everall, M. Towrie, W.F. Finney, and A.W. Parker, " Subsurface Probing in Diffusely Scattering Media Using Spatially Offset Raman Spectroscopy", Appl. Spectrosc. **59**, 393-400 (2005).

(20) A.G. Gonzálvez and A. González-Ureña, "Transmission Resonance Raman Spectroscopy: Experimental Results Vs. Theoretical Model Calculations", Appl. Spectrosc**. 66**(10), 1163-1170 (2012*)*.

(21) P. Matousek, "Deep non-invasive Raman spectroscopy of living tissue and powders", Chem.Soc.Rev. **36,** 1292-1304 (2007).

(22) B. B. Das, F. Liu, and R.R. Alfano, "Time-resolved fluorescence and photon migration studies in biomedical and model random media", Rep. Prog. Phys. **60,** 227–292 (1997), and references therein.

(23) B. Schrader, G. Bergmann, Z. Fresenius, "Die Intensitat des Ramanspektrums polykristalliner Substanzen", Anal. Chem. **225**, 230–247 (1967).

(24) P. Matousek and A.W. Parker, "Bulk Raman Analysis of Pharmaceutical Tablets", Appl. Spec. **60**(12), 1353-1357 (2006).

(25) P. Matousek and A.W. Parker, "Non-invasive probing of pharmaceutical capsules using transmission Raman spectroscopy", J. Raman Spec. **38**, 563-567 (2007).

(26) H. Wang, C.K. Mann, T.J. Vickers, "Effect of Powder Properties on the Intensity of Raman Scattering by Crystalline Solids", Appl. Spectrosc. **56**(12), 1538-1544 (2002).

(27) A. Johansson-Sparen, O. Svensson, S. Folestad, and M. Claybourn, "Quantitative transmission Raman spectroscopy of pharmaceutical tablets and capsules", Appl. Spectrosc. **61**(11), 1211-1218 (2007).

(28) C. Eliasson, N.A. Macleod, L.C. Jayes, F.C. Clarke, S.V. Hammond, M. R. Smith, P. Matousek, "Non-invasive quantitative assessment of the content of pharmaceutical capsules using transmission Raman spectroscopy", Journal of Pharmaceutical and Biomedical Analysis **47**(2), 221–229 (2008).

(29) R. Baker, P. Matousek, K.L. Ronayne, A.W. Parker, K. Rogers, and N. Stone, "Depth profiling of calcifications in breast tissue using picosecond Kerr-gated Raman spectroscopy", Analyst **132**, 48–53 (2007).

(30) N. Stone, R. Baker, K. Rogers, A.W. Parker, and P. Matousek, "Future possibilities in the diagnosis of breast cancer by subsurface probing of calcifications with spatially offset raman spectroscopy (SORS)", Analyst **132**, 899-905 (2007).

(31) P. Matousek and N. Stone,"Prospects for the diagnosis of breast cancer by noninvasive probing of calcifications using transmission Raman spectroscopy", J. Biomed. Opt. **12**(2), 024008 (2007), [doi:10.1117/18934].

(32) A.J. Young, D. Phillipa, A.V. Rubanb, P. Hortonb, and H.A. Frank, "The xanthophyll cycle and carotenoid-mediated dissipation of excess excitation energy in photosynthesis", Pure &Appl. Chern. **69,** 2125-2130 (1997).

(33) A.G. Gonzálvez, A. González-Ureña, R.J. Lewis, and G. van der Zwan, "Spectroscopy and Kinetics of Tyrosinase Catalyzed trans-Resveratrol Oxidation", J. Phys. Chem. B 116, 2553−2560 (2012).

(34) J.J.Strain and I.F.F. Benzie: Antioxidants/diet and antioxidant Defence in Encyclopedia of Human Nutrition, vol. 1, pp. 95-106 (M Sadler, JJ Strain and B Caballero, Editors). London: Academic Press (1999).

(35) A. Cassidy, B. Hanlkey, R.M. Lamuela-Raventós, "Isoflavones, lignans and stibenes-origins, metabolism and potential importance to human health", J. Sci. Food Agric. **80,** 1044-1062 (2000).

(36) L. Fremont, "Biological Effects of Resveratrol", Life Sci. **66,** 663-673 (2000).

(37) J.B. German, R.L. Walzem, "The health benefits of Wine", Annu. Rev. Nutr. **20,** 561-593 (2000).

(38) S. Pervaiz, "Chemotherapeutic potential of the chemopreventive phytoalexin resveratrol", Drug. Res. Updates. **7**, 333-344 (2004).

(39) G.J. Soleas, E.P. Diamandis, D.M. Goldberg, "Resveratrol: A Molecule Who's Time Has Come? And Gone", Clin. Biochem. **30,** 91-113 (1997).

(40) J.B. Jiménez Sánchez, E. Crespo Corral, J.M. Orea, M.J. Santos Delgado, A. González-Ureña, "Trans-resveratrol elicitation by laser resonant irradiation of table grapes", Appl. Phys. B. **87,** 559-563 (2007).

(41) Y. Elad, "Responses of plants to infection by Botrytis cinerea andnovel means involved in reducing their susceptibility to infection", Biol Rev. **72**, 381-422 (1997).

(42) X. Dong, "SA, JA, ethylene, and disease resistance in plants", Curr. Opin. Plant. Biol. **1**, 16-23 (1998).

(43) B.J. Feys, J.E. Parker, "Interplay of signalling pathways in plant disease resistance", Trends Genet **16,** 449-55 (2000).

Capitulo 9

Resumen y Conclusiones

En todos los estudios realizados en el transcurso de esta Tesis Doctoral, el uso de técnicas espectroscópicas Raman - en particular el de Raman de Transmisión y Raman Resonante (o la combinación de ambas) – han ocupado un lugar central. En este trabajo se ha demostrado las ventajas de la técnica Raman de Transmisión respecto de la técnica Raman convencional gracias a su configuración geométrica e insensibilidad a la superficie. Además, se ha evidenciado que esta técnica se puede mejorar con la inclusión del efecto Raman Resonante, por lo que una de las principales motivaciones de la presente Tesis fue el desarrollo de una nueva técnica que combinara la Resonancia Raman con las características operacionales de la Transmisión Raman. De hecho, en términos de desarrollo instrumental, el diseño, construcción y puesta a punto de una nueva técnica basada en la espectroscopia Raman Resonante de Transmisión (TRRS) se ha logrado con éxito, constituyendo uno de los logros más relevantes de nuestro proyecto.

Dicha técnica ha sido aplicada al análisis de carotenoides (principalmente β-caroteno) en muestras estándar y de zanahoria llegando a valores de LOD y LOQ del orden de cientos de picogramos y unos pocos nanogramos por milímetro cúbico, que proporcionan a su vez valores de β-caroteno de 17,3 mg / 100 g de zanahoria

(coincidentes con los bibliográficos). Además el espectrómetro de TRR desarrollado también puede ser aplicado para medir la distribución espacial de carotenoides en frutas y la dependencia de la señal Raman en función del espesor de la muestra (rodaja de zanahoria). Esta dependencia fue investigada y racionalizada utilizando un modelo teórico que describe satisfactoriamente las medidas experimentales.

También se ha investigado el mecanismo de reacción y cinética de algunas reacciones catalíticas en proteínas mediante las técnicas de Espectroscopia Raman Resonante (RRS) y absorción UV-Visible (UV-Vis). En particular, se estudió la catálisis de trans-resveratrol (t-res) inducida por la enzima tirosinasa (ty) mediante las técnicas de RRS y absorción UV-Vis. La absorción UV-Vis ha permitido deducir una cinética de primer orden para esta reacción.

El uso de la espectroscopia Raman Resonante permitió la detección de intermedios de reacción, los cuales son cruciales para la comprensión de algunas de las características y pasos más importantes de la reacción catalítica. Esta investigación ha sido relevante para sugerir inhibidores potenciales en la vía de síntesis de melanina, cuya síntesis es catalizada por la ty, y hoy en día recibe gran atención en la investigación del melanoma.

En el transcurso de este trabajo los fotones láser no sólo se han utilizado como parte del método analítico, sino como un agente (abiótico) para inducir cambios fotoquímicos en los frutos, que mejoren su calidad y estado de salud. Es decir, usando la luz laser bien para inducir estrés abiótico en uva de mesa con el fin de aumentar la producción de metabolitos secundarios, tales como el trans-resveratrol, o carotenoides o como método de análisis para medir su aumento interno utilizando la técnica de TRR.

Para ello se ha diseñado también un espectrómetro Raman Resonante de Transmisión (TRR), basado en un láser de Ar^+ a 514.5 nm de longitud de onda de excitación y un soporte giratorio de 360 °, donde las uvas reciben radiación UV-B LED.

Después de irradiar las uvas durante 30 minutos su contenido de carotenoides se analiza mediante dicho espectrómetro de TRR, observándose un aumento significativo de β-caroteno en uva blanca después de 24 horas de irradiación de la fruta.

El mismo tipo de estudios también fueron llevados a cabo con uvas de mesa, pero utilizando como fuente de fotones un láser UV en lugar de UV-B LED para aumentar el contenido de trans-resveratrol en uvas. Dos longitudes de onda diferentes fueron empleadas, una resonante con la banda de absorción bi-fotónica del trans-resveratrol a 302.1 nm, y otra no resonante a 300 nm. Los análisis microbiológicos y de Reflectancia total atenuada de Transformada de Fourier de infrarrojo mostraron un aumento en la resistencia de la uva a la infección microbiana y una mejora en el contenido de polifenoles respectivamente, cuando la longitud de onda empleada fue la resonante con la absorción bi-fotónica del trans-resveratrol.

Uno de los últimos estudios llevados a cabo en este trabajo se centró en el uso de pesticidas naturales presentes en la propia planta para mejorar la calidad post-cosecha en lugar de utilizar fotones láser, atmósferas controladas o pesticidas químicos. Esta investigación se llevó a cabo para evaluar la capacidad del trans-resveratrol como bio-pesticida natural con la finalidad de mejorar la calidad post-cosecha de las uvas.

Para este propósito se preparó un extracto natural de hojas de vid. Los análisis espectroscópicos y microbiológicos demostraron cómo el uso de tales extractos con

presencia de los bio-pesticidas naturales produjo un aumento significativo de la resistencia natural de la uva a las infecciones microbianas.

A continuación se describen brevemente las principales conclusiones extraídas de este trabajo:

1. Un nuevo Espectrómetro Raman Resonante de Transmisión se ha desarrollado y puesto a punto en nuestro laboratorio combinando la mayor sensibilidad de la espectroscopia Raman Resonante y la poca interferencia de fluorescencia presente en la espectroscopia Raman de Transmisión. La técnica es rápida, no invasiva e ideal para muestras sólidas que muestran una dispersión difusa significativa.

El espectrómetro de TRR se ha aplicado en el análisis de carotenoides en frutos y particularmente en el contenido de β-caroteno en raíces de zanahorias así como la dependencia de la señal Raman en función del espesor de la muestra. Se ha conseguido llegar a un límite de detección de cientos de picogramos por milímetro cúbico o cientos de partes por millón (ppb) que es muy inferior a los contenidos típicos de los pigmentos en los frutos. Se ha desarrollado un modelo teórico de la propagación de dispersión, el cual representa satisfactoriamente la dependencia de la señal Raman respecto al espesor de la muestra.

2. La Absorción UV-Vis y la espectroscopia Raman Resonante han sido utilizadas para la determinación del mecanismo de reacciones enzimáticas, en particular la reacción catalítica t-res-ty. La absorción UV-Vis ha permitido la investigación de la cinética de reacción, sugiriendo la presencia de una cinética de primer orden; mientras que la técnica RRS permitió la identificación de la evolución en

el tiempo de características espectroscópicas asociadas con la presencia de dos intermedios de reacción cruciales para el entendimiento de esta reacción catalítica.

3. Gracias a la información obtenida en el punto **2,** se ha podido estudiar con detalle el mecanismo de la reación enzimática, para la cual, se han estabelecido las siguientes etapas: (i.) la formación del complejo t-res-ty ^{S}P con su enlace O-O, que juega un papel crucial en los primeros pasos de la reacción. Se observó un intermedio de reacción con una banda Raman centrada a 753 cm^{-1} y asignada a la tensión del enlace O-O del μ–η^2: η^2–peroxodicopper (II) correspondiente al complejo t-res-ty ^{S}P. (ii) La hidroxilación del enlace C-H (en posición orto) del complejo t-res usa uno de los átomos de Oxigeno del peróxido produciéndose la ruptura del enlace O-O del centro activo de la ty. (iii) La última etapa implica un intermedio donde los modos vibracionales Cu–O(φ)–Cu) or ν_{AS} (Cu-O(φ)-Cu) correspondientes a la línea Stokes a 642 cm^{-1}, presentan una actividad Raman aumentada por resonancia. Por ello, una de las principales conclusiones alcanzadas en el curso de este estudio fue que los inhibidores potenciales de la tirosinasa deben ser capaces de unirse a los dos iones de Cu (II) de la forma bidentada de la enzima.

4. Respecto a línea de investigación dedicada a “Fotones laser y frutos sanos”, Los fotones UV-B LED se emplearon no como parte del método analítico, sino como un agente (abiótico) capaz de inducir cambios fotoquímicos en los frutos. Como método de seguimiento del aumento del contenido de β-caroteno en uva en

función del tiempo transcurrido desde la irradiación se utilizó la técnica TRRS, observándose que el contenido de β-caroteno en uvas aumenta cinco veces más respecto de la uva control (es decir, aquellas que no recibieron radiación). La relevancia del presente estudio recae en la utilización de dosis bajas de luz UV-B. Asimismo el empleo de la tecnología LED, abre el camino para un desarrollo de protocolos de bajo costo comercial de mejora de la calidad de post-cosecha de frutos, alimentos y vegetales.

5. Análogamente uvas de mesa fueron irradiadas con luz ultravioleta (UV) en lugar de UV- B LED. Al usar radiación UV-B resonante controlada en la piel de la uva, se observó un aumento selectivo del contenido de polifenoles (trans-resveratrol), el cual fue explicado en términos de un aumento en la biosíntesis del polifenol debido a la excitación electrónica siguiendo la absorción resonante bi-fotónica del precursor.

La importancia del presente trabajo recae en el carácter selectivo de los fotones empleados, ya que son seleccionados para ser resonantemente absorbidos por el trans-resveratrol. El empleo de análisis de ATR-FTIR y microbiológicos mostró una mejora en el contenido de polifenoles y una resistencia de la uva de mesa a la infección microbiana, respectivamente, cuando se empleaba una la longitud de onda resonante con la absorción bi-fotónica de trans-resveratrol.

6. En lo que respecta a la cuestión planteada en el capitulo 6, "¿Son los fotones estrictamente necesarios para la mejora de la calidad de los frutos?" La respuesta es afirmativa solo para aquellos casos en los que se desee usar métodos directos y no-invasivos. Sinembarago, hay que señalar que se encontró una mejora significativa de la resistencia de las uvas a su infección y maduración, tras sumergirlas en una disolución de extracto de hojas de vid. La influencia positiva observada de estos extractos naturales se demostró estar asociada a la presencia de polifenoles en base a datos de espectroscopia FTIR, análisis microbiológicos específicos y técnicas de espectrometría de masas acopladas a ionización laser.

Ciertamente, el uso de extractos naturales que contienen bio-pesticidas de la propia planta pueden mejorar de forma significativa la calidad de los frutos, pero cuando se dispone de los fotones láser apropiados o incluso de luz UV-B LED apropiada, su empleo puede constituir un método mucho más rápido, eficiente y no invasivo para mejorar la calidad de post-cosecha de la fruta. En general podría decirse que los fotones adecuados y la fruta sana van de la mano.